2021

Establishing The Transient Mass Balance Of Thrombosis Under Venous Flow: From A Microfluidic Approach To A Reduced Model

Jason Chen
University of Pennsylvania

Establishing The Transient Mass Balance Of Thrombosis Under Venous Flow: From A Microfluidic Approach To A Reduced Model

Abstract

Coagulation kinetics are well established in well plates assays in which human plasma clots isotropically. However, less is known about thrombin kinetics and transport within clots formed under hemodynamic flow. Using microfluidic perfusion of Factor XIIa-inhibited human whole blood over a 250-micron long patch of collagen/tissue factor and immunoassays of the effluent for fragment 1.2, thrombin-antithrombin, and D-dimer (post-endpoint plasmin digest), we sought to establish the transient mass balance for clotting under venous flow. Based upon these measurements under flow conditions, we have developed a highly reduced extrinsic pathway coagulation model (7 ODEs) under flow considering a thin 15-micron platelet layer where transport limitations were largely negligible (except for fibrinogen) and where cofactors (FVIIa, FV, FVIII) were not rate-limiting. By including thrombin feedback activation of FXI and the antithrombin-I activities of fibrin, the model accurately simulated measured fibrin formation and thrombin fluxes. The model required free thrombin in the clot (~100 nM) to have an elution half-life of ~2 sec, consistent with measured albumin elution, with most thrombin being fibrin-bound. Thrombin-feedback activation of FXIa became prominent and reached 5 pM at >500 sec in the simulation, consistent with anti-FXIa experiments. Further, we did a sensitivity analysis by conducting 10,000 Monte Carlo simulations for ±50% variation of 5 plasma zymogens and 2 fibrin binding sites for thrombin. A sensitivity analysis of zymogen concentrations indicated that FIX activity most influenced thrombin generation, a result expected from hemophilia A and B. Averaging all MC simulations confirmed both the mean and standard deviation of measured fibrin generation on 1 tissue factor molecule per μm2. Across all simulations, free thrombin in the layer ranged from 20 to 300 nM with a mean 50 nM. The model also suggested the antithrombotic potency of FXIa inhibitors may vary depending on normal ranges of zymogen concentrations. To sum up, our reduced model, which is supported by experimental data, predicts thrombin and fibrin co-regulation during thrombosis under flow, gives insights into the dynamics of the species involved, and may be useful for multiscale simulation.

Degree Type

Dissertation

Degree Name

Doctor of Philosophy (PhD)

Graduate Group

Chemical and Biomolecular Engineering

First Advisor

Scott L. Diamond

Subject Categories

Biomedical | Chemical Engineering

ESTABLISHING THE TRANSIENT MASS BALANCE OF THROMBOSIS UNDER VENOUS FLOW: FROM A MICROFLUIDIC APPROACH TO A REDUCED MODEL

Jason Chen

A DISSERTATION

in

Chemical and Biomolecular Engineering

Presented to the Faculties of the University of Pennsylvania

in

Partial Fulfillment of the Requirements for the

Degree of Doctor of Philosophy

2021

Supervisor of Dissertation

_____

Scott L. Diamond

Professor, Department of Chemical and Biomolecular Engineering

Graduate Group Chairperson

_____

John C. Crocker

Professor, Department of Chemical and Biomolecular Engineering

Dissertation Committee

Talid R. Sinno, Professor, Department of Chemical and Biomolecular Engineering

Ravi Radhakrishnan, Professor, Department of Chemical and Biomolecular Engineering

Lawrence F. Brass, Professor, Department of Medicine

ESTABLISHING THE TRANSIENT MASS BALANCE OF THROMBOSIS UNDER VENOUS FLOW: FROM A MICROFLUIDIC APPROACH TO A REDUCED MODEL

ACKNOWLEDGMENTS

First, I would like to thank my advisor Dr. Scott Diamond for the assistance and profession. Without his help and dedicated involvement, I wouldn't be able to make it. I would like to thank you for the support, patience, and understanding over these years. I could not have imagined having a better mentor for my Ph.D study. I would also like to show gratitude to the rest of my thesis committee: Dr. Lawrence Brass, Dr. Talid Sinno, and Dr. Ravi Radhakrishnan, for their insightful comments and hard questions. I thank my fellow labmates in Diamond lab especially those who helped me a lot, Dr. Shu Zhu, Dr. Brad Herbig, Dr. Xinren Yu, Dr. Chris Verni, Jason Rossi, and Huiyan Jing. Also, I thank my classmates from CBE program and my Taiwanese friends who supported me through this venture and made my life a little easier. Last but not the least, I am grateful for my parents and family for supporting my all these years.

ABSTRACT

ESTABLISHING THE TRANSIENT MASS BALANCE OF THROMBOSIS UNDER VENOUS FLOW: FROM A MICROFLUIDIC APPROACH TO A REDUCED MODEL

Jason Chen

Scott L. Diamond

Coagulation kinetics are well established in well plates assays in which human plasma clots isotropically. However, less is known about thrombin kinetics and transport within clots formed under hemodynamic flow. Using microfluidic perfusion of Factor XIIa-inhibited human whole blood over a 250-micron long patch of collagen/tissue factor and immunoassays of the effluent for fragment 1.2, thrombin-antithrombin, and D-dimer (post-endpoint plasmin digest), we sought to establish the transient mass balance for clotting under venous flow. Based upon these measurements under flow conditions, we have developed a highly reduced extrinsic pathway coagulation model (7 ODEs) under flow considering a thin 15-micron platelet layer where transport limitations were largely negligible (except for fibrinogen) and where cofactors (FVIIa, FV, FVIII) were not rate-limiting. By including thrombin feedback activation of FXI and the antithrombin-I activities of fibrin, the model accurately simulated measured fibrin formation and thrombin fluxes. The model required free thrombin in the clot (~100 nM) to have an elution half-life of ~2 sec, consistent with measured albumin elution, with most thrombin being fibrin-bound. Thrombin-feedback activation of FXIa became prominent and reached 5 pM at >500 sec in the simulation, consistent with anti-FXIa experiments. Further, we did a sensitivity analysis by conducting 10,000 Monte Carlo simulations for ±50% variation of 5 plasma zymogens and 2 fibrin binding sites for thrombin. A sensitivity analysis of zymogen

concentrations indicated that FIX activity most influenced thrombin generation, a result expected from hemophilia A and B. Averaging all MC simulations confirmed both the mean and standard deviation of measured fibrin generation on 1 tissue factor molecule per μm^2. Across all simulations, free thrombin in the layer ranged from 20 to 300 nM with a mean 50 nM. The model also suggested the antithrombotic potency of FXIa inhibitors may vary depending on normal ranges of zymogen concentrations. To sum up, our reduced model, which supported by experimental data, predicts thrombin and fibrin co-regulation during thrombosis under flow, gives insights into the dynamics of the species involved and may be useful for multiscale simulation.

TABLE OF CONTENTS

LIST OF FIGURES AND TABLES

CHAPTER 1: INTRODUCTION

1.1 Hemostasis and Thrombosis

To prevent bleeding from body, blood will clot in response to injury known as hemostasis. Hemostasis is comprised of two system: platelet aggregation and blood coagulation. A platelet can adhere to the damaged tissue by exposed collagen or von Willebrand Factor (vWF) and undergo an activation process that involves changes in the platelet's surface membrane. The activated platelets release several chemicals from intracellular granules, such as adenosine diphosphate (ADP) and thromboxane A_2 (TXA_2), to further recruit circulating platelets and form a platelet plug. Meanwhile, the exposed tissue factor (TF) triggers the extrinsic pathway of coagulation. The final and main enzyme in the series is thrombin, which cleaves the plasma protein fibrinogen into fibrin monomers. These monomers polymerize, cross-link to form a fibrous mesh and stabilize the aggregate. Together, the platelet aggregate and fibrin mesh constitute the blood clot, and their formation comprises hemostasis, the normal response to vessel injury to prevent blood loss.

These two processes are also the major components of thrombosis, a pathological process that involves formation of a clot inside a blood vessel and that can lead to the complete occlusion of the vessel and consequent blockage of oxygen and nutrients from important organs. Understanding these processes and how they are regulated is of major medical importance.

1.2 Coagulation Cascade

The coagulation cascade has two distinctive and initial pathways, the extrinsic pathway and intrinsic pathway. These pathways are series of reactions. The *extrinsic*

tenase/IXase (TF/FVIIa), formed by tissue factor exposed on disrupted endothelium and circulating factor VII, converts FX to FXa and FIX to FIXa. Initiated by anionic surfaces and along with conversion of activated cofactors FVIIIa and FVa, the *intrinsic tenase* (FIXa/FVIIIa) dramatically amplifies production of FXa. These two pathways lead to *prothrombinase* (FXa/FVa) and generate thrombin. Besides converting fibrinogen to fibrin, thrombin also activates FXIIIa and leads to fibrin crosslink. Thrombin is also responsible for its self-amplification by the FXIa-dependent feedback pathway, which is found to be a promising drug target for thrombosis with minimal bleeding risk.

Fibrin has 'antithrombin-I activity' via two thrombin binding sites: the low affinity site and the high affinity site of the alternative splice variant, γ'-fibrin(ogen). The γ'-fibrinogen splice variant represents about 6-8% of total γ-chains [1]. γ′ fibrinogen has shown to be associated with cardiovascular disease [2]. During thrombosis under flow, thrombin can be captured by the deposited fibrin via tight binding with γ'-fibrin. In acute phase response states γ'-fibrinogen levels can change [3]. It is important to understand thrombin binding to fibrin but few simulations of clotting under flow include these reactions.

1.3 Microfluidics Approaches

Blood clotting is well studied in well plates assays; however, it displays a core/shell structure in hemostatic plugs under flow [4]. Microfluidic devices are ideal technique in the study of blood function. With minimal volume of blood, we are able to control the physiological hemodynamic conditions. Our lab has developed the high-throughput eight-channel device to study human blood clotting under flow *in vitro* [5,6]. With micropatterning techniques, we can control the contribution of tissue factor pathway and contact pathway on the procoagulant surfaces. In addition, low level of tissue factor surfaces allowed observable crosstalk between extrinsic pathway generation of thrombin and FXIa-

dependent feedback pathway [7]. Human whole blood can be perfused at venous or arterial shear rates with platelet and fibrin deposition measured in real time by fluorescence microscopy. These devices have been previously reviewed [5,6].

CHAPTER 2: THE TRANSIENT MASS BALANCE OF THROMBOSIS AND THE REDUCED MODEL

2.1 Establishing the transient mass balance of thrombosis: From tissue factor to thrombin to fibrin under venous flow

2.1.1 Introduction

Upon vessel injury or plaque rupture, platelets rapidly deposit at the perturbed site. Additionally, thrombin is generated by the coagulation cascade triggered by wall-exposed tissue factor (TF). Thrombin functions as a key driver of clotting by promoting human platelet activation via PAR1 and PAR4 and by cleaving fibrinogen for fibrin polymerization. The mouse laser injury model has revealed a heterogeneous clot structure with a tightly packed 'core' of activated platelets and a less stable and loosely packed outer 'shell' of less activated platelets [4,8]. Similarly, in microfluidic experiments with human blood, a P-selectin positive core is detected that is co-localized with thrombin and fibrin. The thickness of the core region depends on the localization of thrombin since thrombin localization detected with a platelet-targeting biosensor [9] is highly correlated temporally and spatially with P-selectin display in the core [10,11]. Under venous conditions, antagonism of fibrin polymerization with the inhibitor gly-pro-arg-pro (GPRP) or blockade of γ'-fibrinogen with an antibody leads to larger clots [11]. Consistent with thrombin localization in the clot core, the core is the location where interstitial permeation is expected to be less due to the lower porosity following contraction [12].

In prior studies using thrombin-antithrombin (TAT) immunoassay on blood flowing over a procoagulant surface [13], little TAT was detectable in the effluent unless fibrin polymerization was blocked with GPRP. Fibrin efficiently captured over 85% of the locally generated thrombin. For flow over a TF surface with fibrin polymerization blocked, the thrombin wall flux increased linearly with time to ~0.5 x 10^{-12} nmol/μm^2-sec over the first

500 sec of clotting. The thrombin flux then increased by a factor of 3-fold by 800 sec of clotting, an increase blocked by anti-Factor XIa antibody (O1A6).

Importantly, the γ'-fibrinogen slice variant represents ~6-8% of the total γ-chains (or equivalently, the γA/γ' heterodimer represents ~12 to 16% of the total fibrinogen) [14,15]. Fibrin presents the weak sites in the E-domain for thrombin exosite 1 (~1.6-1.8 sites/monomer, K_d~2-4 μM) and a high affinity site that targets thrombin exosite 2 via the highly anionic and tyrosine-sulfated γ'-chain sequence (~0.2-0.4 sites/monomer, K_d~0.1-0.4 μM) [16–18]. Despite the measurement of a moderate submicromolar affinity of the γ'-chain of fibrin for thrombin, the binding may actually be much tighter as indicated by fibrin's tight capture of endogeneous by generated thrombin [13] and exogenously added thrombin [18]. In fact, the binding by thick fibers of fibrin has been described as irreversible and unsuited for Scatchard analysis [19] with steric capture/entrapment implicated.

Beyond measuring thrombin production by TAT assay in the presence of GPRP, thrombin generation can also be followed via the release of prothrombin fragment 1.2 (F1.2). F1.2 can be detected in the clot effluent even in the presence of fibrin generation. In contrast to thrombin generation, few if any quantitative measurements have been made of fibrin content of clots formed under flow. Fluorescent fibrinogen or fluorescent anti-fibrin antibody can be added to blood to follow the dynamics of intrathrombus fibrin generation. However, fluorescence is difficult to calibrate and can include platelet binding of fibrin(ogen). As an endpoint measurement, a clot formed on a procoagulant surface can be rinsed with buffer, subjected to plasmin and then assayed by D-dimer immunoassay to give a quantitative measure of intraclot fibrin.

Since γ'-fibrin can capture thrombin, an improved understanding of clot growth requires direct measurement of the co-regulation of local thrombin and fibrin dynamics. For clotting under flow, platelet densities are 50-200X greater than platelet rich plasma

(PRP) [4,20]. Additionally, considerable effort has been directed at computer simulation of tissue-factor driven thrombin generation in tube reactions [21,22] or under flow [23–25]. To our knowledge, this is the first simultaneous measurement of the rate and quantity of thrombin and fibrin generated within a clot formed under venous flow.

2.1.2 Materials and methods

Materials

The following reagents were obtained: Anti-human CD61 (BD Biosciences, San Jose, CA), Alexa Fluor®647 conjugated human fibrinogen (Life Technologies, Grand Island, NY), Collagen Type I Chrono-Par™ aggregation reagent (Chrono-log, Havertown, PA), corn trypsin inhibitor (CTI, Haematologic Technologies, Essex Junction, VT), Phe-Pro-Arg-chloromethylketone (PPACK; Hematologic Technologies, Essex Junction, VT), Dade® Innovin® PT reagent (Siemens, Malvern, PA), Enzygnost® F1+2 monoclonal kit (Siemens Healthcare Diagnostic, Tarrytown, NY), D-dimer ELISA kit (Abcam, Cambridge, MA), Human Fibrinopeptide A (FPA) ELISA Kit (MyBioSource, San Diego, CA), ethylenediaminetetraacetic acid (EDTA, Sigma, St. Louis, MO), H-Gly-Pro-Arg-Pro-OH (GPRP, EMD Chemicals, San Diego, CA), Fluorescein Phe-Pro-Arg-chloromethylketone (fluorescein-PPACK; Hematologic Technologies, Essex Junction, VT), Sigmacote® siliconizing reagent (Sigma, St. Louis, MO), and Sylgard® 184 Silicone Elastomer kit (Dow Corning, Auburn, MI). O1A6 FXI antibody was a gift from Dr. Andras Gruber (Department of Biomedical Engineering, Oregon Health and Science University).

PDMS patterning and flow device

Polydimethylsiloxane (PDMS) devices were fabricated as previously described [13,26]. Devices with a single long channel (250 μm in width, 60 μm in height) were used

to pattern protein onto glass slides. Multi-channel flow chambers were employed for microfluidic thrombosis assay. Each of these devices has 8 individual flow channels (250 μm in width and 60 μm in height) that are diverging from a single inlet and converging into a common outlet where blood sample was collected. PDMS devices can be reversibly fixed to glass slides through vacuum bonding. Glass slides were rinsed with ethanol, dried with filtered compressed air before being treated with Sigmacote® in order to prevent surface triggered blood clotting. Collagen type I (1 mg/mL, 5 μL) was perfused through the main channel on the single channel device to generate a patch (250 μm in length) of aligned collagen fibers on glass slides, followed by bovine serum albumin (0.5% BSA in Hepes Buffered Saline, 5 μL). To add lipidated TF vesicles onto patterned collagen, Dade Innovin® PT reagent (23 nM) was subsequently perfused through the channel [27]. After 30 min of incubation, excessive collagen or vesicles were washed with a final BSA rinse (20 μL). TF surface densities were about ~1 TF molecule/μm^2, based on prior calibration using fluorescent imaging of FITC-annexin V stained vesicles [13,27].

Blood collection and sample preparation

All donors were healthy individuals who provided consent under approval of University of Pennsylvania Institutional Review Board and were self-reported free of any medication or alcohol for at least 72 hr prior to blood donation. Blood was collected via venipuncture into syringes containing high dosage of CTI (40 μg/mL) to prevent contact activation and was subsequently labelled with CD61 antibody (2% by vol.) and fluorescent fibrinogen (1.3 % by vol.) for platelet and fibrin epifluorescence detection, respectively. When needed, GPRP (5 mM) was added to blood sample to block fibrin polymerization. In some experiments, fluorescein-PPACK was added to label the thrombin active site.

Microfluidic thrombosis assay

The multichannel flow chamber was vacuum bonded on glasses slides over the patterned TF bearing collagen patches. The flow channels run perpendicularly to the collagen/TF patches and were primed and incubated with BSA buffer for at least 30 min prior to experiments to block nonspecific protein adsorption during blood perfusion. Labeled whole blood was transferred to BD 1-mL plastic syringes (Becton Dickson, Franklin Lakes, NJ) which were the then mounted on a PHD 2000 syringe pump (Harvard Apparatus, Holliston, MA). All flow experiments were initiated within 10 min after phlebotomy to avoid contact activation due to prolonged blood-surface contact even in the presence of high dosage of CTI. Blood was infused into the flow device at a constant flow rate of 16 μL/min (2 μL/min per channel) which corresponds to an initial wall shear rate of 200 s^{-1} in each channel. Platelet aggregation and fibrin formation were simultaneously monitored and captured with a fluorescence microscope (IX81, Olympus America Inc., Center Valley, PA) equipped with a CCD camera (Hamamasu, Bridgewater, NJ).

F1.2, TAT, D-dimer, and FPA immunoassay

The effluent of the flow device was collected for various immunoassays (**Figure 2-1**). For F1.2 and FPA ELISA, the effluent was treated with 10 μL of quenching buffer containing EDTA (0.5 mM) and PPACK (100 μM). Calcium-dependent thrombin generation was immediately quenched by EDTA and calcium-independent fibrinogen cleavage by thrombin was quenched with PPACK. A blood sample was collected from the outlet every 3 min into individual centrifuge tubes. For TAT assay, the sample was quenched only with EDTA to prevent further thrombin generation but to allow active thrombin to complex with antithrombin. Collected blood samples were centrifuged at 1500 g for 15 min to isolate platelet poor plasma for ELISA. Background levels were determined

by analyzing the plasma sample isolated from blood that was quenched with EDTA/PPACK buffer immediately after phlebotomy. For each mole of generated thrombin, one mole of F1.2 is released from converted prothrombin. Thus, the measured average F1.2 concentration ($\bar{C}_{F1.2}$) within each time interval between sample collections can be converted to an average thrombin flux ($\bar{J}$) using the following equation, where Q is flow rate (16 µL/min) and A is total thrombotic area:

$$\bar{J} = \frac{\bar{C}_{F1.2} Q}{A} \qquad \textbf{Equation 2-1}$$

For the fibrin endpoint determination after 800 sec of clotting, whole blood perfusion was replaced with a HEPES-buffered saline (HBS) rinse and then subjected to high dose plasmin digestion (800 µg/mL for 15 min) followed by digest collection and D-dimer ELISA. Each D-dimer detected was considered equivalent to a single fibrin monomer presenting two D-domains.

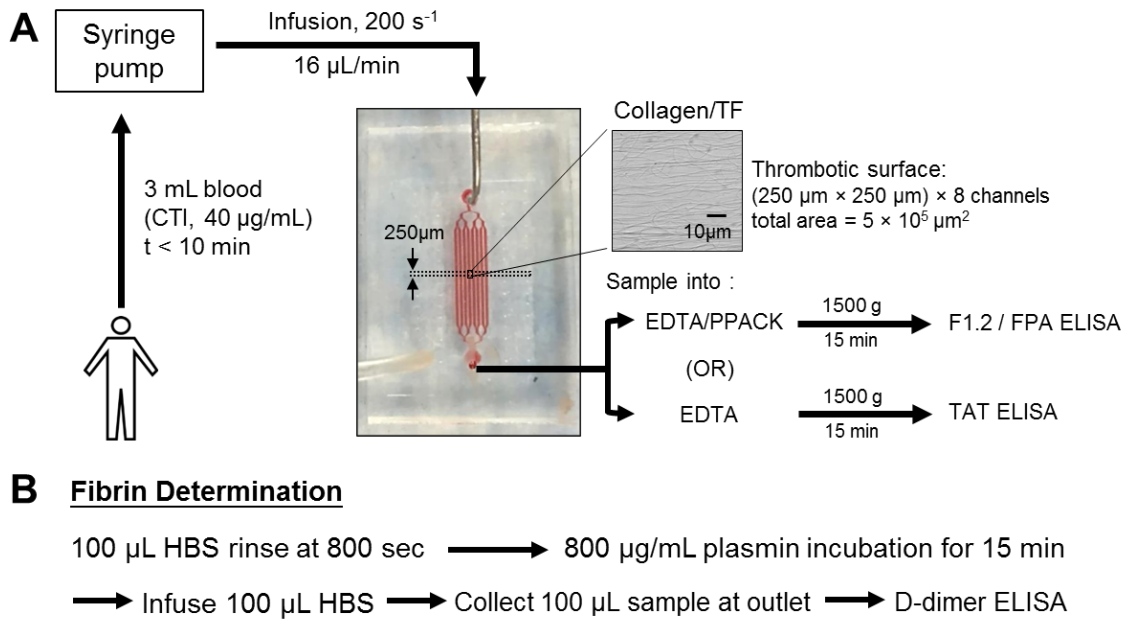

Figure 2-1. Experimental protocol for collecting effluent
Experimental protocol to perfuse whole blood over discrete 250-µm long collagen/tissue factor surfaces while measuring dynamic platelet and fibrin accumulation by fluorescence microscopy and detecting F1.2 and thrombin-antithrombin complex (TAT) in the effluent using immunoassays (**A**). In some experiments, the clot was rinsed in situ and subjected to plasmin digestion to release D-dimer for subsequent immunoassay (**B**).

2.1.3 Results

Intrathrombus thrombin is captured by fibrin via the γ' fibrin(ogen) variant

Human blood was collected in high concentration of FXIIa-inhibitor CTI (40 µg/mL) and immediately perfused over collagen/TF to allow 2-color imaging of platelet and fibrin fluorescence dynamics and collection of effluent samples for assay of TAT, F1.2 (**Figure 2-1A**) or end-point collection of plasmin-lyzed fibrin for D-dimer assay (**Figure 2-1B**). Under venous wall shear rate of 200 s^{-1}, platelets and fibrin intensely accumulated on the collagen/TF patch with dense platelet aggregates surrounded by dense fibrin (**Figure 2-2**). Addition of a low concentration of fluorescein-PPACK (600 nM) did not block fibrin deposition and allowed the detection of the thrombin active site which was highly co-localized with the fibrin (**Figure 2-2, top row**), but considerably less so with platelets. Inclusion of 5 mM GPRP to the assay had little effect on platelet deposition, but ablated

fibrin polymerization and ablated the detection of the thrombin active site with fluorescein-PPACK (**Figure 2-2, middle row**), indicating that capture of tightly-bound thrombin within the clot required fibrin. This result was exactly consistent with the inability to detect TAT in the effluent unless GPRP was present [13]. Inclusion of anti-γ'-fibrinogen antibody had a slight effect on fibrin morphology and completely ablated the detection of the thrombin active site with fluorescein-PPACK (**Figure 2-2, bottom row**), demonstrating that intrathrombus thrombin was captured and localized by γ'-fibrin(ogen).

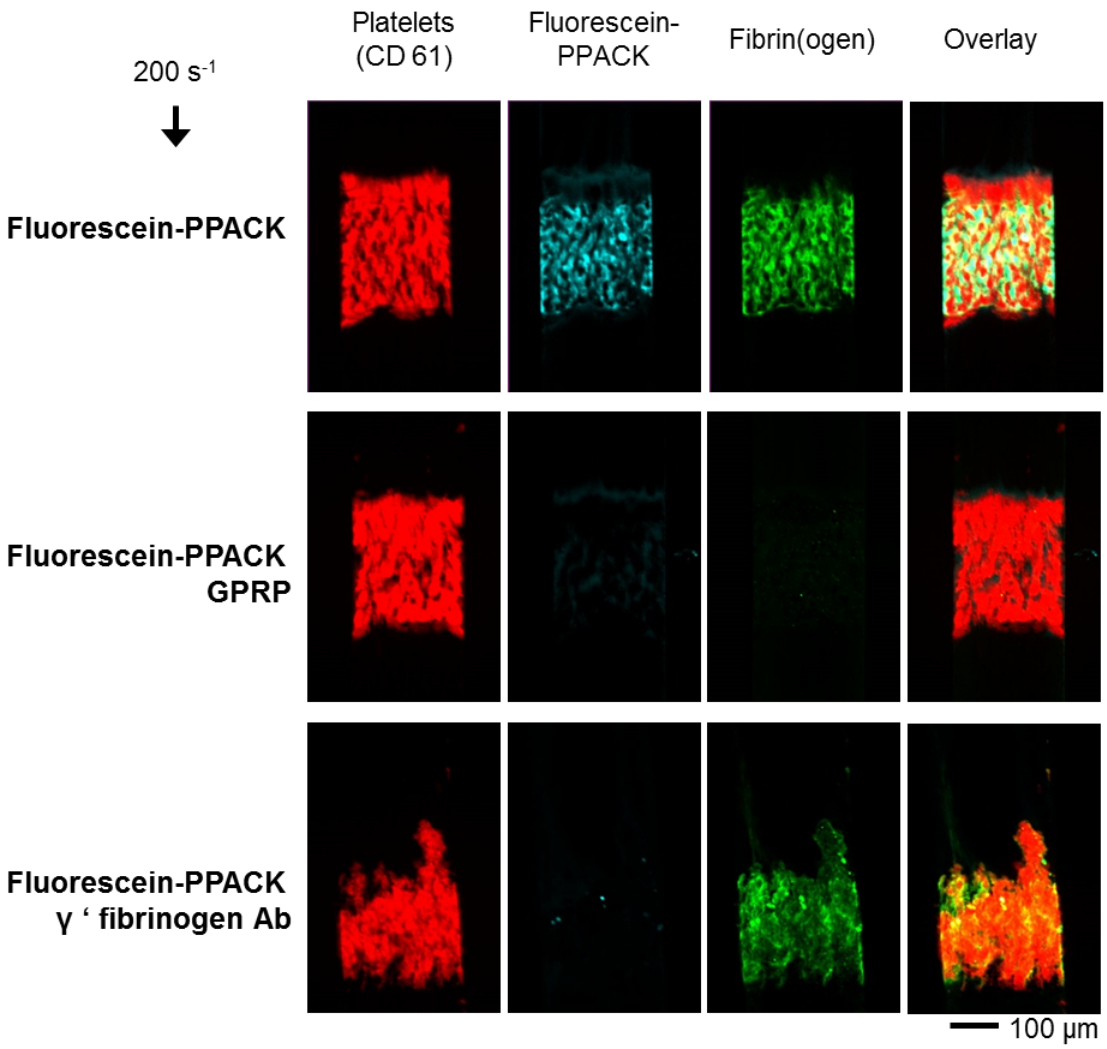

Figure 2-2. Intrathrombus thrombin is captured by fibrin via the γ' fibrin(ogen) variant
Accumulation of fluorescent platelets and fibrin(ogen) on collagen/tissue factor in the presence of low dose fluorescein-PPACK to stain for the thrombin active site under control conditions (top row) or GPRP to block fibrin (middle row) or anti-γ'-fibrinogen antibody (bottom row).

In a separate experimental design, clots were allowed to form (CTI-whole blood over collagen/TF) for 2 min at 200 s^{-1}. Then, fluorescein-PPACK buffer was added for 2 min to label the thrombin active site followed by a 7-min high shear buffer wash at 1000 s^{-1}. Again, the thrombin-active site detected with fluorescein-PPACK was: (1) strongly stained in the clot, (2) highly co-localized with fibrin, (3) largely absent on platelet masses,

and (4) highly resistant to high shear rate wash out over a 7-min time frame (**Figure 2-3**), all consistent with nearly irreversible binding of thrombin by fibrin [13,18,19].

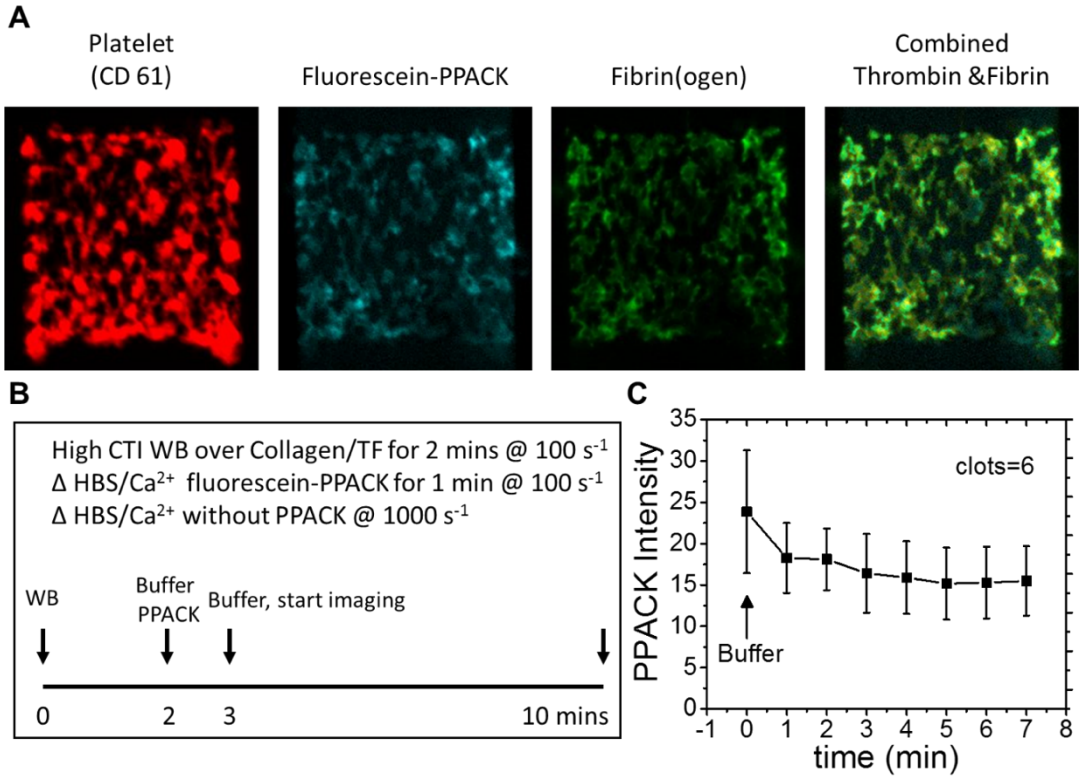

Figure 2-3. High shear rate washout of fluorescein-PPACK stained fibrin over 7 minutes
Washout experiment of fluorescein-PPACK labeled thrombin (A). Clots were formed for 2 min, stained with fluorescein-PPACK for 1 min, and then buffer washed for 10 min (B) to follow the elution of thrombin from the clot (C). Results are expressed as mean ± SD (n=6). All the values are significantly different from zero ($p<0.001$) demonstrating essentially no washout of thrombin.

Thrombin production rates in fibrin rich clots

To measure thrombin production by whole blood clotting on collagen/TF while fibrin was polymerizing (no GPRP), F1.2 was measured in the clot effluent. The concentration of F1.2 increased linearly with time, for the first 500 sec to a thrombin flux value of ~0.5 x 10^{-12} nmole thrombin/μm^2-sec, essentially identical to the thrombin flux determined with TAT assay with GPRP present (**Figure 2-4A**). The amount of F1.2 generated was considerably greater in the presence of GPRP, especially at later times of 400 to 800 sec

where FXIa activity is considered an important contributor to thrombin production in part through a platelet polyphosphate dependent mechanism [13,27]. The increased F1.2 generation in the presence of GPRP was expected since thrombin would not be susceptible to γ'-fibrin sequestration. The late stage role of FXIa on F1.2 generation was shown at the later times between 400-800 sec through the function blocking antibody O1A6 to inhibit FXIa (**Figure 2-4B**). The amount of F1.2 made in the presence of GPRP was ~30-50% greater than the amount of TAT detected in the presence of GPRP (**Figure 2-4A**), which was expected since some of the thrombin released from the clot might be inhibited by C1 inhibitor or α_2-macroglobulin instead of antithrombin. In a control experiment all the F1.2 detected in the effluent was dependent on the TF in the collagen coating since blank chambers lacking collagen/TF produced essentially undetectable levels of F1.2 (regardless of presence or absence of GPRP), also indicating that high dose CTI quenches FXIIa in the inlet reservoir and flow channels of the microfluidic device (**Supplemental Figure II**).

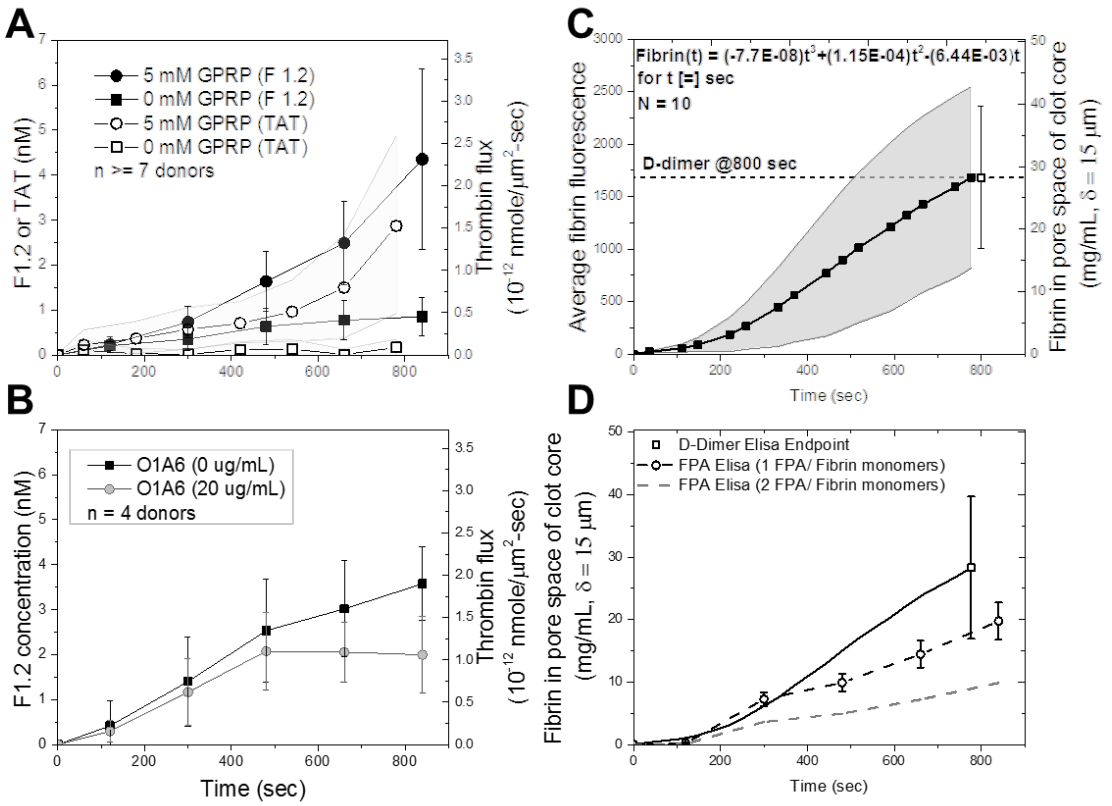

Figure 2-4. The dynamics of thrombin flux and fibrin concentration
Comparison of F1.2 and TAT generation by whole blood clotting under venous flow conditions in the presence or absence of GPRP (A) or anti-FXIa antibody O1A6 (B). Alternatively, clots were formed with fluorescent fibrinogen tracer and then subjected to endpoint plasmin-digest for assay of D-dimer (C). FPA generation was measured from 0 to 800 sec. The result from independently measured D-dimer assay (*dark line*) was compared with assuming 1 FPA/fibrin monomer (*dark dashed line*), and 2 FPA/fibrin monomer (*gray dashed line*) (D). Results are expressed as mean ± SD.

Intrathrombus fibrin can reach levels 10-fold greater than plasma fibrinogen concentration

During the perfusion of whole blood over collagen/TF, the accumulation of fibrin can be followed dynamically with time using fluorescent fibrinogen (**Figure 2-4C**). At the end of the 800 sec experiment, the clot was rinsed and subjected to plasmin degradation to release D-dimer for immunoassay. This 800-sec endpoint measurement allowed the determination of the final fibrin concentration in the clot to be determined to be 30 ± 15 mg/mL (~ 90 μM fibrin; ~10-15 μM γ'-fibrin chains) in the pore space of the clot. This fibrin

concentration depends on several prior known constraints such as the fibrin existing only in the pore space of a platelet mass with porosity of ~0.5 and the core region having a thickness of 15 μm, as previously measured (**Supplemental Figure II**) [10,25,28].

At 800 sec, the measured concentration of fibrin was 10-fold greater than typical average plasma fibrinogen concentration, indicating that fresh fibrinogen was entering the core of the clot where thrombin was generated. Using the endpoint measurement to calibrate the dynamic fluorescence signal obtained by microscopy of venous clotting on collagen/TF, the dynamic intrathrombus fibrin concentration in the pore space of the clot is given as (**Figure 2-4C**):

$$[\text{fibrin, mg/ml}](t) = (-7.7\text{x}10^{-8})\, t^3 + (1.15\text{x}10^{-4})\, t^2 - (6.44\text{x}10^{-3})\, t \text{ , for } t \text{ [=] 0 to 800 sec.}$$

Based on this calibration of the fluorescence signal, the concentration of fibrin generated at 500 sec due to TF was ~15 mg/mL. This post-lysis D-dimer estimate of the clot fibrin includes incorporated fibrinogen that can stably incorporate into D-dimer (even without FXIIIa crosslinking) and assumes that fibrin monomers do not escape from the clot core due to their incorporation into fibrin. FXIIIa crosslinking is expected to be substantial by the end of the 800 sec experiment. For fibrin at a density of 15 mg/mL, the calculated fibrin porosity is ε_{fibrin} = 0.95, based on a fibrin fiber density of 280 mg-fibrin/mL-fiber[29]..

In **Figure 2-4C**, the variability in dynamic fibrin fluorescence across 10 healthy human donors was about ± 50% CV, which was greater than the 8% CV of the D-dimer Elisa and the intrachip clotting/flowrate/sampling error of ~15% CV. The D-dimer endpoint assay was used to calibrate the average dynamic fibrin fluorescence (**Figure 2-4C-D**) since the two signals were highly correlated in individual donor measurements (R^2=0.9592). Similar to the magnitude of the interdonor variability of the fibrin fluorescence signal, the interdonor variability of the D-dimer endpoint assay was about ± 40% CV (**Figure 2-4C-D**).

In a separate control experiment using fibrinopeptide A (FPA) Elisa to corroborate the D-dimer endpoint data, we measured the dynamics of FPA generation from 0 to 800 sec. Assuming 1 FPA/fibrin monomer, the FPA assay was calculated to produce slightly less fibrin than indicated by the independently measured D-dimer assay, albeit within the interdonor variation of the measurements (**Figure 2-4D**). Assuming 2 FPA/fibrin monomer (*dashed line*), the FPA assay predicted only about a third as much fibrin as the D-dimer endpoint assay. The difference between the FPA assay and D-dimer assay might be explained by (1) different donors used for each assay and/or (2) the incorporation into the fibrin of fibrinogen, single-cleavage des(A)-fibrin monomer, or even small amounts of des(B)-fibrin monomer.

Intrathrombus fibrin/thrombin ratio demonstrates thrombin has a short half-life < 100 msec.

By measuring the thrombin flux with time (**Figure 2-4A**) with F1.2 assay as fibrin is made dynamically (**Figure 2-4C**), it is possible to determine the total amount of thrombin and fibrin made during the assay. By 500 sec before the contact pathway engages, a total of 92000 molecules of thrombin and 203,000 molecules of fibrin were generated per single molecule of TF (or per μm^2 of surface area). By TAT assay, it is estimated that 15% of the thrombin can escape the clot as detectable TAT and that most (~ 70%) of this escaping thrombin complexes with antithrombin with 30% captured by other inhibitors and undetected by TAT assay. Assuming that all fibrin monomers are captured within the fibrin of the clot, the ratio of intrathrombus fibrin to thrombin was remarkably low. There were only ~3 fibrin monomer equivalents generated per thrombin molecule. Regarding FPA generation, the overall rate R is given as $R= k_{cat} * [(S_o/(S_o+K_m)]$ where $S_o = \alpha$A-chains = 2[fibrinogen]. For $k_{cat} = 77\ s^{-1}$ and $K_m = 5.7\ \mu M$ [30] or $k_{cat} =84\ s^{-1}$ and $K_m = 7.2\ \mu M$ [31],

the overall rate is R = 60 FPA per thrombin per sec. For this rate of generation of desA-fibrin monomer by thrombin mediated release of fibrinopeptide A (FPA) of 60 FPA per thrombin per sec [30,31], the average lifetime (t_{avg}) of thrombin in the thrombus can be estimated to be t_{avg} ~ 100 msec by:

[72,300 thrombin] * (60 FPA/thrombin-sec) * (t_{avg}) = 203,000 fibrin monomers * (2 FPA/monomer)

For a half-life $t_{1/2}$ ~ 0.693 (t_{avg}), the half-life of thrombin in a clot with fibrin is $t_{1/2}$ ~ 70 msec, considerably shorter than the protein diffusional escape time of ~ 5-10 sec as calculated by simulation [32] or measured with flash-activated albumin in clots [33]. The short half-life of 70 msec is fully consistent with typical association rates of proteins with each other and the observation that almost all of the thrombin is captured by fibrin with minimal elution out of the clot [13].

Calculation of free thrombin within the clot assuming equilibrium with fibrin

Based upon F1.2, TAT, and D-dimer assay, the concentrations within the core pore space of the clot at 500 sec were estimated to be 15 μM thrombin and 45 μM fibrin (**Figure 2-5**). Both these intrathrombus concentrations were considerably greater than the plasma concentration of prothrombin (1.4 μM) and fibrinogen (9 μM). From the TAT assay, intraclot fibrin displayed ample capacity to bind substantial amounts of endogeneously generated thrombin. Based upon equilibrium of 15 μM thrombin with 45 μM fibrin that presents 72 μM weak sites and 13.5 μM strong sites (following [18]), we calculated that the free concentration of thrombin within the clot core was on the order of 100-200 nM (~10-20 U/mL) for a γ'-site K_d of ~0.2 μM.

However, the value of K_d for endogeneously generated thrombin incorporated into endogenously generated fibrin may be different from values obtained with exogenously

added thrombin and may depend on the exact concentration and polymerization conditions of thrombin and fibrin used in the measurement. The lack of washout of fluorescein-PPACK stained fibrin over 7 minutes (**Figure 2-3**) was indicative of a very slow off-rate. Given the lack of measurements on extremely high density intrathrombus fibrin, we explored computationally (*see* **Supplemental Methods**) a range of K_d values for the γ'-site, assuming the weak site in the E-domain was between 1 and 5 μM (**Figure 2-6**). Free intrathrombus thrombin concentrations were calculated to range from about 20 to 200 nM under conditions of tighter binding (γ'-site K_d ~1 to 50 nM). These estimates do not include binding of free thrombin to platelet GPIbα (K_d~100 nM) or consumption by fibrin-linked α_2-macroglobulin or α_1-antitrypsin [34].

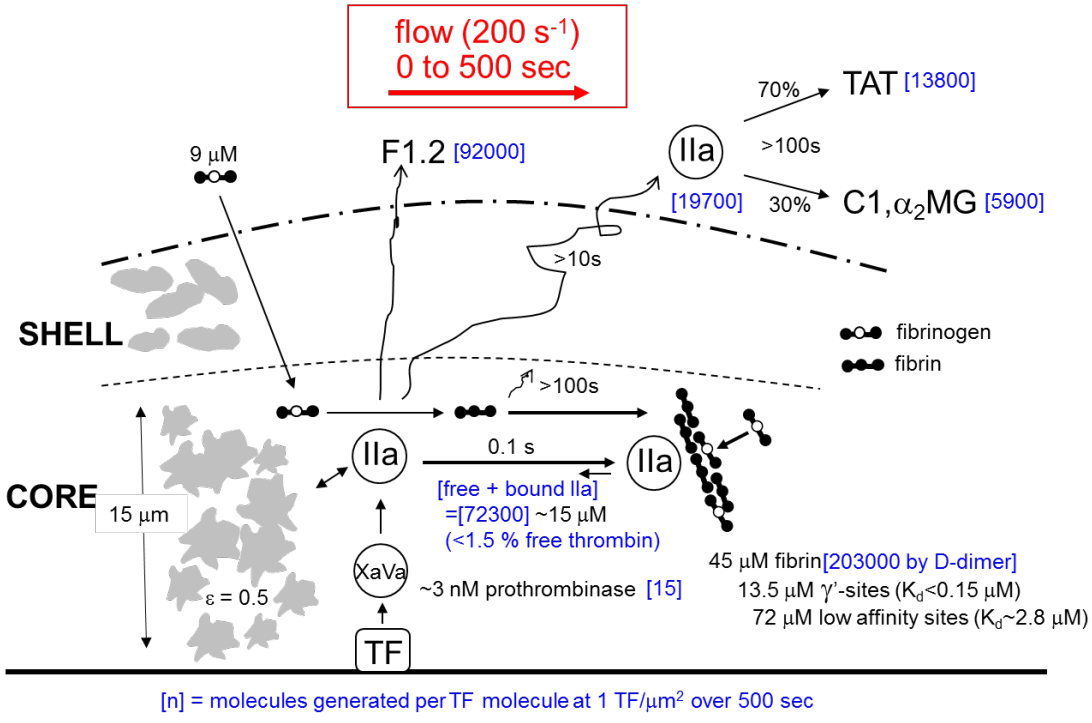

Figure 2-5. Transient mass balance for production in the thrombus core over 500 sec
Transient mass balance for production in the thrombus core (15 μm thick, porosity~0.5) of thrombin and fibrin over 500 sec of venous thrombosis on collagen/tissue factor. Over 500 sec, the copy number [*blue*] per unit area of 1-μm^2 (at 1 TF/μm^2) in a pore volume of 7.5 μm^3 was calculated for total thrombin generation (based upon F1.2 assay), amount of thrombin escape in the presence of

fibrin (based upon TAT assay), deposited fibrin (based upon D-dimer assay), and active prothrombinase (based upon known kinetic constants).

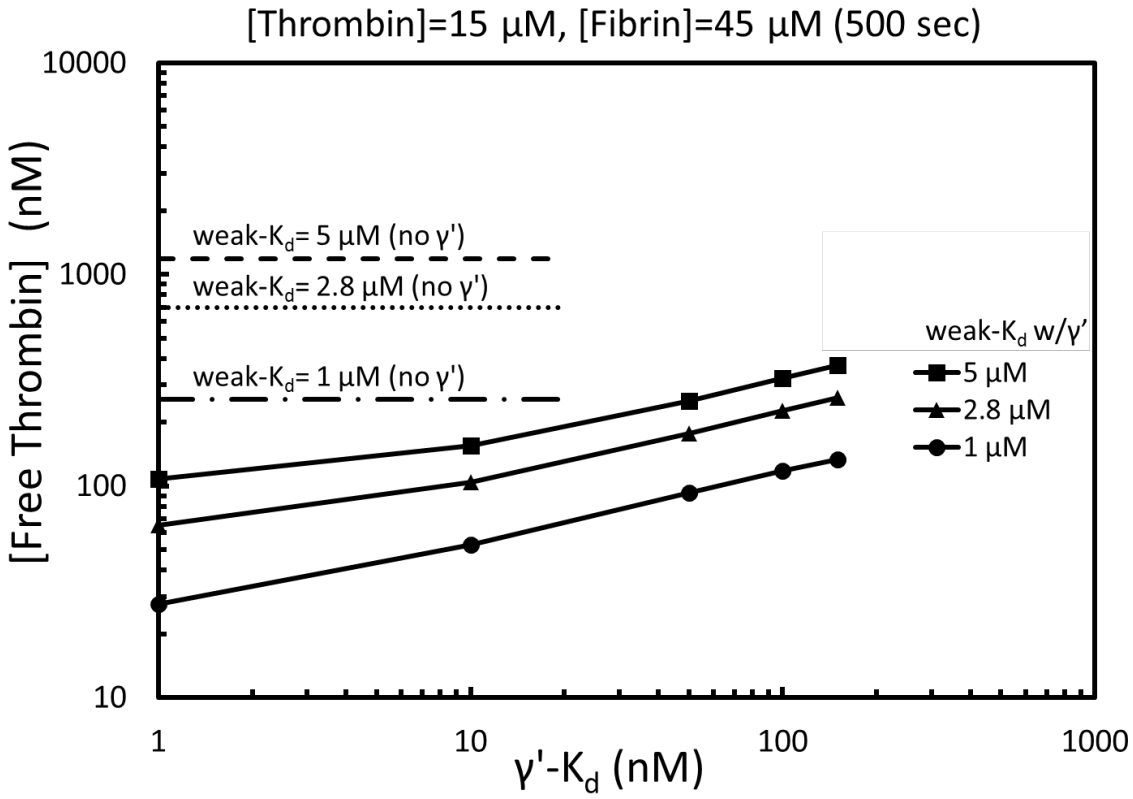

Figure 2-6. Calculation of free thrombin within the clot assuming equilibrium
Calculation of free thrombin within the pore volume of the thrombus core at 500 sec based upon a total thrombin concentration of 15 μM and total fibrin concentration of 45 μM. The free thrombin concentration is shown for weak sites (E-domain) only with K_d of 2.8, 5 μM (*dotted lines*) or for weak sites in combination with the γ'-site with the γ'-K_d varied from 1 to 200 nM *(solid lines* for weak K_d of 1 μM (*circle*), 2.8 μM (*triangle*), or 5 μM (*square*). The weak and γ'-site concentrations were calculated to be 72 μM and 13.5 μM, respectively, following [18].

Using known kinetic constants [35], we calculated that ~15 molecules of active prothrombinase (Xa/Va) per μm^2 were produced over the first 500 seconds of clotting in order to generate 92000 molecules of thrombin (*See* **Supplement Method**). For a core height of δ=15 μm and porosity ε=0.5, the platelet volume of the core (7.5 μm^3) over 1 μm^2 contains approximately the equivalent volume of a single platelet (~10 μm^3). By 500 sec, there were ~15 active prothrombinase complexes per platelet. Based on the half-lives of

FXa and prothrombinase, it is likely that ~10^2 molecules of Xa, Xa/Va, inhibited-Xa, and inhibited-Xa/Va were made per platelet over the 500 sec distal of 1 molecule of TF. Interestingly, the effective concentration of 1 molecule of TF per 7.5 μm^3 pore volume in the core corresponds to a relatively high TF concentration of 220 pM.

2.1.4 Discussion

Blood clotting on a procoagulant surface under flow involves hundreds of reactions within activating platelets and the coagulating plasma. The autocatalytic nature of coagulation is remarkable, with a single molecule of TF found to generate 92,000 molecules of thrombin over a 500-sec clotting window. This generation of thrombin was first measured [13] using TAT assay in the absence of fibrin using GPRP. We now confirm this measurement using F1.2 assay as a gold standard for the first measurement of thrombin generation in the presence of fibrin polymerization under flow conditions. Clearly, fresh prothrombin can enter the clot. Using the D-dimer assay, the first measurement of intrathrombus fibrin concentration revealed that fresh fibrinogen substrate can also continually enter the clot and be converted to fibrin monomer and incorporated into fibrin. While the binding of thrombin into fibrin has been studied in the literature[36], the conditions of a thrombus formed under flow are unique relative to those found in a tube of clotting blood or plasma. Clearly γ'-fibrin can bind endogeneously produced thrombin to a significant extent (**Figure 2-2** and **Figure 2-3**). The intrathrombus concentration of fibrin is quite high (5-10X), relative to fibrinogen levels in plasma. While fibrin bound thrombin is active against small peptide substrates and protected against antithrombin, fibrin-bound thrombin has relatively little activity against fibrinogen (*see* [37,38] showing only ~1-10% conversion of fibrinogen over 30 min by fibrin-bound thrombin). Clot-bound thrombin may also have some potential role in wound healing.

Unique to a thrombus formed under flow, free thrombin was predicted to have a very short half-life due to fibrin binding and a low fibrin generating yield of only a few fibrin monomers per thrombin molecule. Prior computer simulations of TF-activated PRP clotting in a tube have considered combined production of thrombin and fibrin [22]. However, most flow simulations predict thrombin to elute from the clot followed by a slower inhibition by antithrombin [23–25] with little consideration of γ'-fibrin binding of thrombin. In this flow assay, the addition of high dose heparin (4 units/mL) was found to ablate fibrin formation, indicating that the FXa-ATIII, FXa/Va-ATIII, and thrombin-ATIII reactions can be catalyzed to out-compete fibrin monomer generation by thrombin. For example, heparin is known to accelerate ATIII inhibition of thrombin by >1000-fold [39] and FXa/Va by 4800-fold [40]. The data presented in **Figure 2-4** should allow improved validation of simulations that seek to predict dynamic concentrations of prothrombinase (FXa/FVa), intrathrombus thrombin, and fibrin polymerization, as well as FXIa-mediated pathways that occur between 500 and 800 sec of clotting.

In this transient mass balance, we sought to account for all the thrombin molecules and fibrin monomers that are generated on a surface over time. It is a transient mass balance because the system is never at steady state (eg. the thrombin flux increases with time in **Figure 2-4A**). We used various proxies including TAT, F1.2, FPA, and D-dimer to obtain a consistent view that: (1) F1.2 and FPA leave the clot even when fibrin is made, (2) almost all the thrombin in the clot is captured by the deposited fibrin via tight binding with γ'-fibrin, and (3) thrombin is short lived within the clot due to the antithrombin-I activity of fibrin. While the role of γ'-fibrinogen in arterial thrombosis is less established, it is increasingly clear that low levels of γ'-fibrinogen are a risk factor for venous thrombosis [41,42]. Using human blood, we have observed previously that γ'-fibrin has an important role in limiting clot growth under venous flow conditions [11]. In future work on clotting

under venous and arterial flow conditions, the effects of low and high γ'-fibrinogen levels on thrombin production, fibrin production, fibrin/thrombin ratio, and clot growth rate may prove clinically relevant, particularly in acute phase response states where γ'-fibrinogen levels can change [3].

2.2 Reduced model to predict thrombin and fibrin generation during thrombosis on collagen/tissue factor under venous flow: Roles of γ'-Fibrin and Factor XI

2.2.1 Introduction

The reaction network and kinetics of human blood clotting impact diseases such as coronary thrombosis, stroke, deep vein thrombosis, hemophilia, disseminated intravascular coagulopathy (DIC), and traumatic bleeding. Numerous therapeutics are designed to either inhibit or catalyze reactions of the coagulation cascade. Despite decades of study, new reaction modulators (eg. platelet polyphoshate [43] and reaction pathways (eg. direct conversion of FVIIIa by TF/FVIIa/Xa [44]) are still being discovered. In some cases, the significance of a particular reaction studied in a purified system may be difficult to resolve since pM-levels of factors formed transiently in whole blood are challenging to measure directly.

Excluding platelet metabolism other than the availability of anionic phospholipid, isotropic kinetic models of plasma coagulation in a closed system can include 50 to 100 reactions, 1 to 3 kinetic rate coefficients per reaction, and about 10 initial conditions for zymogen or cofactor concentrations [21,22,45]. Fortunately, these large ODE models can be parameterized and solved with minor computational expense. In these models, a trigger at t=0 is required such as 1 to 10 pM tissue factor (TF) along with 1% of FVII being in a cleaved yet zymogen-like state as free FVIIa. Alternatively, if no TF is present, a source term for FXIIa generation or non-zero levels of cleaved factors is required to drive clotting [22]. In closed systems, the concentration of substrates and products can undergo $>10^3$-fold changes as clotting proceeds non-linearly through initiation, propagation/amplification, and exhaustion (inhibition and substrate consumption). Calibrated automated thrombinography (CAT) assay reports these dynamics for platelet-poor or platelet-rich plasma with typical time lags of 3.1 and 8.1 min, peak thrombin levels of 458 and 118 nM at 10 min, and reaction completion by 25 min [46].

As clotting progresses, the *extrinsic tenase/IXase* (TF/FVIIa) converts FX to FXa and FIX to FIXa. Along with conversion of activated cofactors FVIIIa and FVa, the *intrinsic tenase* (FIXa/FVIIIa) dramatically amplifies production of FXa, while *prothrombinase* (FXa/FVa) generates thrombin (releasing fragment F1.2). Thrombin cleaves platelet PAR-1 and PAR-4 and converts fibrinogen to fibrin monomer by release of fibrinopeptides A and B (FPA/B). The reaction of thrombin and antithrombin to form thrombin-antithrombin (TAT) is relatively slow (~1 min) unless catalyzed by heparin. Fibrin monomers associate into protofibrils that laterally aggregate into bundles. Thrombin also activates FXIIIa, a transglutaminase that crosslinks fibrin. Plasmin-mediated fibrinolysis of crosslinked fibrin releases various fibrin degradation products (FDP) including D-dimer. These reactions can be studied in closed systems, ± fluid mixing and ± spatial gradients. To mimic thrombosis at a specific wall location (an open system), blood treated with the FXIIa inhibitor corn trypsin inhibitor (CTI) can be perfused over a defined thrombotic surface containing TF. Clotting on a surface under flow includes mathematically complex physical phenomenon such as platelet margination to the wall [47], convective/diffusive transport, concentration boundary layers, pressure-driven permeation, and moving boundaries [20,48]. Solving large sets of partial differential equations (PDEs) for coagulation species transport and reaction is expensive and non-trivial [49]. Generally, enzyme-substrate interactions at the single molecule level are considered unaffected by macroscopic flow forces.

Fibrin has 'antithrombin-I activity' via thrombin binding to the low affinity site in the E domain and the high affinity site in the D-domain of the alternative splice variant, γ'-fibrin(ogen). The γ'-fibrinogen splice variant represents about 6-8% of total γ-chains, with γA/γ' heterodimer representing 12-16% of total fibrinogen [1]. γ′ fibrinogen level is associated with cardiovascular disease [2]. During thrombosis under flow, thrombin co-

localizes on fibrin [50,51]. A recent observation is that little thrombin (detected as TAT) leaks out of a growing clot unless fibrin polymerization is inhibited with Gly-Pro-Arg-Pro (GPRP) [52]. By immunoassays for TAT and F1.2 (± fibrin inhibitor, GPRP) and D-dimer (post-plasmin treatment), the dynamics of thrombin and fibrin generation have only recently been measured for flow of human whole blood over defined collagen/TF surfaces [50].

To our knowledge, no model has calculated intrathrombus thrombin generation and fibrin polymerization under flow conditions where fibrin is being formed dynamically and local thrombin is reversibly binding fibrin through the weak (E-domain) and strong binding sites (γ'-variant). We present a reduced model where key assumptions are supported by direct experiment measurements. This reduced model deploys a thin film assumption for the clot core (thickness ~ 15 microns) where zymogen levels in the clot are set to be identical to those in the flowing plasma. This assumption did not hold for fibrinogen transport, which is not surprising given that fibrinogen (340 kDa) is considerably larger than the other coagulation factors. For a set of prevailing plasma concentrations for Factors FVIIa, FIX, FX, FXI, prothrombin, fibrinogen as well as initial surface $[TF]_o$, the reduced model makes quantitatively accurate predictions of thrombin and fibrin levels under venous flow conditions. Fibrin appears to allow for explosive but feedback-inhibited production of thrombin. After a clotting episode, the large amount of fibrin-bound thrombin was predicted to take a few hours to elute into the circulation to form TAT. This reduced model may be particularly useful for multiscale simulations of thrombosis over vessel length scales of mm to cm.

2.2.2 Methods

A reduced kinetic model of coagulation under flow was formulated to include extrinsic tenase/FIXase activity, intrinsic tenase activity, prothrombinase activity, feedback activation of FXIa by thrombin, fibrin generation, and thrombin binding to fibrin(**Figure 2-7**) using measured Michaelis-Menton kinetic parameters (**Table 2-1**). The reduced model employs various physical and biochemical features of clotting under flow that are supported by experimental measurement:

#	Reactions	Enzyme	$[S]_0$	k_{cat} (s^{-1})	K_m (μM)	α (s^{-1})	η	Ref.
1	$X \xrightarrow{TF^*} Xa$	TF/VIIa	X_0=0.17 μM	1.15	0.24	0.46	1	[35]
2	$IX \xrightarrow{TF^*} IXa$	TF/VIIa	IX_0=0.09 μM	1.8	0.42	0.32	1	[22]
3	$X \xrightarrow{IXa} Xa$	IXa/VIIIa	X_0=0.17 μM	8.2	0.082	5.42	1	[22]
4	$II \xrightarrow{Xa} IIa$	Xa/Va	II_0=1.4 μM	30	0.3	24.7	0.18	[22,35,53]
5	$\alpha - fbg \xrightarrow{IIa} desA - Fn1 + FPA$	IIa	α-fbg_0=18 μM	80	6.5	5.88	0.05	[22,54]
6	$XI \xrightarrow{IIa} XIa$	IIa/p*	XI_0=31 nM	$1.3x10^{-4}$	0.05	$4.98x10^{-5}$	0.36	[22]
7	$IX \xrightarrow{XIa} IXa$	XIa/p*	IX_0=0.09 μM	0.21	0.2	0.065	1	[22,36]
	thrombin binding to fibrin			**K_d (μM)**	**k_f ($\mu M^{-1}s^{-1}$)**	**k_f (s^{-1})**		
1	$IIa + E\ site \leftrightarrow IIa \cdot E\ site$			2.8	100	280		[18]
2	$IIa + \gamma\ site \leftrightarrow IIa \cdot \gamma\ site$			0.1	100	10		[18]

Table 2-1. Reactions and kinetic parameters used in the ODEs model.
Simplified clotting reactions neglecting limits in activated cofactor generation, plasma zymogen concentrations, and kinetic parameters of coagulation where η is the effectiveness factor (actual rate with transport limits/theoretical maximum rate). For each reaction, $\alpha_o = k_{cat}\,[S]_o/(K_m+[S]_o)$. Reversible binding of thrombin to the weak and strong site in fibrin was treated as kinetically-controlled, reversible adsorption.

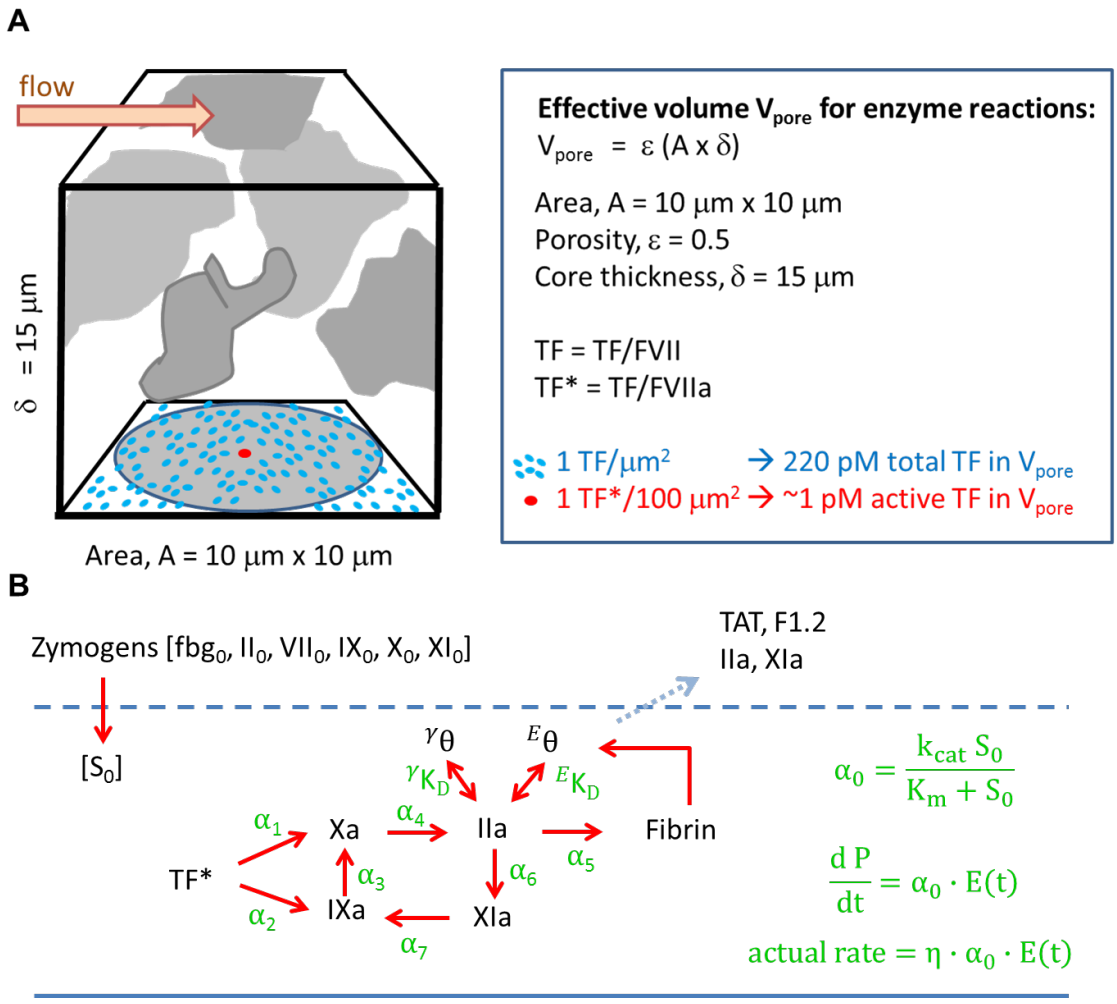

Figure 2-7. Schematic of the simplified ODEs model.
The concentration of active TF* is defined as TF/FVIIa which is homogenized over the porous core volume V_{pore} (A). All zymogens were assumed to enter the clot core by diffusion to maintain their plasma level $[S]_o$. All active enzymes had a 1-minute half-life, with TF* set to 3 min (since FVIIa generation was ignored). Free thrombin and FXIa eluted by diffusion from the core with a 2-sec half-life. The thrombin core thickness was set to 15-μm, with 50% of platelets by vol. Only the activated proteases are shown for simplicity.

Core thickness. The porosity used in the model is an estimate of the spatially averaged porosity over the entire 250 um x 250 um clotting region of the microfluidic assay, recognizing that this averages over both platelet/fibrin dense regions surrounded by fibrin dense regions. It is expected that the lower porosity decreases the effective diffusion of thrombin.

Substrate delivery. Substrate concentrations in the clot core are considered to be constant at plasma levels (S_o). Thus, the Michaelis-Menton reactions to generate product [P] become linearized with respect to [E, enzyme] as $dP/dt = [k_{cat} (S_o/(K_m+S_o))] \bullet E(t) = \alpha \bullet [E(t)]$ (**Table 2-1**). For species without diffusion limitations, the effectiveness factor $\eta = 1$ (actual rate/ideal rate without diffusion limits). If a species experience transport limits, then $\eta < 1$ and $dP/dt = \eta \bullet \alpha \bullet [E(t)]$. This approach is supported by direct measurements of TAT, F1.2, FPA, and D-dimer that indicate local clot associated product levels (thrombin and fibrin) are in excess of plasma levels (prothrombin and fibrinogen) demonstrating continual substrate delivery into the core of the clot [50].

Product escape from the clot core. Just as substrates can enter the core, free thrombin and FXIa were considered to escape the clot. The escape time was set to the measured half-life of 2 sec for albumin within the clot core [55] where $k_{elute} = \ln(2)/2$ sec. This half-life in the thin-film for product escape = $k_{elute} \bullet [E]$ is conceptually and mathematically similar to the use of a mass transfer coefficient k_c with units of 1/time as defined in [23].

Although the binding characteristics of F1.2 to fibrin are unknown, we hypothesize that the observation that fibrin suppresses F1.2 elution may be consistent with fibrin inhibiting the thrombin-feedback pathway involving FXIa which in turn results in less prothrombin conversion. The small Fragment F1.2 was considered to leak out of the clot core as fast as thrombin was generated in the core. For TAT, 70% of the thrombin eluted from the clot was considered complexed with antithrombin with the remaining 30% of eluted thrombin complexed with other inhibitors [50]. Based upon all thrombin and F1.2 begin generated in the pore space V_{pore} of the clot core (**Figure 2-7A**), the flux J-F1.2 and the flux J-TAT leaving the clot were calculated as:

$$\text{Flux, J-F1.2(t)} = \eta_4 \bullet \alpha_4 [Xa(t)] (V_{pore}/\text{area}) = \eta_4 \bullet \alpha_4 [Xa(t)] \delta \qquad \text{Eqn. 1}$$

$$\text{Flux, J-TAT(t)} = 0.7 \bullet k_{elute} [IIa(t)] (V_{pore}/\text{area}) = 0.7 \bullet k_{elute} [IIa(t)] \delta \qquad \text{Eqn. 2}$$

Cofactors not rate limiting. For healthy non-hemophilic blood, the generation of cofactors (FVa, FVIIIa) was treated as non-rate limiting. Thus, the intrinsic tenase FIXa/FVIIIa = "FIXa", and prothrombinase FXa/Va = "FXa".The availability of FIXa and FXa (not FVa or FVIIIa) controlled the enzymatic cleavage of their substrates according to the reactions parameterized in Table 1.

Initial surface concentration. FVII and FVIIa in plasma were assumed to instantaneously equilibrate with surface TF such that [TF*] = TF/FVIIa = 1 % of $[TF]_0$ where $[TF]_0$ = 1 molecule/μm^2 set experimentally. No additional TF* was allowed to be generated in the model, equivalent to the quenching dynamics via platelet coverage invoked by Kuharsky and Fogelson. [23].

Order of 1-minute enzyme half-lives. The inhibition mechanisms of coagulation proteases via TFPI, ATIII, C1-inhibitor and α_2-macroglobulin are complex and diverse and not fully resolved. Inhibition was treated uniformly to be a pseudo-first order reaction. Enzyme half-lives were set to be on the order of 1-min for FXa, FIXa, FXIa, FIIa (and 3 min for TF* since FVIIa generation was neglected). In other words, inhibition was clearly not as rapid as 0.1 min and clearly not as slow as 10 min. Thus, k_i = ln(2) /60s as a first approximation.

Thrombin adsorption to fibrin. Reversible thrombin binding to the weak E-domain site ($^{E}K_D$= 2.8 μM) and the strong γ'-site ($^{\gamma}K_D$ = 0.1 μM) was consider to have diffusion-limited association (k_f = 100 μM^{-1} s^{-1}). Fibrin-bound thrombin was considered to

be fully resistant to inhibition. All fibrin monomer generated in the clot core was assumed to be fully incorporated into fibrin.

The delivery of plasma zymogens and platelets to the surface of a growing clot would be even faster at arterial flow conditions, however the increased shear forces tend to enhance platelet removal. Unfortunately, it is difficult to measure eluted FPA, F1.2, or TAT under arterial conditions due to their 10-20X greater dilution in the exit flow stream compared to the venous measurement [52]. Importantly, arterial syndromes tend to be drugged with anti-platelet agents, not anticoagulants.

For the reaction topology shown in Fig. 1, these assumptions result in a reduced clotting model with only 8 ODEs for 6 reactive species undergoing 7 reactions (**Table 2-1**) and 2 fibrin sites for reversible binding of thrombin. These 8 ODEs were solved in Matlab R2016b using the ODE sovler *ode15s.*

ODE 1. $$\frac{d\,TF^*}{dt} = -k_{i,TF} \cdot TF^* \;\; for\; k_{i,TF} = \ln(2)/180s$$

ODE 2. $$\frac{d\,Xa}{dt} = \alpha_1 \cdot TF^* + \alpha_3 \cdot IXa - k_i \cdot Xa$$

ODE 3. $$\frac{d\,IXa}{dt} = \alpha_2 \cdot TF^* + \alpha_7 \cdot XIa - k_i \cdot IXa$$

ODE 4. $$\frac{d\,XIa}{dt} = \eta_6 \;\cdot\; \alpha_6 \cdot IIa - k_{elute} \cdot XIa \; - k_i \cdot XIa \;\; for\; \eta_6 = 0.23$$

ODE 5. $$\frac{d\,Fibrin}{dt} = \eta_5 \;\cdot\; \alpha_5 \cdot IIa \quad for\; \eta_5 = 0.05$$

where : $^{E}\theta_{total} = (1.6) \cdot \text{fibrin}$ and $^{\gamma}\theta_{total} = (0.3) \cdot \text{fibrin}$

ODE 6. $\frac{d\,IIa}{dt} = \eta_4 \cdot \alpha_4 \cdot Xa - \left(\frac{d\,{}^{E}S}{dt} + \frac{d\,{}^{\gamma}S}{dt}\right) - k_{elute} \cdot IIa - k_i \cdot IIa \quad for\ \eta_4 = 0.25$

ODE 7. $\frac{d\,{}^{E}S}{dt} = {}^{E}\mathrm{k}_f \cdot IIa \cdot ({}^{E}\theta_{total} - {}^{E}S) - {}^{E}\mathrm{k}_r \cdot {}^{E}S$

ODE 8. $\frac{d\,{}^{\gamma}S}{dt} = {}^{\gamma}\mathrm{k}_f \cdot IIa \cdot ({}^{\gamma}\theta_{total} - {}^{\gamma}S) - {}^{\gamma}\mathrm{k}_r \cdot {}^{\gamma}S$

This reduced model for blood clotting on a collagen/TF surface under flow uses 19 parameters, only 3 of which were adjusted to fit the experimental data:

7 kinetic coefficients (α_i) based on measured kinetics and plasma zymogen levels (**Table 2-1**)

1 initial surface TF* level based on specified $[TF]_o$=1 TF/μm^2 and [FVIIa]/[FVII] = 0.01.

3 binding parameters: ${}^{E}K_D$, ${}^{\gamma}K_D$, k_f

2 known stoichiometric coefficients: 1.6 E-sites/monomer, 0.3 γ'-sites/monomer

1 elution rate: k_{elute} = ln(2)/2s for free species of thrombin and FXIa

2 inhibition rates: k_i = ln(2)/60s for FXa, FIXa, FXIa, FIIa; $k_{i,TF}$=ln(2)/180s for TF*

3 effectiveness factors (η_4, η_5, η_6) ≠ 1, adjusted to fit experimental data.

Diffusion of thrombin from fibrin layer into a flow field

For simulations of thrombin equilibrated to fibrin (no thrombin generation) followed by desorption-controlled elution of thrombin, a full PDE simulation was solved for a 2D rectangular domain (1000 μm long x 60 μm high) representing a channel of the microfluidic device [50]. At a location 150 μm downstream of the entrance, a porous fibrin reaction

zone (250-μm long x 15-μm high) was defined as the clot core, with fibrin concentration set by D-dimer ELISA experiment. A thrombin flux was imposed along the bottom plate to allow thrombin diffusion through the fibrin (in the presence of two binding sites (1.6 $^{E}\theta$-sites per fibrin monomer; 0.3 $^{\gamma}\theta$–sites per fibrin monomer) with binding kinetic parameters given **Table 2-1**. COMSOL was used to solve the convection-diffusion-reaction equation for thrombin transport in two steps. First, the Free and Porous Media Flow module was first solved with a Stationary study step to get the velocity field (u). Second, the mass transport was solved by the Transport of Diluted Species in Porous Media (thrombin) coupled with General Form PDE for weak and tight thrombin binding was solved with a time-varying time-step, with a relative tolerance of 0.0001.

The thrombin binding by fibrin was described by the following equations:

$$\frac{\partial C_{IIa}}{\partial t} = -\nabla \cdot (-D\nabla C_{IIa}) - u \cdot \nabla C_{IIa} - \frac{\partial {}^{E}S}{\partial t} - \frac{\partial {}^{\gamma}S}{\partial t}$$

$$\frac{\partial {}^{E}S}{\partial t} = {}^{E}k_f \cdot C_{IIa}({}^{E}\theta_{total} - {}^{E}S) - {}^{E}k_r \cdot {}^{E}S$$

$$\frac{\partial {}^{\gamma}S}{\partial t} = {}^{\gamma}k_f \cdot C_{IIa}\left({}^{\gamma}\theta_{total} - {}^{\gamma}S\right) - {}^{\gamma}k_r \cdot {}^{\gamma}S$$

2.2.3 Results

Thrombin and fibrin production for blood flow over 250-μm collagen/TF

For perfusion of CTI-treated whole blood across a 250-μm long patch of collagen/TF (1 molecule-TF/μm^2), platelets rapidly accumulate and create a sheltered reaction environment triggered by TF for production of thrombin and fibrin [52,56]. The effluent can be sampled and subjected to immunoassays to determine the measured species flux for a 250-long x 250 μm-wide patch of collagen/TF for TAT and F1.2, in the presence and absence of fibrin assembly (± GPRP) (**Figure 2-8A, C**). The dynamic accumulation of fluorescent fibrin in the experiment was converted to a fibrin concentration by end-point immunoassay of D-dimer, post-plasmin treatment (**Figure 2-8E**). For the 7 reaction rate coefficients (α_1- α_7) (**Figure 2-7B, Table 2-1**), only 3 rates required adjustment ($\eta_4,\ \eta_5,\ \eta_6$) from their literature values in order to simulate thrombin and F1.2 elution and fibrin polymerization in the presence and absence of GPRP. The adjustments for prothrombinase activity ($\eta_4 = 0.18$) and thrombin activation of FXIa were modest ($\eta_6 = 0.36$) and could involve either transport rate limits or just as possible the difference of the reaction in the whole blood milieu in comparison to dilute buffer conditions used in enzyme studies. The adjustment in thrombin mediated activation of fibrinogen was markedly pronounced, requiring a 20-fold reduction in the rate ($\eta_5 = 0.05$). This 20-fold reduction in rate corresponds either to a ~80-fold increase in K_m (unlikely) or an 80-fold decrease in the intraclot level of fibrinogen substrate relative to plasma levels. In the experimental measurement, the generation of fibrin per thrombin molecule was unexpectedly low, given the known speed of FPA release by thrombin (k_{cat} = 80 s^{-1}). In considering the value η_5 as an effectiveness factor (actual rate/ideal rate in the absence

of transport limits), the penetration of fibrinogen (340 kDa) into the dense fibrin-rich core of the clot is hypothesized, and required in the model to be diffusion-limited.

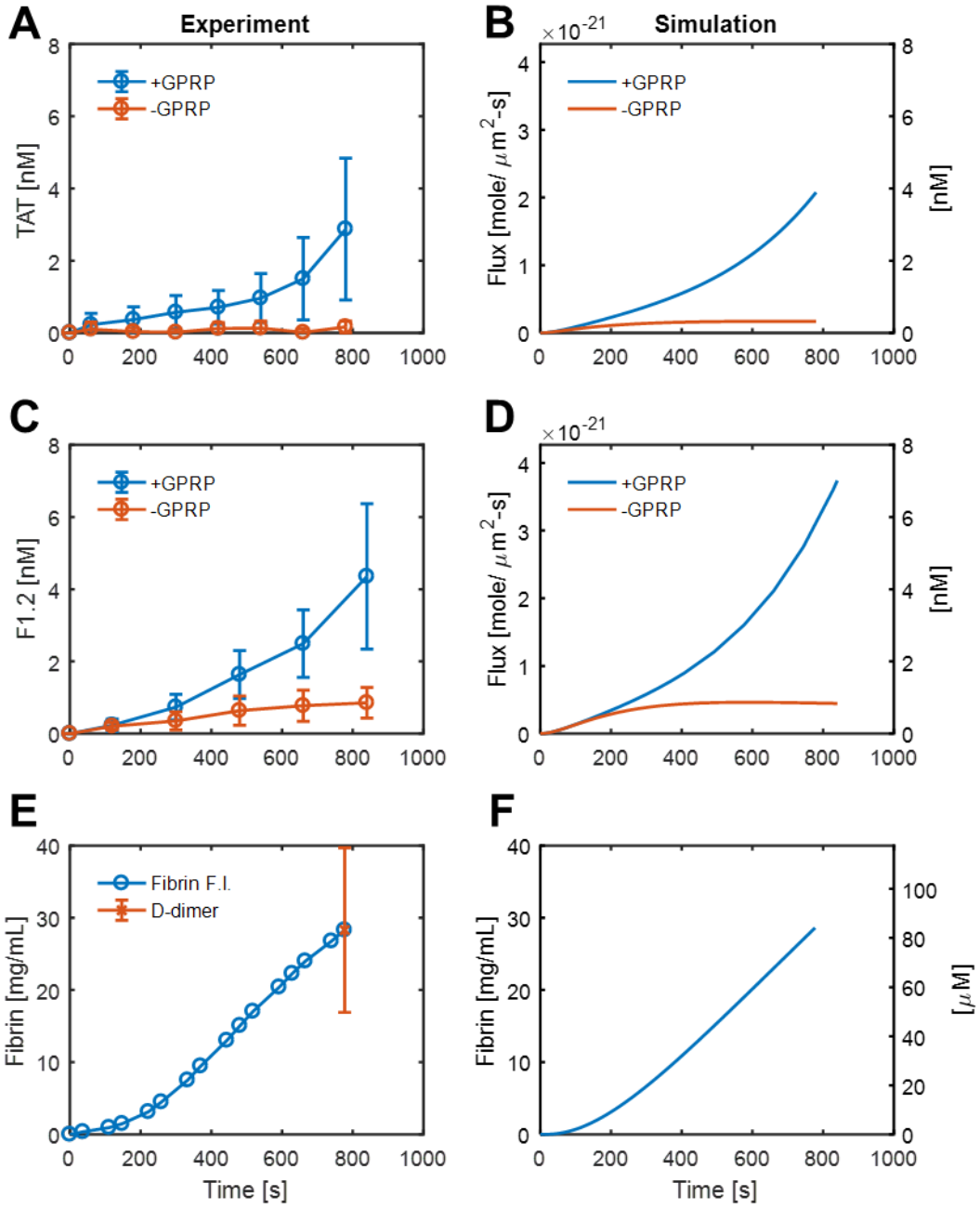

Figure 2-8. Comparison of experiment and simulation for TAT, F1.2, and fibrin dynamics. Thrombin-antithrombin (TAT) and Fragment F1.2 elution from clots in the presence or absence of fibrin (± GPRP) for experimental perfusion of whole blood over collagen/TF (A,C) and in simulations under identical conditions (B, D). Fibrin was measured dynamically by fluorescent fibrinogen incorporation and then calibrated by end-point D-dimer assay following plasmin degradation (E), while the intrathrombus fibrin concentration was simulated (F).

The model clearly predicts that thrombin has difficulty eluting from the fibrin due to fibrin binding (**Figure 2-8A-B**). Once fibrin is prevented from forming in the simulation or binding thrombin (α_5=0 or setting K_D>10 M) or the experiment (+GPRP), the TAT flux increases linearly with time for the first 500s and then increases even faster from 500 to 800s. As thrombin is generated, a small fragment F1.2 is released as a result of the prothrombinase activity. In both experiment and simulation, F1.2 elutes from the clot even in the presence of fibrin (**Figure 2-8C-D**). Additionally, more F1.2 is made than TAT, since thrombin can be inhibited by other inhibitors such as C1 and α_2-macroglobulin; the simulation accounts for this (Note the value of 0.7 in Eqn. 1 for J-F1.2). With GPRP to eliminate fibrin's antithrombin-I activity and facilitate FXIa-mediated feedback pathway, more F1.2 is detected both in the experiment and in the simulation (**Figure 2-8C-D**). Under flow conditions, fibrin reached a concentration that was 10-fold greater than plasma fibrinogen concentration (3 mg/mL, 9 μM) (**Figure 2-8E**).

Dynamics of intrinsic tenase and prothrombinase

The dynamics of intrinsic tenase generation, prothrombinase production, and thrombin binding to fibrin were explored in the model under various conditions. In the model, intrinsic tenase ("IXa" = FIXa/FVIIIa) reaches a level of 30 pM by 200 sec. By turning off thrombin-feedback activation of FXIa (setting α_6 = α_7 = 0), the model demonstrates that most of the intrinsic tenase is generated in the first 200 sec is from tissue factor (**curve *c*, Figure 2-9A**) while after 500 sec, most of the intrinsic tenase is a result of the feedback activation of FXIa by thrombin as seen in curve *b* = (*a* – *c)* (**Figure 2-9A**). FXIa reaches a level of only 5 pM in the simulation (**dashed line, Figure 2-9A**) demonstrating how potent FXIa can be for FIXa production and thrombin production. Similarly, the intrinsic tenase can be turned off (i.e. severe hemophilia) by setting α_2 = α_3

= 0 such that all of the prothrombinase is the direct result of the extrinsic tenase (**Figure 2-9B**). In this case, very little prothrombinase is generated, as expected for extreme hemophilia A/B. The role of FXIa in prothrombinase generation can be seen, especially after 500 sec, where most of the prothrombinase is a downstream result of the generation FXIa (**Figure 2-9B**). In the simulation, little thrombin is made when the extrinsic tenase/FIXase (TF*) cannot generate FIXa (α_2=0), again consistent with the circumstances of severe hemophilia. As expected from the dynamics for prothrombinase, the majority of thrombin made at times >500 sec was the result of thrombin-feedback activation of FXIa (**Figure 2-9C**). Thrombin reached 18 μM-levels after 800 sec of clotting with almost all of it bound to the weak (E-domain) and strong (γ') site and about only 1% of the thrombin (~100 nM) existing as a free species (**Figure 2-9D**). By 800 sec of clotting, the full effect of cascade amplification is seen in that an initial surface concentration of $[TF]_o$ = 1 molecule-TF/μm^2 (2.2 pM TF/VIIa = TF* in the core) results in the generation of 30 pM intrinsic tenase, ~15 μM prothrombinase, ~18 μM thrombin (100 nM free thrombin), and ~90 μM fibrin (30 mg/mL).

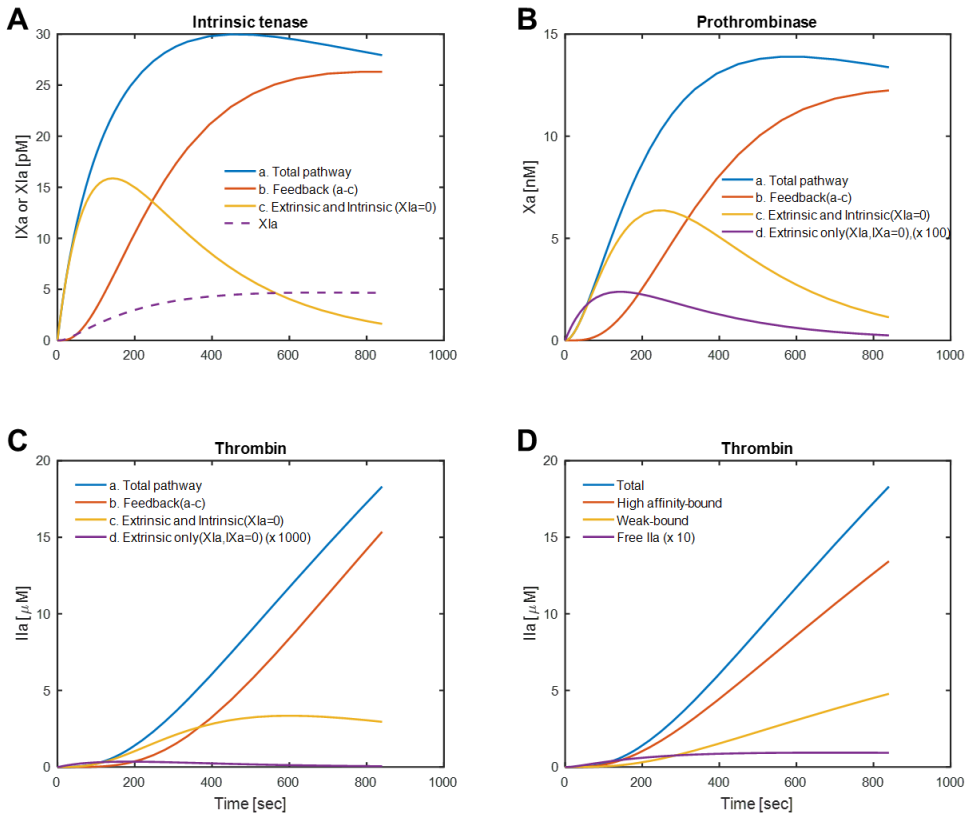

Figure 2-9. Concentration of the procoagulants predicted by the ODEs model.
The concentration of FIXa (ie the intrinsic tenase, FIXa/FVIIIa) generated by all pathways (a,blue), in the absence of feedback with FXIa=0 (c, orange) and by the FXIa-feedback pathway (b, red) calculated via a-c. (A). FXIa is shown as dashed-line. The concentration of FXa (ie. Prothrombinase, FXa/FVa) generated by various pathways (B) demonstrating that only a minor fraction of FXa is derived from TF/VIIa in the simulation. The concentration of thombin generated via various pathways (C). The majority of intrathrombin thrombin is bound to the γ'-site in fibrin with <100 nM as free thrombin (D).

Role of γ' fibrinogen level

The range of γ' fibrinogen concentrations can vary in healthy individuals [57], with a reference range of 0.088 to 0.551 mg/mL. Additionally, fibrinogen is an acute response gene and the fraction of splice variant can change. The concentration of γ' fibrinogen concentrations and the γ' fibrinogen/total fibrinogen ratio have been reported to be relevant in thrombosis, and different in different stages of disease, potentially with some protectant

effect in venous thrombosis [41]. In the simulation, we varied the γ' fibrinogen concentration to explore the effect on the co-regulation of fibrin and free thrombin concentration. With more γ' fibrinogen, there was slightly more high-affinity sites for thrombin, therefore, sequestering more thrombin and decreasing the fibrin and free thrombin concentration (**Figure 2-10A-B**). In contrast, a 50% reduction in $\gamma\theta$ caused a slight increase in the level of free thrombin and the amount of fibrin made. However, the effect of γ'-fibrinogen levels were not particularly marked, a reasonable result given the excess fibrin that is formed relative to thrombin, but still suggestive of a protective or regulating contribution in venous thrombosis.

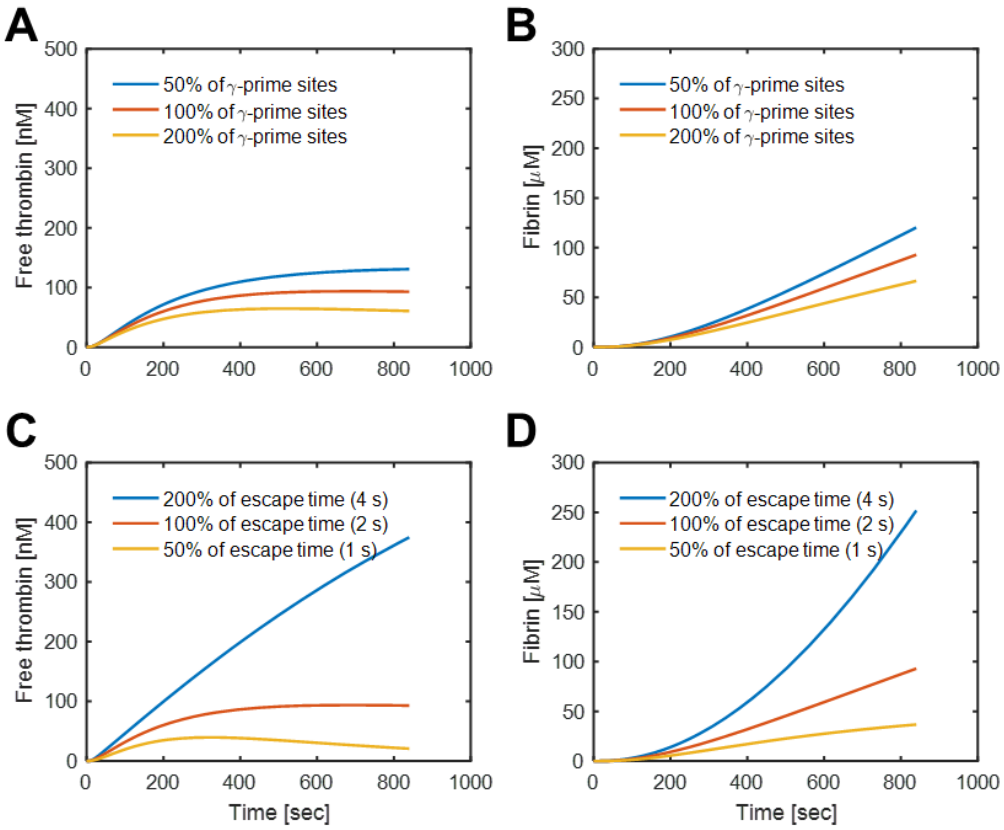

Figure 2-10. Effect of γ' site concentration and escape time on thrombin and fibrin. The thrombin (A) and fibrin concentration (B) at 50%, 100%, and 200% of normal levels of γ'-fibrinogen. The thrombin (C) and fibrin concentration (D) for different diffusional escape times of free thrombin from the clot.

Protein escape time

As reported previously, platelet contraction can alter protein transport [55] with soluble proteins retained longer in the core of the clot than the less dense outshell shell. In the laser injury mouse model, albumin half-life in the clot core has been measured to be about 2 sec. In the simulation, we artificially adjusted the escape time between 1 sec and 4 sec to explore how intrathrombus diffusion influences local free thrombin and, consequently, fibrin production. A longer escape time of 4 sec resulted in dramatically higher intrathrombus concentration of fibrin and free thrombin, indicating the model was

very sensitive on escape time. The concentration of thrombin increase more than 3-fold with a doubled escape time to 4 sec (**Figure 2-10C-D**).

Convection-diffusion simulation of thrombin loading and elution from fibrin

To simulate dynamic concentrations of intrathrombus thrombin in the core, the velocity field and convective-diffusive transport of thrombin was calculated by COMSOL (**Figure 2-11A-B**). The empirically measured flux of thrombin $J_{IIa}(t)|_{Y=0}$ (via F1.2 ELISA) was set at the bottom boundary condition of the core region. The empirically measured time-varying fibrin concentration fibrin(t) (calibrated by end-point D-dimer ELISA) was set uniformly in the core region. The concentration of $^{E}\theta$ and $^{\gamma}\theta$ sites were to 1.6x fibrin(t) and 0.3x fibrin(t), respectively. After 800 sec, the thrombin flux entering the domain was set to zero in order to explore long term thrombin elution from the clot. The time-averaged flux into and out of the clot outlet (**Figure 2-11C-D**) revealed that >90% of the thrombin was captured by the fibrin, via both sites. By 500 sec, the concentration of intrathrombus thrombin was only 61 nM, only about 1% of total thrombin (5.5 μM) in the clot (**Figure 2-11C-D**), indicating that the literature K_D values for binding were consistent with actual

independent measurements of TAT elution. The transient concentrations of total thrombin, intrathrombus free thrombin, and bound thrombin to each site, are shown in **Figure 2-11E**. After 800 sec, the thrombin flux from the bottom plate was set to zero and the thrombin in the clot was allowed to be eluted by diffusion under prevailing flow conditions. The binding of thrombin by fibrin was sufficiently strong under a venous shear rate with an apparent half-life in the clot of 1.1 hour (**Figure 2-11F**). Thrombin eluted slowly into the flow field, relative to its half-life in the presence of antithrombin, such that its concentration would not be expected to perturb the hemostatic balance in the circulation.

Thus, circulation levels of TAT can accumulate over hours and be measured in patients, even when ~90% of the thrombin made in the first 800 sec is fibrin bound.

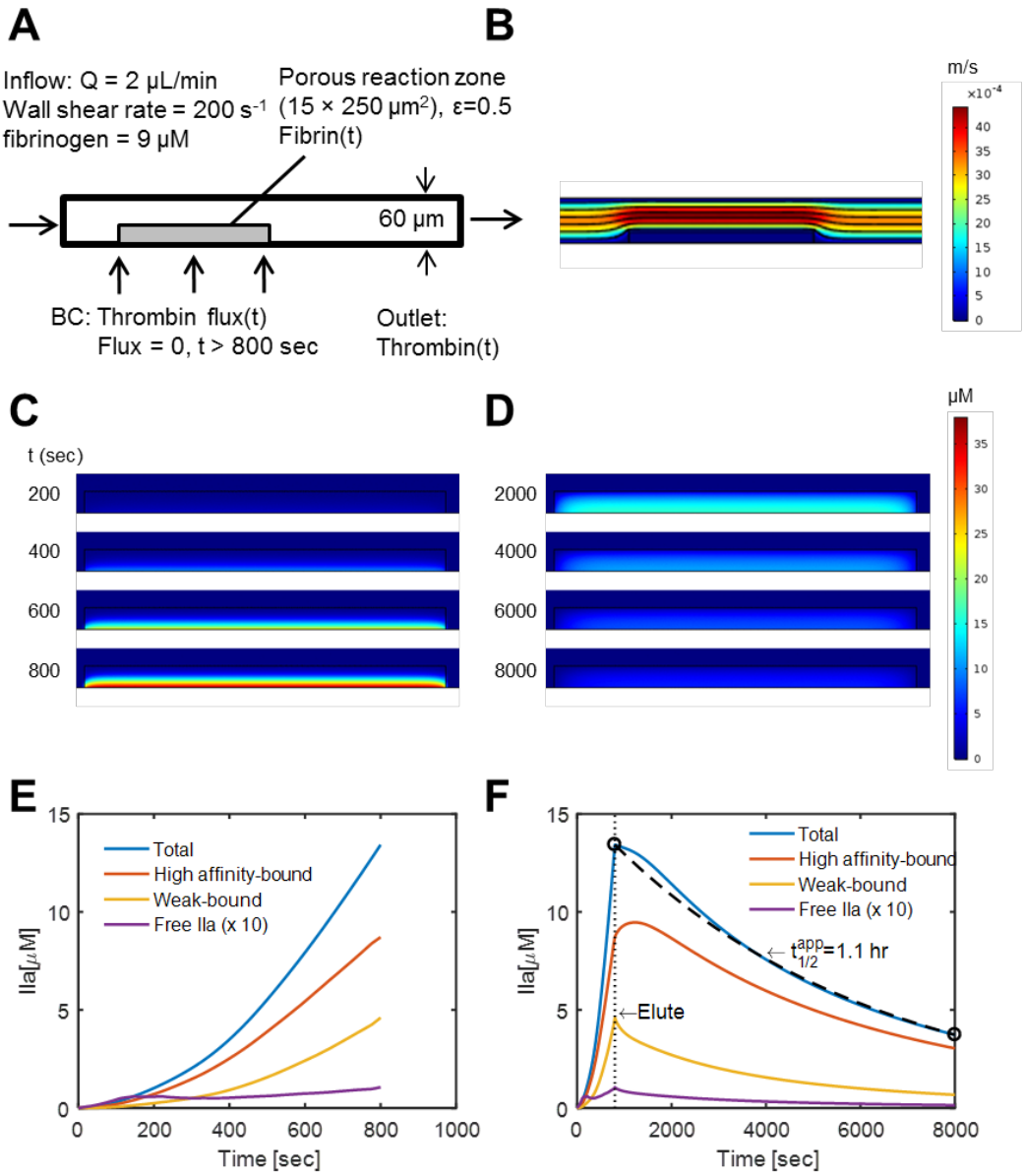

Figure 2-11. Transient convection-diffusion of thrombin into and out of a fibrin domain exposed to venous flow.
The 2D simulation domain and imposed boundary conditions (A) allowed determination of the velocity field (B) and the intrathrombin thrombin transport dynamics over time (C, D). The average concentration of total, free, and bound thrombin in the clot domain are shown for imposed thrombin flux and fibrin concentrations (E). After 800 sec, no fresh thrombin was delivered into the clot and the elution of thrombin from the clot domain was followed (F).

2.2.4 Discussion

By assuming plasma zymogens can enter a thin clot at a rate significantly greater than their consumption, a highly reduced and essentially linearized ODE model provided a reaction topology suitable for accurate prediction of blood clotting on collagen/TF under venous flow. The thin film assumption was first formalized in Kuharsky-Fogelson model [23] to generate a large systems of ODEs describing clotting under flow. With the well mixed, thin film approximation, we were able to simplify clotting under flow to 8 ODEs and 19 parameters. A total of 16 parameters were from literature and only 3 were adjusted in order to fit the measured TAT and F1.2 and fibrin generation data (± GPRP). Of the 3 adjustable parameters, only the rate of fibrinogen activation by thrombin appeared to be strongly diffusion-limited ($\eta_5 = 0.05$). This result was not particularly surprising given the enormous size of fibrinogen in comparison to the other coagulation factors. While ignoring cofactor activation of FVa and FVIIIa as non-rate limiting appeared to be compatible with predicting clotting of healthy blood, the generation of FIXa was absolutely required for robust thrombin production.

As an ODE model, the actual transport physics were mainly parameterized by the rate of free thrombin elution from the clot, guided by experimental measurements of ~2-sec half-life of flash-activated albumin in a clot subjected to flow along its outer boundary. In the presence of thrombin binding to fibrin, the elution rate of free thrombin from the clot appears to be an important regulator of clotting (**Figure 2-10C-D**). The 2-sec elution half-life for proteins was consistent with (i) in vivo mouse measurement, (ii) the human blood microfluidic measurements, and (iii) the average time it takes a protein to diffuse an average distance of 15 microns.

The roles of FXIIa in mouse thrombosis models [58] and platelet released polyphosphate to amplify thrombin-mediated feedback activation of FXIa [7] have

motivated the pharmaceutical development of FXIIa, FXIa, and polyphosphate inhibitors. In **Figure 2-9A**, FXIa reaches ~5 pM by 500 sec of clotting and the amount of thrombin generated between ~500 and 800 sec is largely FXIa-dependent (**Figure 2-9C**). This is exactly consistent with microfluidic experiments conducted with anti-FXI antibody that blocked the increase of TAT and F1.2 flux and fibrin deposition after 500 sec [7,50,52].

By calibrating the model on measured thrombin and fibrin generation rates, the simulation provides insights, based on Table 1 kinetics, into pathways proximal to thrombin. The concentrations of FIXa/FVIIIa and FXa/FVa and FXIa were particularly low and would be difficult to measure directly inside the clot under flow conditions. Over 800 sec of clotting, the model revealed "cascade amplification" from 30 pM levels of intrinsic tenase to 15 nM prothrombinase to 15 μM thrombin to 90 μM fibrin, with FXIa pathways contributing significantly after 500 sec. Interestingly, little thrombin results directly from the FXa produced by TF/FVIIa, consistent with severe hemophilic blood producing little fibrin following perfusion over TF surfaces [59].

For the thin core region within the rapidly formed platelet deposit, the kinetics of thrombin and fibrin production are largely sheltered from the prevailing flow on the outer boundary of the clot. The current model may have some applicability to core dynamics during TF-driven arterial thrombosis since the core thickness (thrombin and fibrin and P-selectin positive region) has been measured to be relatively similar between the venous (100 s^{-1}) and arterial (2000 s^{-1}) condition [60].

As a model analyzing dynamics limited to the thin, core region using ODEs, the model was not designed to predict clot growth and spatial dynamics over distances of 100s or 1000s of microns. However, the TF-dominated thrombin generation rate in the core region could be coupled to spatial models of platelet deposition and FXIa-enhanced thrombin generation. The reduced model focuses on concentration changes of thrombin

and fibrin in the thin “core” region which is only 15-microns thick. Since proteins can diffuse this short distance in ~10 sec, the well-mixed assumption of this thin region is reasonable, although not suited for predicting longer distance wave propagation such as found for clotting in stagnant plasma over millimeter distances [61–63].

The full biochemical and spatial complexity of human coagulation (typically involving >50 reactions in reality and in simulation) may relate more to the kinetic demands of hemostasis and its strong selective pressure (eg. surviving child birth), rather than to the complexities of thrombosis in older adults of modern times. The reduced model exploits the thin-film approximation under flow to emphasize a few key zymogen activation events at constant zymogen concentration. Despite its simplicity, this reduced model may have a useful implementation within more complex spatial thrombosis models that include platelet activation and accumulation [25,64].

The reduced model is not directed at describing the full progression of a thrombotic event over large spatial distances in large vessels, particularly where platelet accumulation dominates the growth process. However, this model may be very useful in establishing a surface TF-dependent thrombin flux and fibrin regulation that is a time-dependent boundary condition to a larger multi-species PDF model where platelets continue to accumulate and thrombin production transitions to platelet polyphosphate/FXIa-dependent.

Few simulations of clotting under flow include the role of anti-thrombin-I activity of fibrin or γ’-fibrinogen levels. The ratio of γ’-fibrinogen to total fibrinogen may be clinically relevant. Reduced γ’-fibrinogen levels have been associated with an increased venous thrombosis risk [15,41] Here, we demonstrated a simplified ODEs model to simulate the thrombin and fibrin generation. This reduced model may be particularly useful in

multiscale simulations that seek to account for single platelet phenomenon [65], microscopic attributes of a wound site [56], and whole vessel dynamics [25,35].

CHAPTER 3: SENSITIVITY ANALYSIS OF A REDUCED MODEL OF THROMBOSIS UNDER FLOW: ROLES OF FACTOR IX, FACTOR XI, AND γ'-FIBRIN

3.1 Introduction

Blood clotting occurs under flow conditions in many circumstances of hemostasis or intravascular thrombosis. When tissue factor is exposed to the blood the coagulation cascade is triggered, resulting in the eventual generation of thrombin and the polymerization of fibrin. The molecular events of this protease cascade are well studied and computer simulations of isotropic coagulation (TF added to plasma) typically include 20 to 60 individual parameterized reactions [21,22,45]. The complexity is increased by the presence of flow, the participation of platelets in clot growth, and various strong couplings and feedbacks [49,65,66]. Detailed models of coagulation under flow often require 20 to 50 PDEs and more than 100 parameters. Numerous reviews have discussed both continuum and particle-based numerical approaches [20]. The further goal of multiscale modeling seeks to deploy complex vascular flows with realistic models of platelet signaling and coagulation function [64,67,68], all of which is extremely demanding from a computation point of view. Reduced models offer advantages in bridging scales and in handing 3D coupled reaction-diffusion-convection problems.

For clotting isotropically in a tube or clotting under flow conditions, plasma zymogen variations can be studied by Monte Carlo simulation or with highthroughput experiment to explore sensitivity to initial condition [22]. Blood plasma contains zymogens whose concentrations can vary in the healthy population [69]. These variations impact coagulation time as was seen in a sensitivity analysis that highlighted early FVIIa participating reactions [70]. Often, the time to generate thrombin is the key parameter used in sensitivity analysis [71]. For example, using a sensitivity analysis of thin film

compartment model of clotting under flow, Leiderman et al. identified an unexpected competitive reaction involving Factor V that influenced hemophilic severity. However, these models have reaction networks that do not include the dynamics of fibrin generation and the binding of thrombin to fibrin via a weak site and a strong site. Fibrin has 'antithrombin-I activity' which includes (i) thrombin exosite I binding to the low affinity (Kd~2.8 uM site) in the E Domain, (ii) thrombin exosite II binding the high affinity site (Kd~0.1 uM) in the D-domain of the alternative splice variant, γ'-fibrin(ogen), (iii) a potential bivalent interaction, and (iv) irrerversible entrapment [72]. The γ'-fibrinogen splice variant represents about 6–8% of total γ'-chains, with γA/γ' heterodimer representing 12–16% of total fibrinogen [1].

Typically, simulating reactions under flow requires PDE models, however the thin film approach can reduce the system to ODEs that include mass transfer coefficients [24] or accommodate transport limits with effectiveness factors (η = actual rate/ideal rate) [73]. In the present study, we explored the sensitivity of an extrinsic pathway model for a 15-micron film that was previously shown to simulate fibrin formation dynamics and thrombin generation dynamics.

3.2 Materials and Methods

The reduced model supported by experimental data to predict thrombosis under flow was described in detail previously[74]. Briefly, the model simulates blood clotting under venous flow over collagen/ TF (1 TF/ μm^2) with 15-micron thick "core" region (δ = 15 μm, porosity ~0.5) supported by direct imaging. The model includes extrinsic tenase/ FIXase activity, intrinsic tenase activity, prothrombinase activity, feedback activation of FXIa by thrombin, fibrin generation, and thrombin bindings to fibrin. Thin film assumption allowed the linearization of the Michaelis-Menton kinetics from publications. The reduced model (7 rates, 2 KD, enzyme half-lives~ 1 mins) only required 3 adjustments from published values measured under static conditions to predict the elution rate of thrombin-antithrombin (TAT), fragment F1.2 with or without fibrin formation, and intrathrombus fibrin. The schematic of the reduced model is shown in **Figure 3-1A**. The experimental data of fibrin dynamics and F1.2/ TAT flux with/without fibrin formation are shown in **Figure 3-1B-D**. The effective volume for enzyme reaction and initial conditions are shown in **Chapter 2**. The simulation results compared to experimental data are shown in **Chapter 2**.

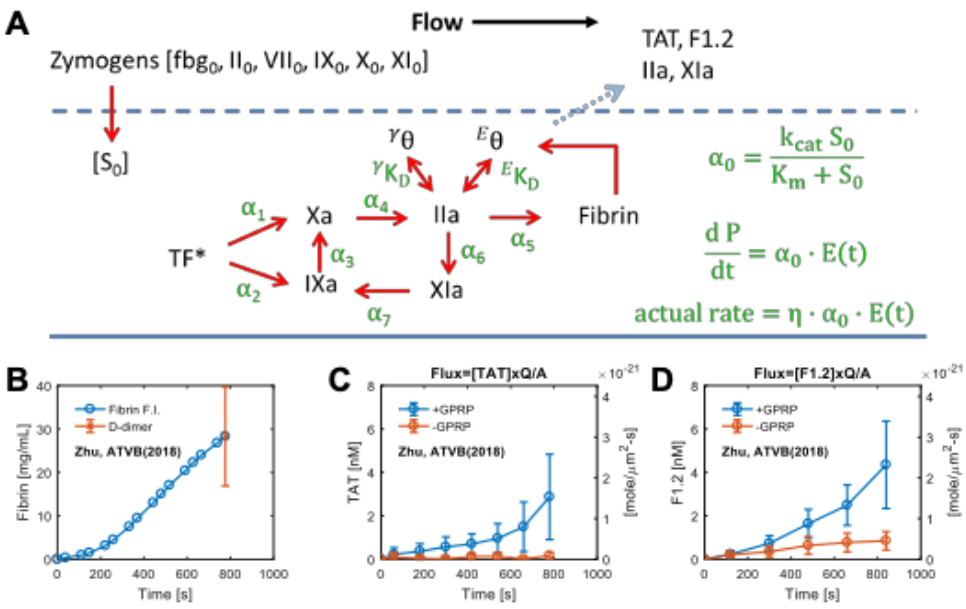

Figure 3-1. Schematic of the reduced model.
With 7 reactions, only the activated proteases are shown (A). All zymogens were assumed to enter the clot core by diffusion to maintain their plasma level $[S]_0$. All active enzymes had a 1-minute half-life, with TF* set to 3 min. Elution rate from the core was set to 2-sec half-life. The dynamic of fibrin from 8-channel device of the fibrin fluorescence intensity with the end-point concentration determined by D-dimer ELISA (B). Thrombin flux from the collagen/TF surface determined by thrombin-antithrombin complex (TAT) ELISA with and without GPRP to allow fibrin formation (C). Thrombin flux from the collagen/TF surface determined by fragment F1.2 ELISA with and without GPRP to allow fibrin formation (D).

The initial concentration of 5 plasma zymogens (FXI, FIX, FX, FII, fibrinogen) and 2 fibrin binding sites (weak sites and γ'-sites) are obtained from literature value and shown in **Table 2-1**. The results of baseline initial concentration all outputs are shown in **Supplement Figure III**, including the dynamics of FIXa, FXa, FXIa, thrombin on different sites, Fibrin, and F1.2/ TAT flux. Sensitivity analysis evaluate the effect of each variable on model predictions, and we followed a similar sensitivity analysis used by a recent study [71]. Although there is other way for sampling [70], we varied the concentration of 7 variables (5 zymogens and 2 thrombin binding sites) ± 50% described in [71]. First, we performed a local sensitivity test where the variables were changed one-at-a-time. For visualization, the change of the maximum concentration of each species over 800 sec, instead of whole dynamics, was shown with respect to a range of variant. We then

performed 10,000 Monte Carlo simulations where all the variables were sample uniformly and independently between 50-150% from their baseline concentration.

The dynamics of fibrin deposition in 8-channel devices has been used to evaluate coagulation in whole blood under flow [27,75–77]. Therefore, we marked the top 2% and bottom 2% of simulations that produced maximal and looked at the distribution of the 7 variables. To evaluate the potency of a perfect FXIa/FXI inhibitor, we can turn off the feedback pathway described in [74] by setting α_6 and α_7 (in **Table 2-1**) to zero.

3.3 Results

3.3.1 Local sensitivity analysis

By thin film assumption, we were able to simplify the perfusion of CTI-treated whole blood clotting over collagen/ tissue factor surface (250 μm, 1 TF/ μm^2). Only 3 parameters were adjusted from literature to fit the measured TAT, F1.2 and fibrin generation data (± GPRP). The reactions and kinetic parameters used in the reduced model are shown in the **Table 2-1**. With well mixed, substrate concentrations in the clot are set to be constant at plasma levels from literatures. The dynamics of the procoagulants, thrombin distribution, fibrin, flux of F1.2 and TAT predicted by the reduced model with the baseline of plasma protein levels and thrombin binding sites are shown in **Supplement Figure III**.

However, the levels of plasma zymogens and fibrin binding sites for thrombin vary within a range naturally [69]. Here, we analyze the sensitivity of the reduced model output of all species (FIXa, FXIa, FXa, thrombin on different sites, TAT/F1.2 flux and fibrin). We first used the method of changing a variant one-at-a-time to quantify the sensitivity of each output, which was used by [71]. We changed a variant one-at-a-time at a range of 50% to 150% of normal with others fixed. The local sensitivity of thrombin concentration on different sites of fibrin are shown in **Figure 3-2**. The results suggest that FIX level is the most important factor for thrombin. When FIX level is increased 50% from the baseline, total thrombin and thrombin binding on to weak sites increase by 100% and 140%, and free thrombin and thrombin on γ'-sites increase by around 75% compared to baseline. Maximum thrombin concentration is less sensitive to the variation on both thrombin binding sites. A stronger effect is seen when the γ'-sites decreases by 50%, thrombin on weak sites and free thrombin increase by 80% and 40% more. The variation leads to similar trend on procoagulants (FIXa, FXa, FXIa), and the results are shown on **Figure 3-3**. Variation in FXI has more effect on FXIa. Fibrin as the final product of the coagulation

cascade doesn't change dramatically with the variants. The fibrin concentration stays within ± 50% by varying each inputs. Lastly, there are similar effects of F1.2 and TAT flux (**Figure 3-3 E, F**), but the effect on F1.2 is stronger.

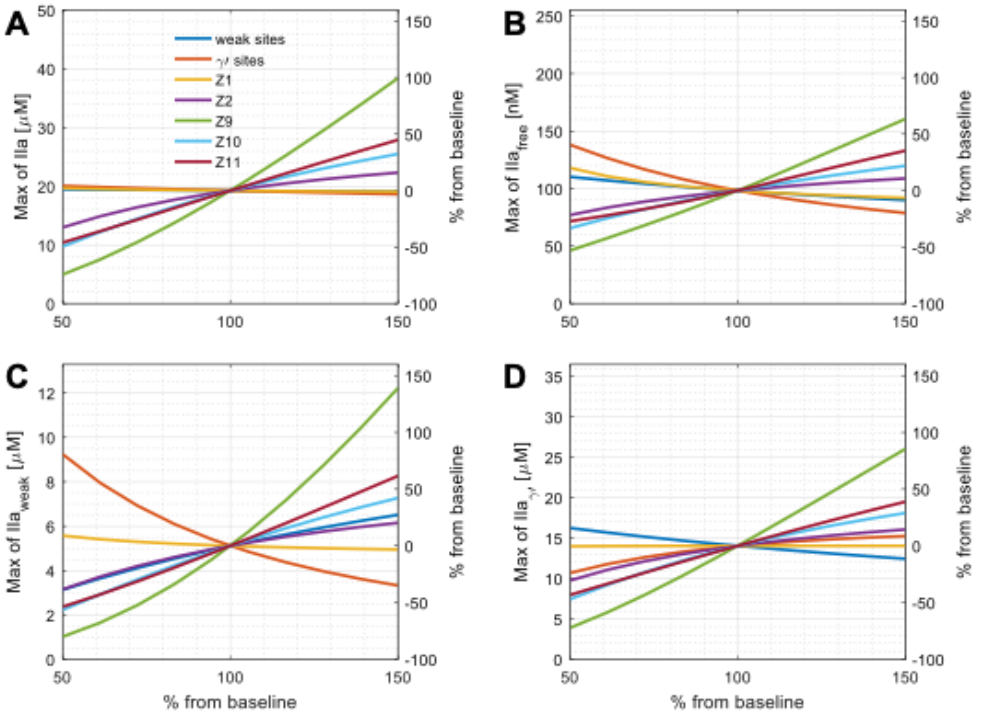

Figure 3-2. Local sensitivity analysis of total thrombin, free, and bound thrombin in the clot. The change of intrathrombus thrombin concentration on different sites due to the variation of plasma protein levels or thrombin binding sites on fibrin. The levels were changed one-at-a-time.

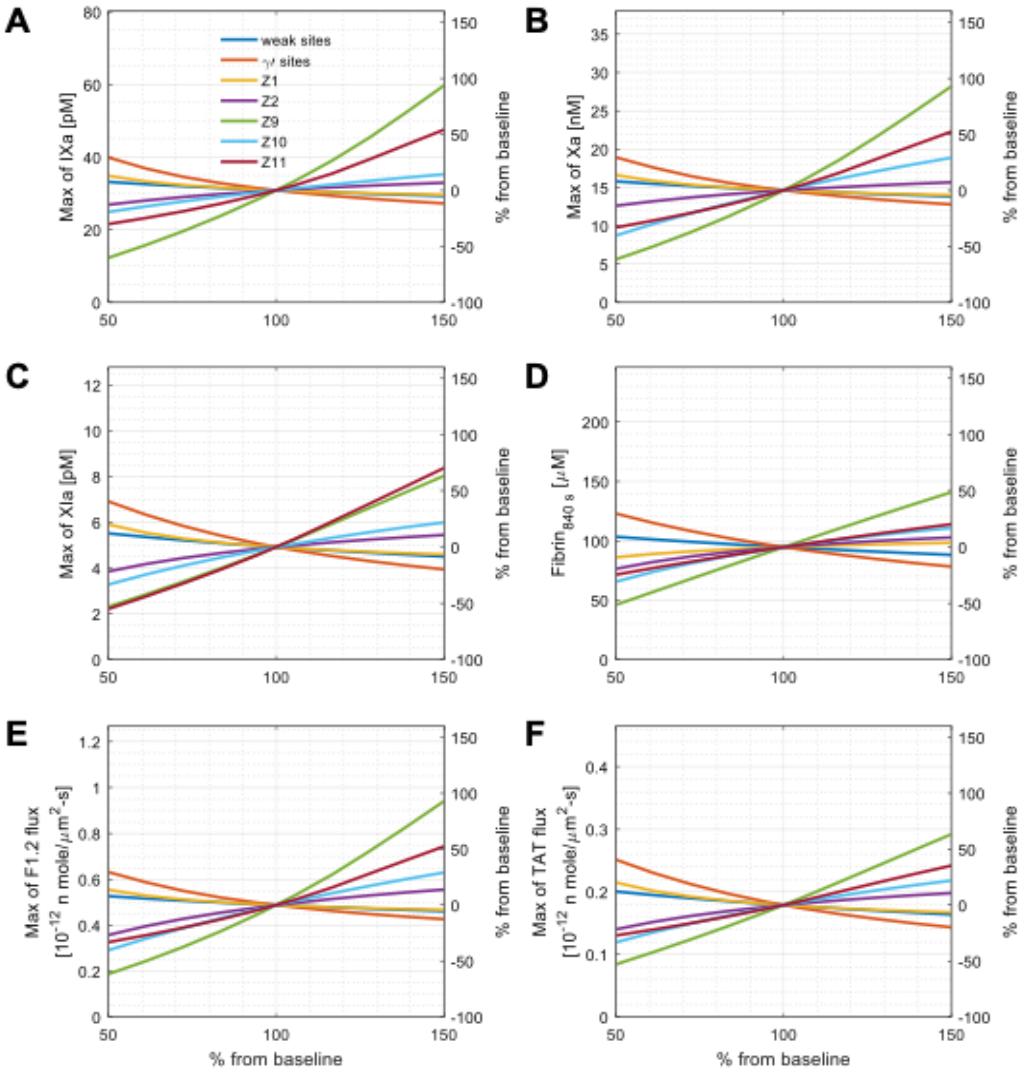

Figure 3-3. Local sensitivity analysis of procoagulants, fibrin, F1.2 flux, and TAT flux. The concentration change of FIXa (A), FXa (B), FXIa (C), fibrin (D), and flux of F1.2 (E) and TAT(F) due to the variation of plasma protein levels or thrombin binding sites on fibrin. The levels were changed one-at-a-time.

3.3.2 Global sensitivity test

To further investigate how the variants would affect the results of reduced model, a global sensitivity analysis was performed. 10,000 Monte Carlo simulations were conducted with 7 variables including the levels of 5 plasma protein and 2 thrombin binding sites. Each variable was sampled between 50 and 100% of their baseline uniformly and

independently for every simulation. The results fibrin concentration for every simulation are shown in **Figure 3-4A**. The mean, standard deviation and range are shown in **Figure 3-4B**, and the fibrin concentration distribution at 780 sec are shown in **Figure 3-4C**. The mean and standard deviation of fibrin concentration are similar to the experimental results, shown in red in **Figure 3-4A B**, where whole blood was perfused over collagen/TF surface followed by plasmin digestion and D-dimer ELISA [50]. The dynamic results and the distribution at 800 sec of thrombin and other species are shown in **Figure 3-5**. Normal range variation of 7 inputs leads to free thrombin ranging most from 20 to 300 nM. The simulation results of TAT and F1.2 Flux are shown in **Figure 3-6**, and they agree with experimental data (shown in red, [50]) of ELISA analysis of effluent.

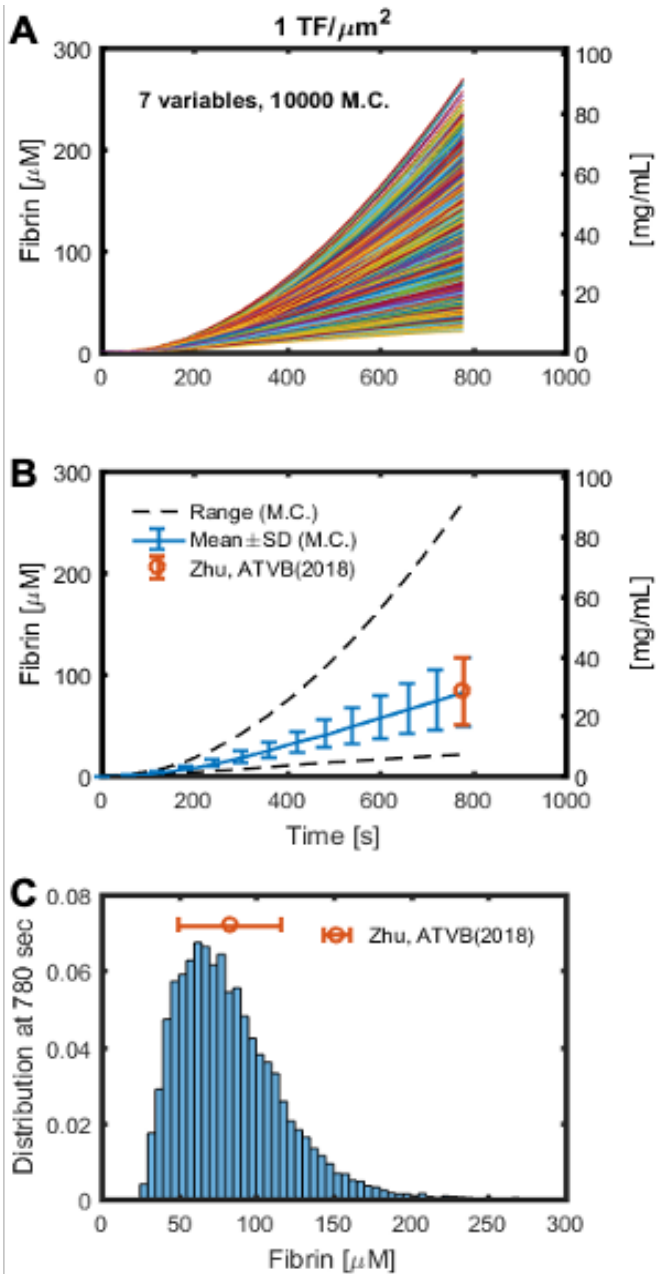

Figure 3-4. Fibrin concentration of 10,000 simulations compared to experimental data of blood clotting over collagen/ TF under venous flow rate.
Fibrin concentration of 10,000 Monte Carlo simulations of 7 variables (A). The mean, standard deviation, range (B), and the distribution (D) of the simulations, with the experimental end-point estimation of fibrin concentration from the D-dimer ELISA (shown in red). The 7 variables of plasma protein levels and thrombin binding sites were generated uniformly and independently.

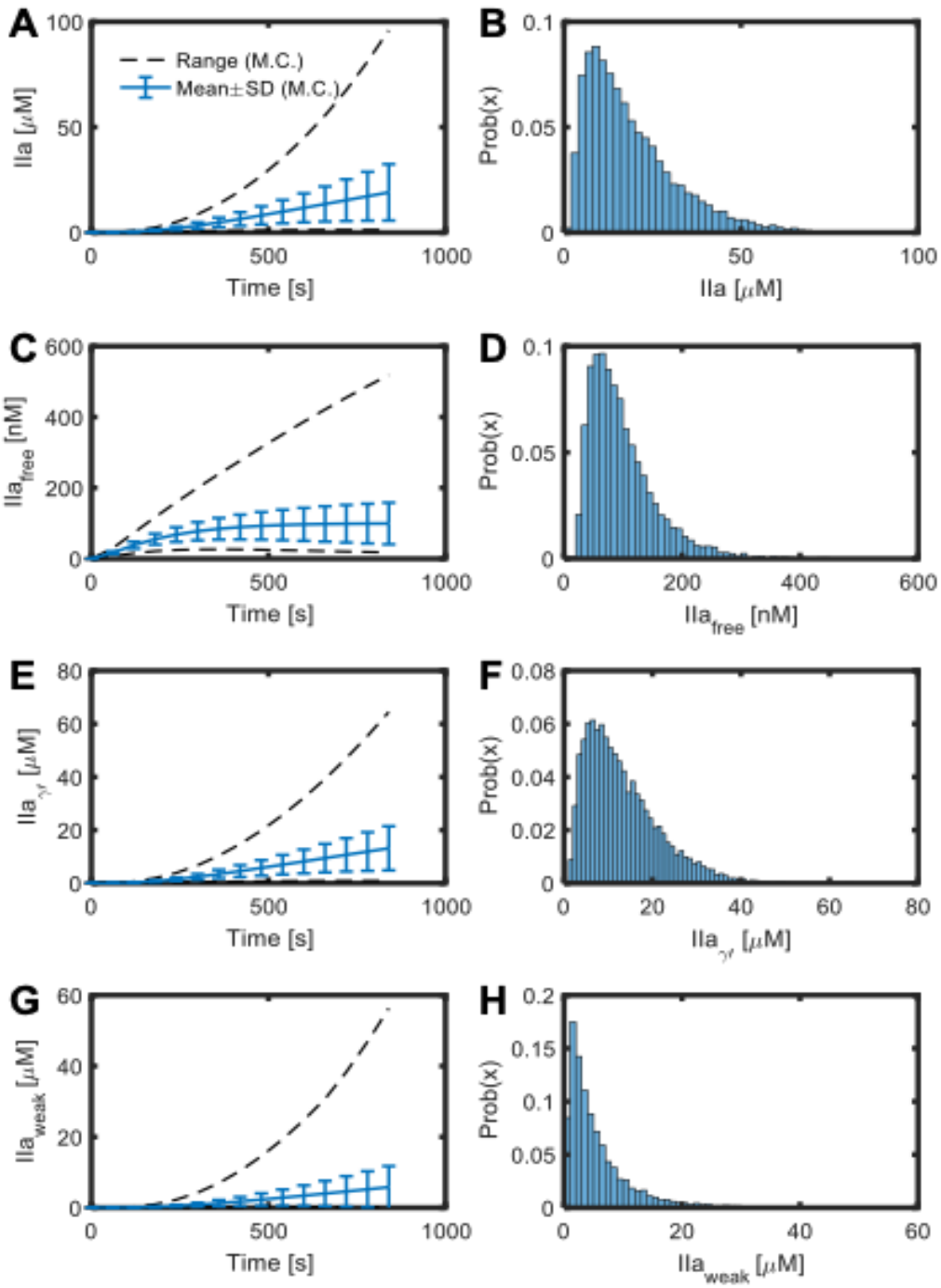

Figure 3-5. Total, free, and bound thrombin of 10,000 simulations of blood clotting over collagen/ TF under venous flow rate.
The mean, standard deviation, range (A, C, E, G) and the distribution at 800 sec (B, D, F, H) of thrombin on different sites of 10000 MC simulation varying plasma protein levels and thrombin binding sites ± 50% uniformly and independently.

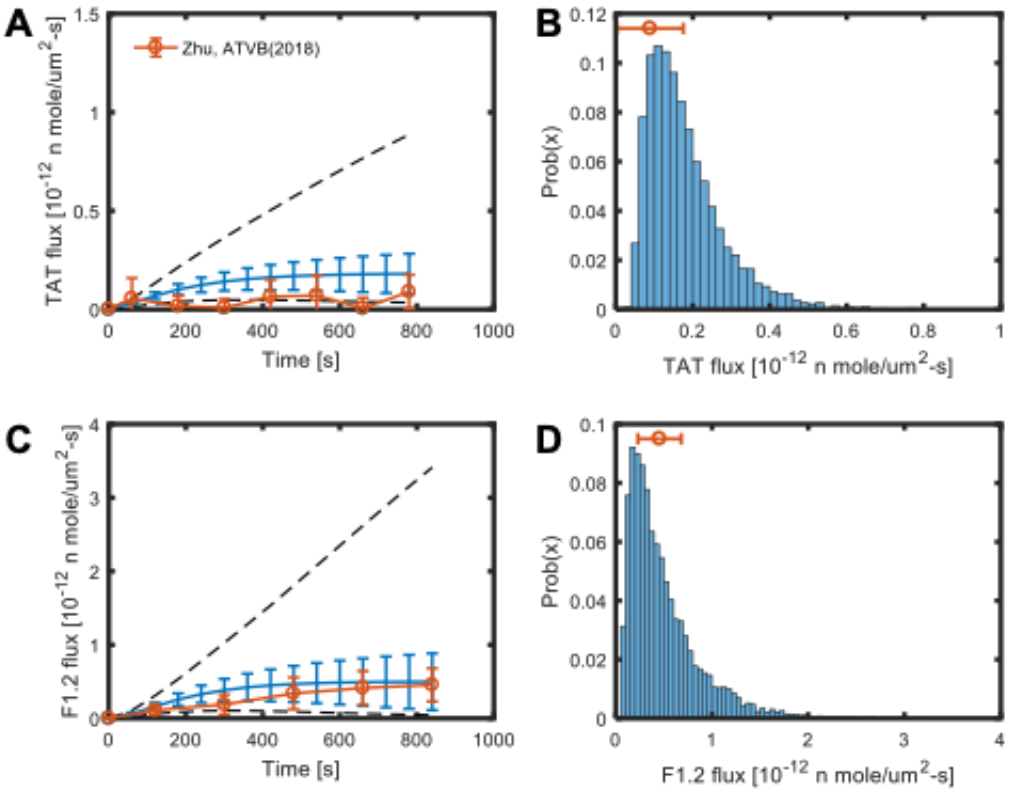

Figure 3-6. Transient convection-diffusion of thrombin into and out of a fibrin domain exposed to venous flow.
The mean, standard deviation, range (A, C) and the distribution at 800 sec (B, D) of TAT and F1.2 flux of 10000 MC simulations varying plasma protein levels and thrombin binding sites ± 50% uniformly and independently. The experimental data of blood clotting over collagen/TF from ***Zhu, ATVB(2018)*** are shown in red.

3.3.3 Conditioned inputs distribution

We performed 10,000 Monte Carlo simulations by varying 7 variables independently. We further focused on the model's result on fibrin production and marked the top and bottom 2% of the final fibrin concentration shown in **Figure 3-7A**. The distribution of the plasma protein levels and thrombin binding sites of top and bottom 2 % are shown in **Figure 3-7B-C**. By looking at the subset of top 2% of fibrin generated, the distribution of plasma FIX, FXI levels and gamma'-sites are narrower and skewed away from 100%. These suggest that the high levels of FIX and FXI and less γ'-sites are

important and lead to more fibrin, which agree to our local sensitivity analysis. For the subset of bottom 2%, low levels of FIX and FX lead to less fibrin.

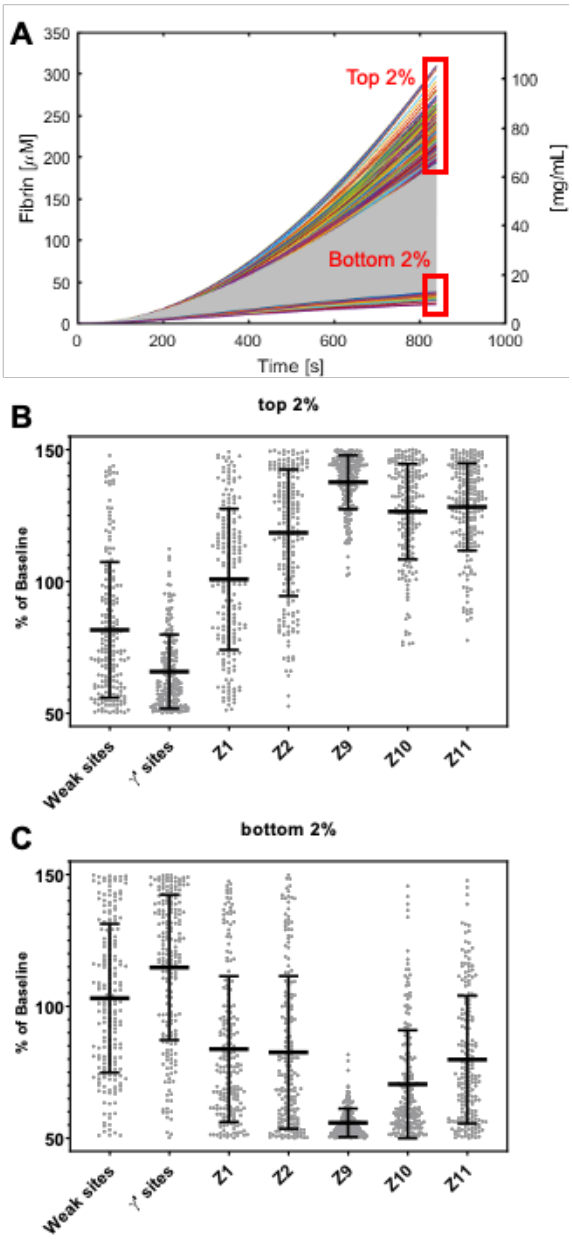

Figure 3-7 Plasma protein levels and thrombin binding sites distribution of the subsets of top and bottom 2% of fibrin concentration of 10,000 simulations.
Fibrin concentration of 10,000 Monte Carlo simulations of 7 variables varying uniformly and independently. Top 2% and bottom 2% are labeled (A). Plasma protein levels and thrombin binding sites distribution of top 2% (B) and bottom 2% of the simulations (C).

Feedback pathway has emerged as a novel target for antithrombosis with little effects on hemostasis [78]. Here we evaluated the effect of blockage of FXIa by turn off feedback pathway in our simulations. We first labeled the 2%, middle 50% and bottom 2% of the final fibrin concentration in the 10,000 simulations, and then set the FXIa to zero to see the efficacy of the inhibitor. The results are shown in **Figure 3-8**. The top 2% lead to 71% fibrin reduction by an ideal FXIa inhibitor, while the middle 50% and bottom 2% of the simulation only has 50% and 33% fibrin reduction. Here we showed that the efficacy of feedback pathway inhibitor may vary within a normal range of zymogens.

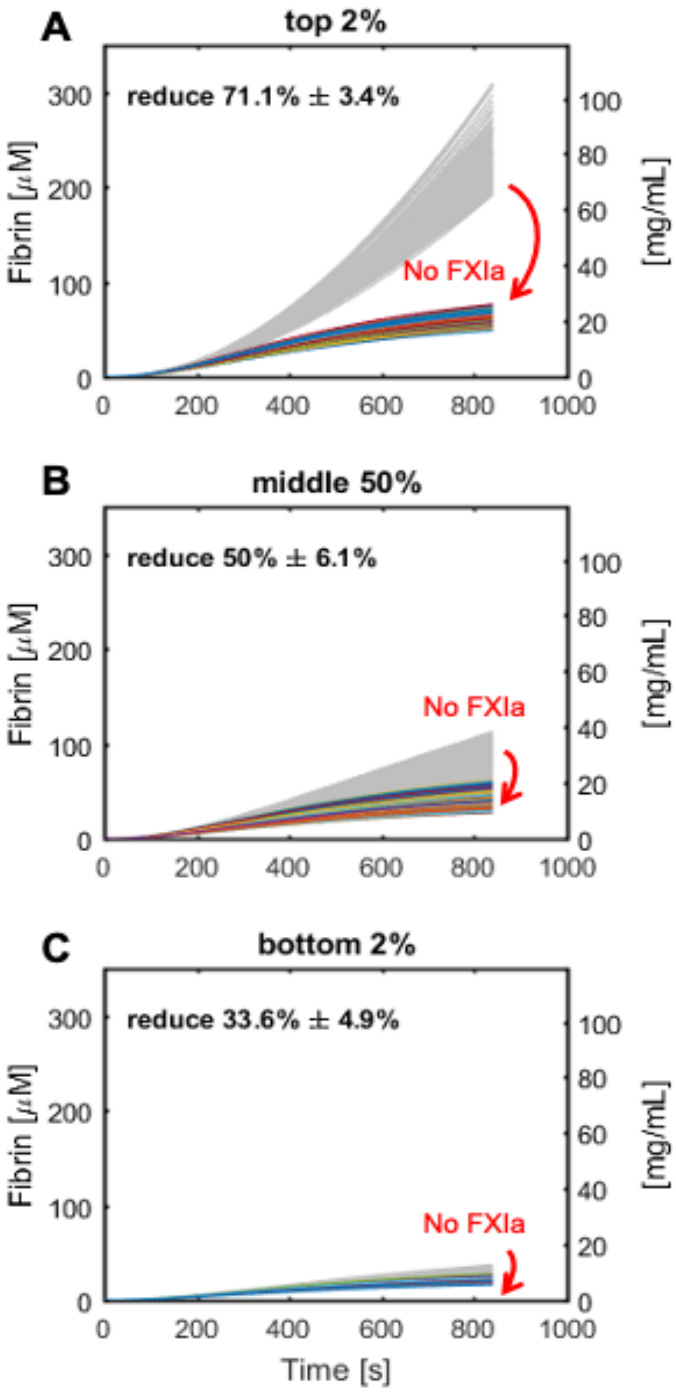

Figure 3-8. The potency of the blockage of FXIa varies over the subsets of fibrin concentration.
The effect of inhibition of FXIa on fibrin concentration of top 2% (A), middle 50% (B), and bottom 2% (C) of 10,000 simulations.

3.4 Discussion

In this study, we extended our reduced model and performed sensitivity analysis of an extrinsic pathway coagulation ODE-model under flow. We first performed the local sensitivity analysis where each of 5 plasma zymogens and 2 fibrin binding sites for thrombin is varied ±50% from their published data one-at-a-time. This indicated that the level of FIX and γ'-binding sites are the most important variables for most of the matrices. For the global sensitivity analysis, 7 variables are changed simultaneously and independently within 50-150%. With 10,000 Monte Carlo simulations, we shown the distribution of each procoagulants in the model and found that the mean and standard deviation of fibrin generation and TAT/ F1.2 flux met with the data measured from healthy donors[50,52]. We also showed that the FXIa inhibitor may have different potency across normal ranged plasma protein and thrombin binding sites, and the top 2% of the final fibrin concentration has the stronger effect of 71% fibrin reduction.

Plasma levels vary within individual in normal range [69]. Review has summarized that high levels of coagulation factor are associated with thrombosis [79]. In a large population-based, case–control study studies, Leiden Thrombophilia Study, research showed that elevated FIX [80] and FXI [81] are related to higher risk for thrombosis. Models has been developed to study the sensitivity to initial clotting factor concentration, both static [70,82] and under flow [71]. However, Link et al's model has small sensitivity to normal variation of initial clotting factors. This might be due to no fibrin cleavage reaction or thrombin binding was included and the matrices they chose (lag time, max relative rate, and final thrombin concentration). With the reduced model, we are able to identify FXI and FIX as risk factors for thrombosis.

It has been shown that thrombin binds to fibrin clot nearly irreversibly and localizes by γ'-fibrin [50]. The bindings of thrombin in the clot not only minimize downstream

coagulation, but also protects thrombin from antithrombin inhibition [18]. Studies suggested that the variant interacts with other plasma protein and influences on clot formation and strength [83,84]. Fibrinogen γ' level varies in patients, changes during inflammation and associates with arterial and venous thrombosis clinically [85]. Although the association between γ'/total fibrinogen ratio and thrombosis remain unclear and sometimes shows the opposite [42], studies suggested that decrease ratio are associated with higher risk for thrombosis [41]. Our reduced ODEs-model demonstrates that low level of γ'-fibrin is the dominant factor in top 2% fibrin generation and it increases thrombin flux and fibrin generation. These results confirm with the explanation that the antithrombin-I activity of fibrin affects coagulation and reduces thrombin and its further activation.

Simulations give insights and help experimental design for further discovery in coagulations [86]. Recently, Link et al used the computationally driven approach to identify FV as modifier for hemophilia, further confirm it with experiment, and propose a potential mechanism. Although there are limitations and our model only describe the thrombosis under venous flow over TF-surface, it emphasized crucial reactions which have been often overlooked. With emerging strategies targeting FXI [87], our results provide insights in variation in potency of the inhibitors within normal range of clotting factors. Despite of the simplicity, this reduced model may be useful for its coagulation phenotype and further implementation with multiscale modeling which includes platelet accumulation [64,65,67].

CHAPTER 4: A MICROFLUIDIC APPROACH FOR DRUG TESTING

4.1 Dual antiplatelet and anticoagulant (APAC) heparin proteoglycan mimetic with shear-dependent effects on platelet-collagen binding and thrombin generation

4.1.1 Introduction

Antithrombotic drugs are typically classified into one of three major categories: antiplatelet, anticoagulant, or fibrinolytic agents [1,2]. Common antiplatelet therapeutics include aspirin and clopidogrel which both inhibit secondary platelet agonist generation (thromboxane A2 and ADP, respectively) [88–90], as well as inhibitors of the integrin αIIb/β3 [91]. Anticoagulants are responsible for preventing thrombin generation and fibrin polymerization. Warfarin and various heparins have been used as an oral and parental anticoagulant for several decades, but recent advances have focused on specifically targeting coagulation factors, such as thrombin and factor Xa [88]. Finally, fibrinolytic or thrombolytic drugs (most notably tPA: tissue plasminogen activator) promote the generation of plasmin, an enzyme that cleaves fibrin [92].

With increasingly complex cardiovascular disease states comes a need for the administration of multiple antithrombotics with different mechanisms of action. While certain classes of drugs have the potential to function synergistically, there is an associated increased bleeding risk as the number of drugs increases [93,94]. Therefore, identifying a method for combining the antithrombotic functions of antiplatelet and anticoagulant agents into a single therapy can have a potentially great impact on the field, as uncertainty regarding optimal use remains [94].

Heparin (usually referred to as unfractionated heparin; UFH) is yet another common clinically-used antithrombotic agent which carries anticoagulant behavior through its binding and activation of antithrombin. Antithrombin then works to deactivate circulating thrombin and factor Xa to hinder the coagulation process [95]. Heparin can bind directly

to thrombin (K_d=100 nM) resulting in anticoagulant behavior [96]. Heparin is derived from mast cells which line the vascular walls usually in the same general location as tissue factor (TF). Upon tissue injury, mast cells are activated and release heparin proteoglycans (HEP-PGs) which are much higher in molecular weight than UFH [97,98]. These structures have been shown to exhibit both anticoagulant features, as does heparin typically [99], as well as specific antiplatelet properties, most notably involving the platelet-collagen interaction and subsequent aggregation and fibrin polymerization [97]. The unconventional ability for a heparin-based entity to impact collagen-dependent platelet activation could be attributed to the fact that type I collagen has binding sites for heparin, in addition to the heparin binding site to von Willebrand Factor (vWF) bridging platelets with collagen, relevant under arterial shear rates [100]. The concept of designing synthetic HEP-PG mimetics, structured with a protein core and conjugated with UFH, has been demonstrated [97,98,101,102].

Despite various results comparing the ability of HEP-PGs and UFH to inhibit collagen-mediated platelet aggregation and serotonin release under flow conditions [97], previous work with dual anticoagulant and antiplatelet (APAC) conjugates has been focused primarily on *in vitro* platelet aggregometry studies and *in vivo* vascular models [98,102]. The importance of understanding the functionality of APACs, as is the case with any novel therapy, in more pathophysiologic scenarios *in vitro* is crucial. Thus, the focus of this work was to compare the results obtained from various *in vitro* experimental techniques to gain a broader understanding for the potential therapeutic effect of synthetic HEP-PG mimetics with varying heparin conjugation levels (CL10, CL18, HICL).

4.1.2 Materials and methods

Reagents

Reagents were obtained as follows: Anti-human CD61 (BD Biosciences, San Jose, CA), Alexa Fluor® 647 conjugated human fibrinogen (Life Technologies, Waltham, MA), corn trypsin inhibitor and D-Phe-Pro-Arg-chloromethylketone (CTI and PPACK, respectively; Haematologic Technologies, Essex Junction, VT), Sigmacote® siliconizing reagent (Sigma, St. Louis, MO), Dade® Innovin® PT reagent (Siemens, Malvern, PA), collagen Type I Chrono-Par™ aggregation reagent (Chrono-log, Havertown, PA). Whole blood was drawn via venipuncture from healthy donors following University of Pennsylvania Institutional Review Board approval into a syringe loaded with 100 μM PPACK (to inhibit thrombin activity altogether for the study of platelet deposition on collagen only) or 40 μg/mL CTI (to inhibit contact pathway and measure platelet and fibrin deposition). Prior to each blood draw, donors self-reported to be free of any medications for 7 days and alcohol use for 48 hours. Additionally, female donors self-reported to not using oral contraceptives.

Three different APAC molecules were synthesized (Aplagon, Helsinki, Finland) as previously described [98,102]. In brief, dual antiplatelet and anticoagulant (APAC) conjugate comprises of protein core, where UFH chains are bound by covalent di-sulfide bridges provided by a cross-linker molecule to reach various conjugation levels (CL) of heparin.

Microfluidic assays

Microfluidic experiments were run as previously described [103]. Glass slides were treated with Sigmacote®. A volume of 5 μL of collagen was perfused through a patterning channel device (250 μm wide and 60 μm high) to create a single strip of fibrillar collagen.

Lipidated TF was then sorbed to the collagen surface by introduction of 5 μL of Dade Innovin PT reagent (20 μM stock concentration). The Dade Innovin PT reagent was incubated with the collagen for 30 min without flow and then blocked and rinsed with 20 μL of bovine serum albumin (1% BSA in Hepes-buffered saline). An 8-channel microfluidic device was vacuum-mounted perpendicularly to collagen/TF surfaces forming 8 parallel-spaced prothrombotic patches (250 x 250 μm). APAC (CL10 7.12 mg/mL; CL18 11.94 mg/mL or HICL 6.71 mg/mL in phosphate-buffered saline, PBS, 10 mM Na_2HPO_4, 0.137 M NaCl, pH 7.5) was diluted in 1% BSA for appropriate concentrations for the analysis. Vehicle (1% BSA) or APAC-treated blood was perfused across the 8 channels at an initial wall shear rate controlled by a syringe pump (Harvard PHD 2000; Harvard Apparatus, Holliston, MA). Each thrombus was formed under constant flow rate (constant Q). Platelet and/or fibrin deposition were monitored simultaneously by epifluorescence microscopy (IX81; Olympus America Inc., Center Valley, PA). Images were captured with a charged coupled device camera (Hamamatsu, Bridgewater, NJ) and were analyzed with ImageJ software (National Institutes of Health). To avoid side-wall effects, fluorescence values were taken only from the central 75% of the channel. The background-corrected fluorescence values were fitted by use of a log (inhibitor concentration) vs. response routine in GraphPad Prism 5.00 (GraphPad Software) to calculate the half-maximal inhibitory concentration (IC50).

4.1.3 Results and discussion

APAC has antiplatelet activity in the absence of thrombin under venous shear rate upon collagen

The 8-channel device, developed by Maloney et al [26], has been used to investigate platelet function and coagulation in whole blood under flow. Briefly, eight inlets of treated or untreated blood were perfused over collagen (with or without TF) while platelet and fibrin deposition can be monitored. The first aim was to determinate the antiplatelet effectiveness alone, without the influence of thrombin and fibrin. PPACK, a direct thrombin inhibitor, was added as an anticoagulant and blood was perfused over collagen at a shear rate of 200 s^{-1}. CL18 (30 μg/mL) inhibited platelet deposition (**Figure 4-1A**) at both early times (100 s) of attachment to collagen and at later times (180 to 420 s) where secondary deposition was occurring, via ADP/thromboxane enhancement [104,105]. CL18 caused a dose-dependent inhibition (IC50 = 27 μg/mL, based on endpoint fluorescence at 400 s) (**Figure 4-1B-C**). In similar tests with PPACK-treated whole blood, HICL also reduced platelet deposition (IC50 = 57 μg/mL), while CL10 had unclear effect of inhibition on platelet deposition (IC50, not determined) (**Table 4-1, Figure 4-3A**).

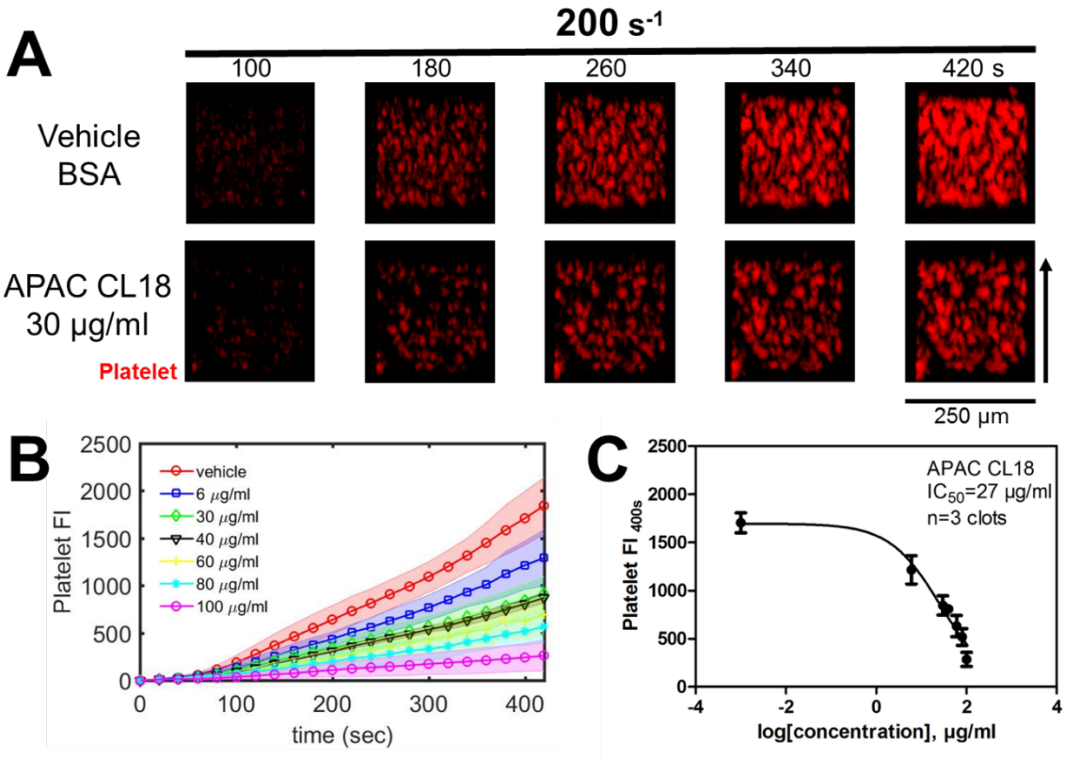

Figure 4-1. Platelet deposition is dose-dependently reduced by APAC in the absence of thrombin under 200 s^{-1} over collagen in microfluidic assay.
Vehicle (1% BSA) and APAC (CL18, 30 µg/mL) was added to PPACK-treated whole blood and perfused over collagen under venous shear rate. (A) images of platelet deposition, (B) dynamics of platelet deposition and (C) dose-response curve and IC50 (± standard deviation [SD]).

	IC_{50} (µg/ml), 200 s^{-1}		
	PPACK	High CTI	
	Platelet	Platelet	Fibrin
APAC CL10	Not determined	25	0.6
APAC CL18	27	71	5.4
APAC HICL	57	90	0.5

Table 4-1. IC50 values calculated at venous shear rate for PPACK and CTI-treated whole blood.
IC50 values were calculated for each APAC species (CL10, CL18, and HICL) under two different anticoagulated whole blood conditions (PPACK and CTI). Since PPACK inhibits all thrombin activity, APAC-driven inhibition was only observed on platelet deposition. CTI-treated whole blood enabled the calculation of IC50 for both platelet deposition and fibrin polymerization.

APAC shows both antiplatelet and anticoagulant activity under venous shear rate upon collagen/TF

High level of CTI (40 μg/ml), a FXIIa inhibitor, was used to avoid clot formation in the reservoir, which allowed the combined study of platelet deposition in the presence of thrombin/fibrin production. Blood was perfused (at 200 s^{-1}) over collagen/TF strip to initiate extrinsic pathway. HICL at 30 μg/mL reduced both platelet and fibrin deposition at venous flow condition with fibrin production strongly antagonized (**Figure 4-2A**). HICL produced a dose-dependent inhibition of both platelet (IC50 = 90 μg/mL) and fibrin deposition (IC50 = 0.5 μg/mL) (**Figure 4-2B-E, Figure 4-3H-I**). Similar tests were run for CL10 (Platelet IC50 = 25 μg/mL; Fibrin IC50 = 0.6 μg/mL) and for CL18 (Platelet IC50 = 71 μg/mL; Fibrin IC50 = 5.4 μg/mL) (**Table 4-1, Figure 4-3B-C, Figure 4-3E-F**). For the 3 APAC constructs tested at venous thrombotic conditions, each construct was considerably more potent (>13 to 180-fold) against thrombin generation/fibrin deposition in comparison to inhibition of platelet deposition.

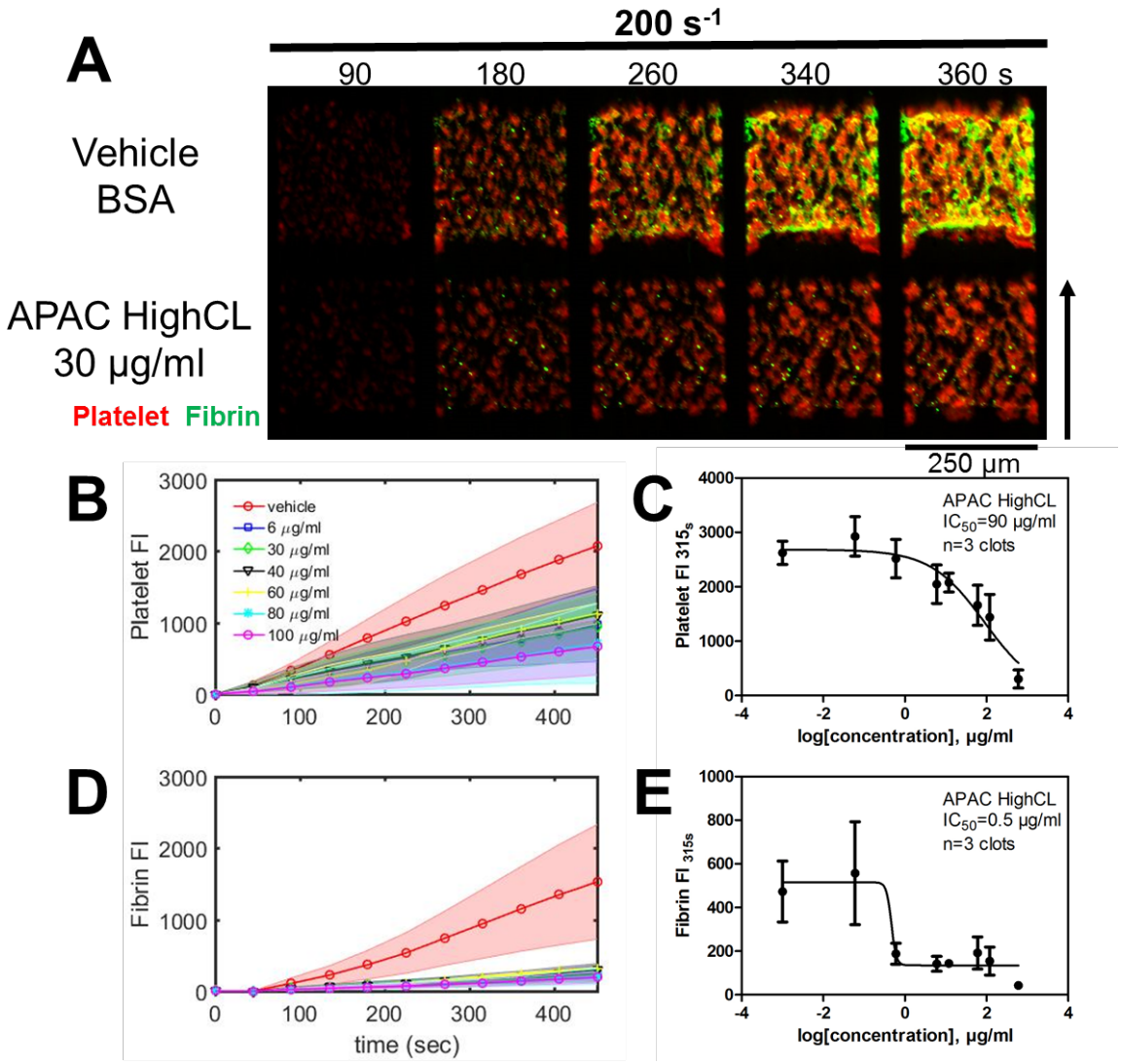

Figure 4-2. APAC inhibits platelet deposition dose-dependently with simultaneous anticoagulant efficacy under 200 s^{-1} over collagen/TF in microfluidic assay.
Vehicle (1% BSA) and APAC (HICL, 30 µg/mL) was added to CTI-treated whole blood and perfused over collagen/TF under venous shear rate. (A) images of platelet and fibrin deposition, (B) dynamics of platelet deposition, (C) dose-response curve and IC50 for platelet deposition, (D) dynamics of fibrin polymerization, (E) dose-response curve and IC50 for fibrin polymerization (± standard deviation [SD]).

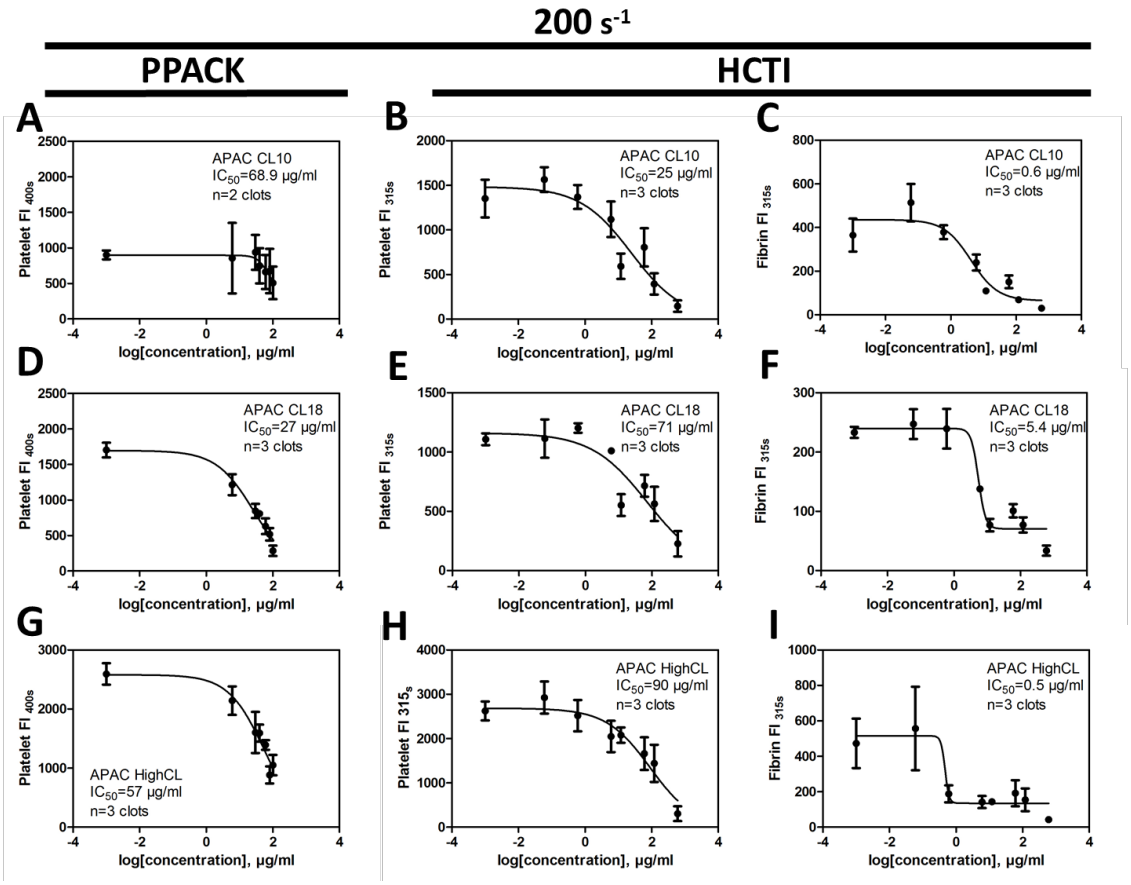

Figure 4-3. Dose-response curves for each APAC species at venous shear rate.
Inhibition on platelet deposition and fibrin formation under two anticoagulated whole blood conditions (PPACK and CTI) at venous shear rate (200 s^{-1}) of CL10 (A), (B), (C). CL18 (D), (E), (F). HICL (G), (H), (I) (± standard deviation [SD]).

APAC in whole blood is more potent as an antiplatelet agent under arterial than venous flow

Microfluidic methods allow the rapid testing of non-anticoagulated, freshly-drawn whole blood, enabling the determination of clotting in the presence of FXII [103]. Blood samples need to be carefully handled and minimally perturbed. The concentration of APAC was chosen to be 10 µg/mL to match the IC50 order in the previous experiment. Whole blood treated with CL10 (10 µg/mL) was immediately perfused over a collagen/TF surface at either venous (200 s^{-1}) or arterial (1000 s^{-1}) perfusion. At this low concentration under venous perfusion, there was little antagonism of platelet deposition, but strong

antagonism of fibrin deposition (as shown in **Table 4-1**). In contrast, under the arterial perfusion condition, CL10 displayed considerable potency against both platelet and fibrin deposition (**Figure 4-4**), suggesting that CL10 may antagonize vWF pathways required for platelet deposition at arterial flow conditions. As expected, there was considerably less fibrin generated under control conditions (no CL10) at arterial flow compared to venous flow (**Figure 4-4E-F**). Finally, APAC and vWF interaction was confirmed by immunoprecipitation, where APAC (CL10, biotinylated) was captured by vWF under static conditions with collaborators' help.

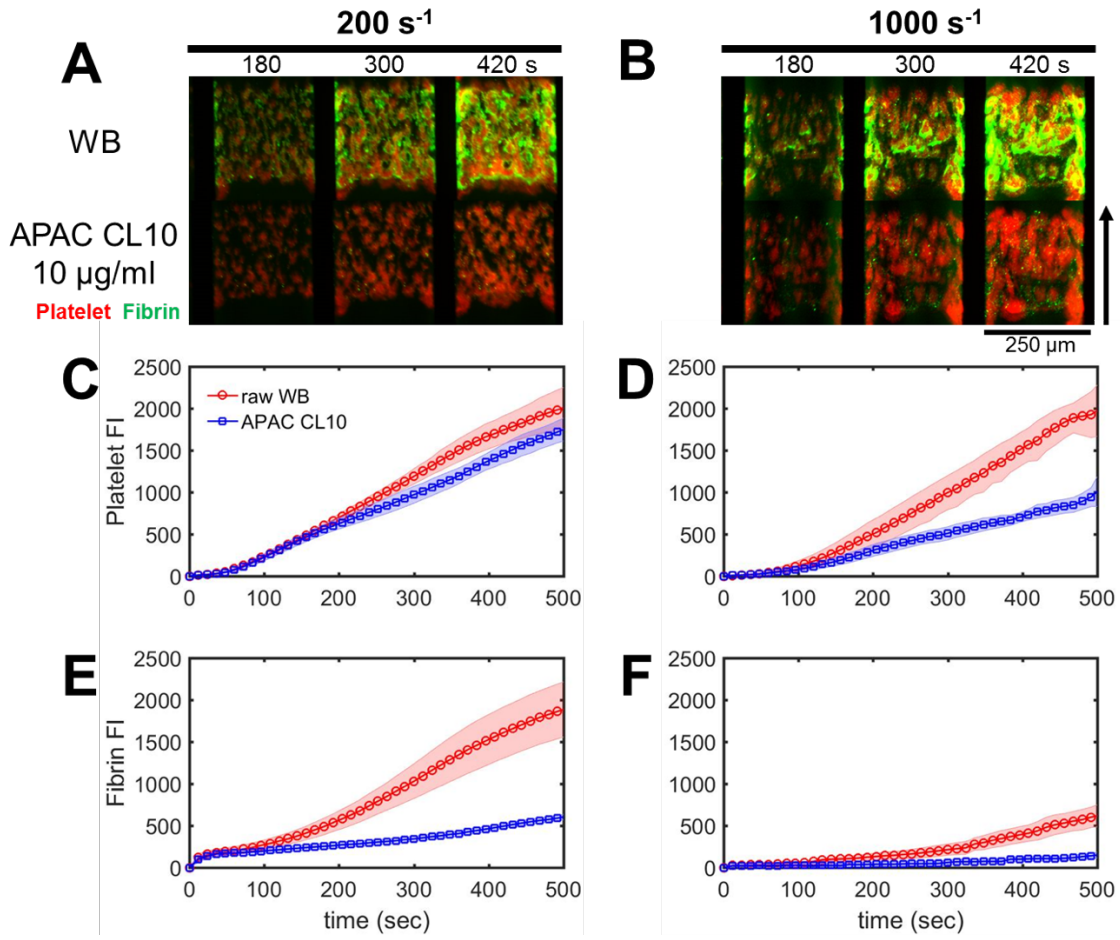

Figure 4-4. APAC is more efficient in antiplatelet activity under arterial shear rate compared to venous shear rate.
APAC (CL10, 10 µg/mL) was added to untreated whole blood and perfused over collagen/TF under (A) venous shear rate and (B) arterial shear rate. APAC has stronger effect on inhibition of platelet deposition. (C), (D) dynamics of platelet deposition and (E), (F) dynamics of fibrin generation (± standard deviation [SD]).

Concern of bleeding risks associated with combinations of two or more blood modulating drugs have sparked interest in developing cardiovascular therapies with dual antiplatelet and anticoagulant (APAC) activity. Using naturally-produced HEP-PGs as a framework for synthetic alternatives, protein functionalized with conjugated UFH chains offers a promising route [98,102]. With our 8-channel device, we demonstrated APAC antiplatelet activity with PPACK-treated blood perfused upon collagen. Secondly, we analyzed the ability of APAC to interfere with the thrombus growth when CTI-treated blood

was perfused upon a collagen/TF surface. We also provide evidence that APACs can directly interact with collagen to reduce platelet deposition under flow and to decrease collagen-induced calcium mobilization. Additionally, the increased inhibitory activity against platelets under arterial flow conditions suggests that APAC when studied in the absence of any other anticoagulant may also reduce vWF binding to collagen or modulate the VWF-GPIbα interaction. APAC interaction with vWF was supported by the immunoprecipitation studies where vWF captured APAC. A schematic summarizing the major results is shown in **Figure 4-5**.

Other than its traditional anticoagulant mechanism, heparin has been implicated to exhibit other antithrombotic effects such as inhibiting endoperoxide metabolites that lead to thromboxane A2 production, suggesting aspirin-like functions [106]. Also, collagen has previously been reported to have unique heparin-binding sites separate from those involved in heparin-triggered thrombin inactivation [100,107,108]. Though the functional significance of heparin-collagen binding is still unclear, it may explain the observed inhibitory phenomenon of heparin proteoglycans and synthetic APAC conjugates on collagen-induced platelet aggregation, especially under blood flow.

Though certain explanations may be incorrect, and collagen and thrombin appear to be the sole targets, more work should be performed to further refine the specific antiplatelet and platelet anticoagulant mechanisms of APAC.

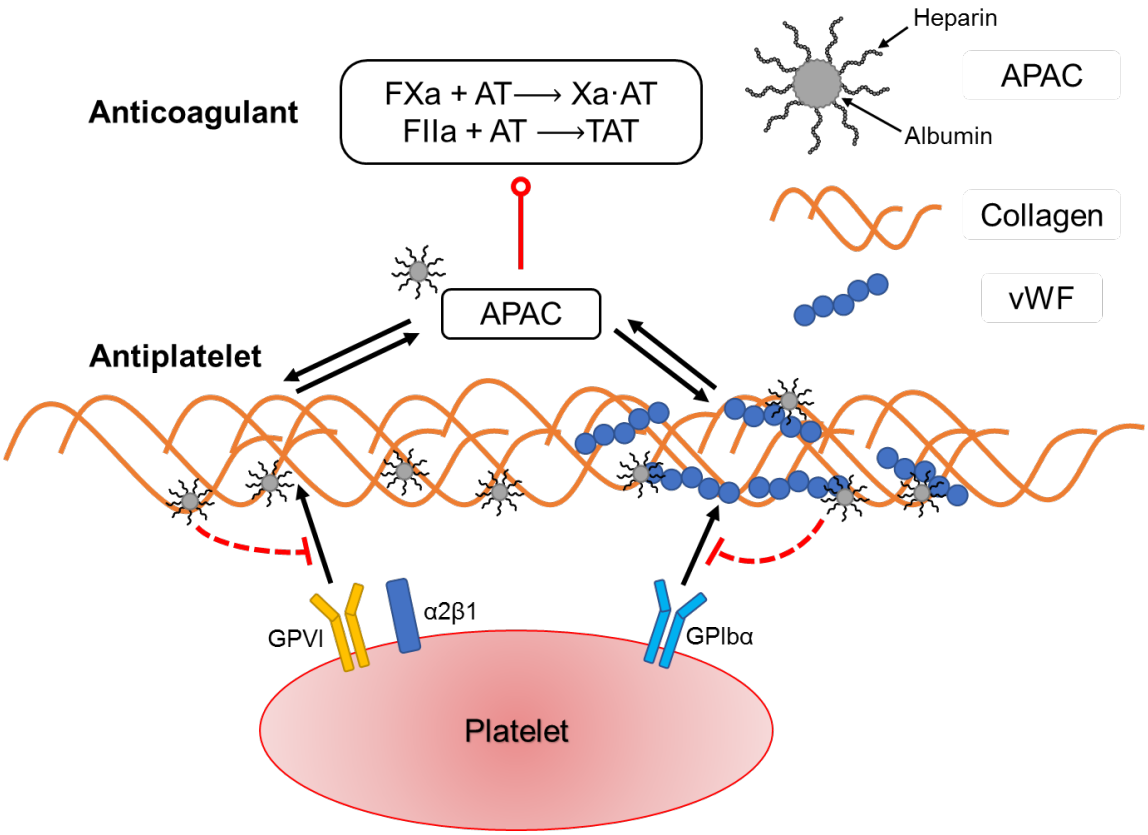

Figure 4-5. Schematic of APAC functionality as both antiplatelet and anticoagulant agent. APAC has anticoagulant effect by accelerating the inactivation of thrombin and factor Xa through an antithrombin-dependent mechanism. Its antiplatelet activity results from inhibition on platelet-collagen interactions. APAC strongly inhibited platelet deposition under high shear rate by attenuating GPIbα-VWF mediated activation.

4.2 Using microfluidic assay to characterize PAR4 & FXIa antagonist as potential antithrombotic targets

Most of the approved antithrombotic agents interfere with hemostasis, leading to an increased risk of bleeding. FXIa and PAR4 inhibitors have been shown to be safer antithrombotic drugs under different assays [87,109]. However, in our microfluidic assay, the collagen/TF surface is too potent to show the effect. Here, we collaborated with Bristol Meyers Squibb and tried to utilize customized pattering surface to evaluate them as antithrombotic drugs under flow. The schematic figure is shown in **Figure 4-6**.

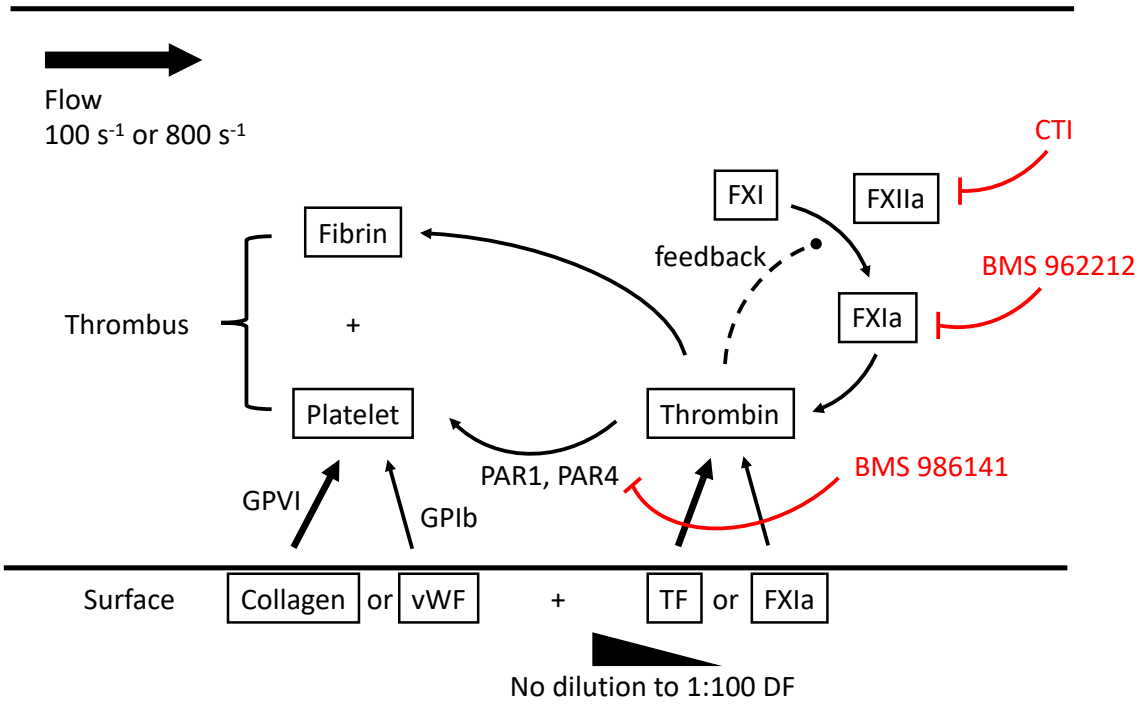

Figure 4-6. Schematic of the simplified coagulation cascade model.
Blood coagulation can be initiated via contact pathway or extrinsic pathway. We can modify our surface to trigger different pathway. Collagen can capture and further activate platelet, while vWF is highly adhesive for platelet, which allows us to investigate the activation of platelet via PAR1 and PAR4 by thrombin.

FXIIa and thrombin can activate FXI, resulting in sustained thrombin generation. While FXIa plays a key role in thrombosis because of the thrombin-mediated-feedback pathway, it only plays a minor role in hemostasis, especially with high tissue

factor[27,110]. We evaluated a small molecule that inhibits FXIa, BMS-962212. FXIa inhibitor only shows difference at later time point under high TF because TF on the surface is potent. However, it can inhibit fibrin formation earlier under low TF and display dose-dependent response in **Figure 4-7A-B**. BMS 962212 can also inhibit fibrin formation triggered by FXIa surface, and display dose-dependent response shown in **Figure 4-7C-D**.

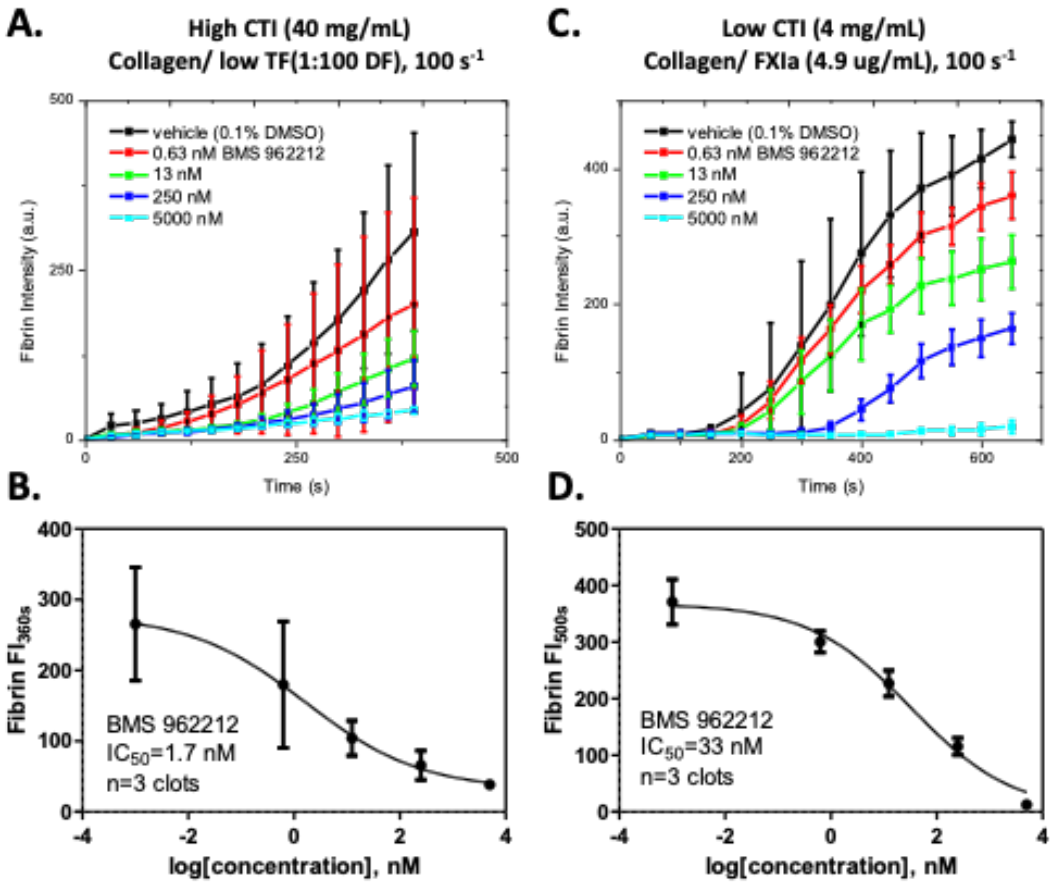

Figure 4-7. The effects of FXIa inhibitor over different surface.
FXIa inhibitor inhibits fibrin formation under low TF (A) , with the dose-response curve (B). FXIa inhibitor inhibits fibrin formation triggered by FXIa surface (C), with the dose-response curve (D).

Thrombin activates platelets by protease-activated receptors PAR1 and PAR4. PAR1 is thought to be the main receptor because of its high affinity and sensitivity and is therefore regarded as promising antiplatelet target. However, it has been reported for the

rising bleeding risk with the FDA-approved vorapaxar. Small molecule antagonists of PAR4 has demonstrated antithrombotic activity in human model in chambers [111]. The potential of PAR4 as an antiplatelet target has not been well characterized under flow[112]. Here, we characterized the pharmacology of BMS-986141, a potent and selective PAR4 antagonist, in a microfluidics model of thrombosis. Arterial plaque rupture thrombosis was simulated by flowing blood through microfluidics channels patterned with von Willebrand Factor to allow platelet adhesion and lipidated tissue factor to trigger thrombin generation.

Our labmate Christopher Verni [113] has shown that BMS-986141 specifically blocked calcium mobilization by PAR4 agonist peptide (AYPGKF, IC50~1.3 nM). The PAR4 antagonist reduced the secondary phase of calcium mobilization in platelets challenged with 200 nM thrombin, without affecting the initial peak calcium, as expected for slower more sustained PAR4 signaling compared to the rapid, short lived signaling of PAR1. However, BMS 986141, showed no significant effect of PAR4 antagonist under strong platelet activation by collagen/TF surface. Therefore, we switched to vWF surface, on which the platelet can adhere, so that we can see the subtle effects of PAR 4 antagonist. For corn trypsin inhibitor (CTI)-treated whole blood perfused over vWF/TF surface under high shear rate (800 s^{-1}) in **Figure 4-8**, BMS-986141 reduced platelet deposition by ~ 20 %, but not fibrin deposition (N=7 donors, 27 clots; $p < 0.03$).

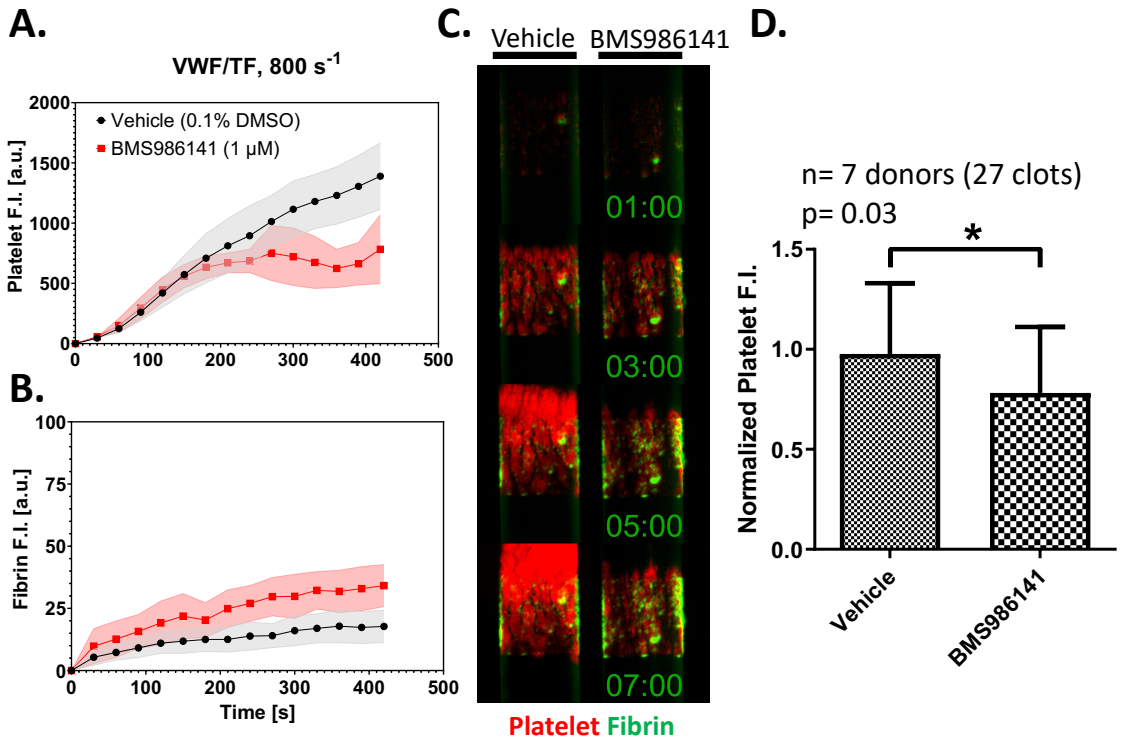

Figure 4-8. PAR4 antagonist, BMS-986141, reduces platelet deposition on a vWF/TF surface at 800 s^{-1}.

In conclusion, BMS-962212, a FXIa inhibitor, showed no effects on high TF surface but displayed inhibition on fibrin formation on low TF surface. The small molecular also showed strong effects on fibrin over FXIa surface in a dose-dependent way. In the future, it would be interesting to determine the surface concentration of the FXIa by using the inhibitor conjugated to fluorophores. BMS-986141 is a highly specific antagonist of PAR4. This small molecule reduced platelet deposition in a microfluidic assay of perfused CTI-treated whole blood over patterned surfaces of vWF/TF, which simulate conditions of arterial thrombosis. Future work will be to test the effect of PAR 4 antagonist with the combination of thrombin/ factor Xa inhibitors and other antiplatelet drugs.

4.3 $P2Y_{12}$ inhibition of platelet deposition under different shear rate with or without thrombin generation

ADP is an important agonist that induces platelet aggregation through its receptors $P2Y_1$ and $P2Y_{12}$, which is crucial in both hemostasis and thrombosis. $P2Y_{12}$ antagonists has been widely used to demonstrate the role of $P2Y_{12}$ in platelet function [114,115]. Cangrelor has been evaluated in clinical trials of thrombotic diseases for its rapid action [116,117]. However, less is known for the role of P2Y12 antagonist on platelet under different shear rate in the presence of thrombin. Here, we used the microfluidic thrombosis assay to investigate cangrelor under various well-controlled conditions.

Cangrelor can inhibit platelet deposition at venous shear rate under low/no thrombin condition

The 8-channel device was used to investigate cangrelor effects under flow in various conditions. Previously, platelet sensitivity to p2y12 inhibitor under flow was studied. $P2Y_{12}$ antagonist, 2MeSAMP [114], was shown to reduce both primary platelet deposition and secondary aggregation in the absent of thrombin. Our first aim was to study the antiplatelet effect of cangrelor without the influence of thrombin. Human whole blood was treated with a direct thrombin inhibitor, PPACK, and perfused over collagen at 100 s^{-1} shear rate. Platelet deposition was greatly reduced by Cangrelor at early time points (200 s) in the absence of thrombin at venous flow rate over collagen (**Figure 4-9**). At later times, we can also see the decrease of platelet fluorescence intensity. From the images, we saw only a thin layer of platelet with cangrelor at 30 and 1000 nM.

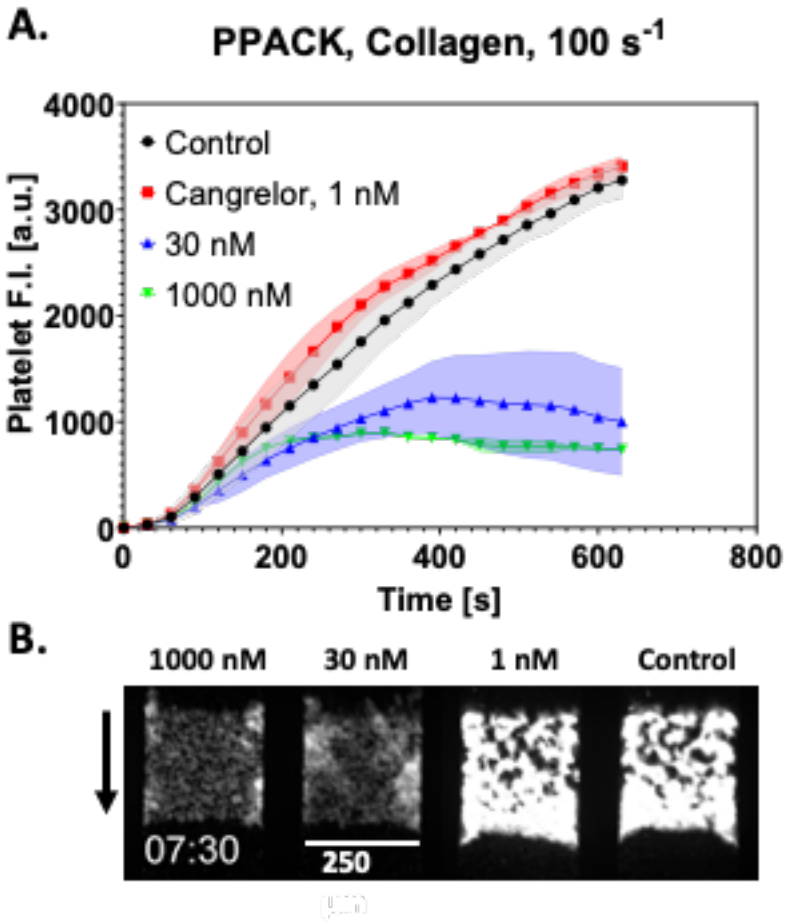

Figure 4-9. Platelet deposition is greatly reduced by Cangrelor in the absence of thrombin at venous flow rate over collagen.
Cangrelor was added at different concentration to PPACK (100 uM)-whole blood and perfused over collagen at 100 s^{-1}. (A) Dynamics of platelet fluorescent intensity. (B) Images of platelet deposition 7.5 mins.

Cangrelor at lower concentration can inhibit platelet deposition only at arterial shear rate at the absent of thrombin

Cangrelor at 30 nM had great effect on platelet deposition without thrombin. We here tested cangrelor at lower concentration (6.6 nM) at different shear rate (**Figure 4-10**). We also added P-selectin antibody to investigate cangrelor effect on P-selectin (+) core region. There was no significant difference in both platelet deposition and P-selectin between cangrelor at low concentration (6.6 nM) and control at 100 s^{-1}. However, with

same conditions, cangrelor reduced both both platelet deposition and P-selectin signals at 800 s^{-1}. Cangrelor had early effect on platelet depostion at 100 s and reduced around 30% at the end of experiment (500 s).

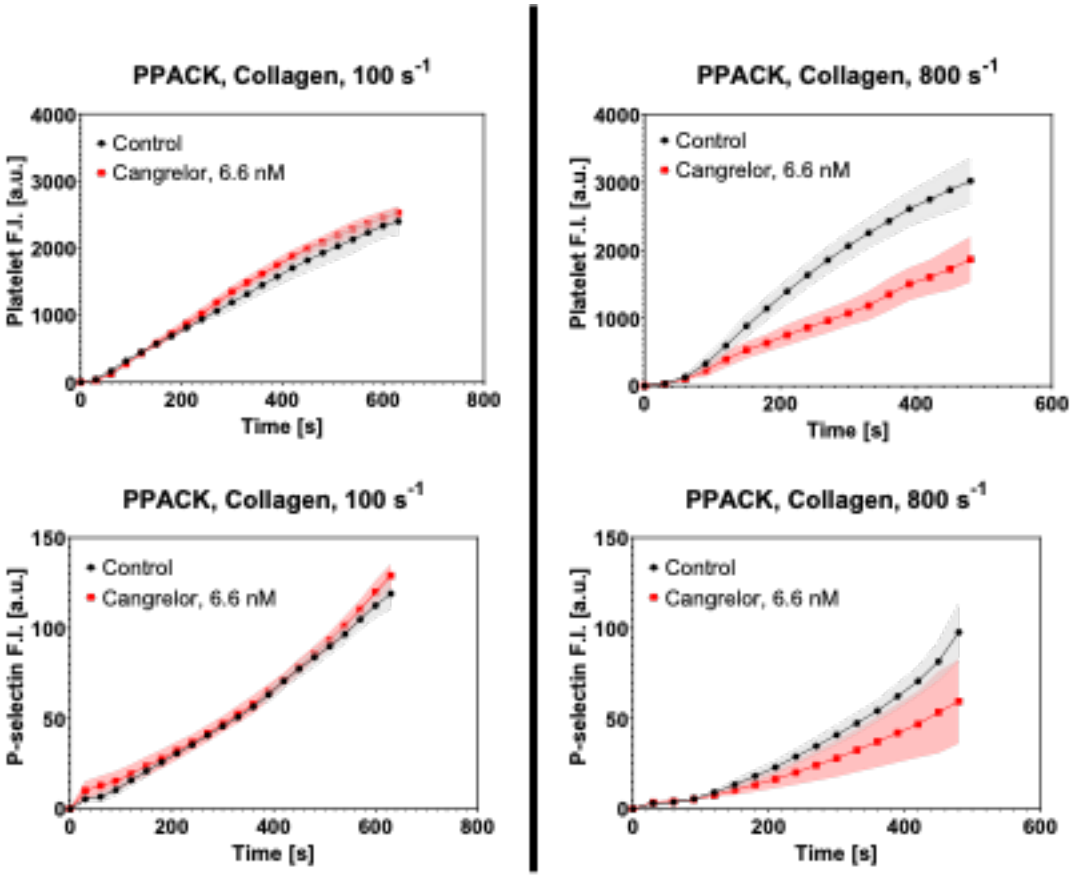

Figure 4-10. Cangrelor at low concentration shows shear-dependent effects on both platelet deposition and P-selectin (+) in the absence of thrombin.
Cangrelor (6.6 nM) was added to PPACK (100 μM) -treated whole blood and perfused over collagen at 100 s^{-1} (first column) and 800 s^{-1} (second column).

In the presence of thrombin, Cangrelor only inhibit platelet deposition at arterial shear rate but not venous shear rate

To study cangrelor in the present of thrombin and fibrin, blood treated with high CTI (40 μg/mL), a FXIIa inhibitor, was perfused over collagen/ TF. We first tested it with a range of concentration. Even at high concentration of cangrelor (1000 nM), there was little effects on platelet deposition over collagen/TF at 100 s^{-1} in the presence of thrombin

(**Figure 4-11**). However, at 800 s^{-1}, cangrelor at 30 and 1000 nM reduced platelet deposition at early times and around 70% at the end of the experiement (500 s). These experiments suggest that cangrelor has shear-dependent effects on platelet in the presence of thrombin.

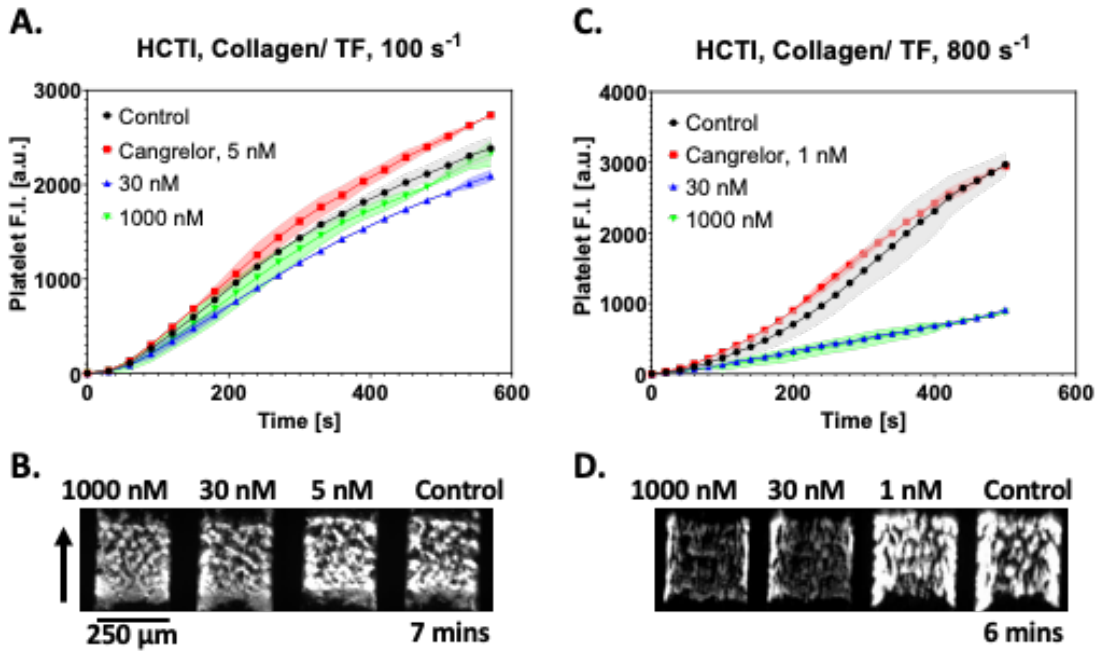

Figure 4-11. Cangrelor reduced platelet deposition in the presence of thrombin at arterial shear rate but not venous shear rate over collagen/TF.
Cangrelor was added at different concentration to HCTI-treated whole blood and perfused over collagen/TF. (A) Dynamics of platelet fluorescent intensity at 100 s^{-1} (B) Images of platelet deposition 7 mins. (C) Dynamics of platelet fluorescent intensity at 800 s^{-1} (D) Images of platelet deposition 6 mins. (HCTI: High CTI)

We added P-selectin antibody to characterize cangrelor effects on platelet structure. Agreed with previous experiment, even at 1000 nM, cangrelor didn't reduce the platelet deposition at venous flow rate in the presence of thrombin (**Figure 4-12**). However, cangrelor affects the morphology of the clot from the images Also, it reduces P-selectin (+) core region around 25% at venous shear rate in the presence of thrombin.

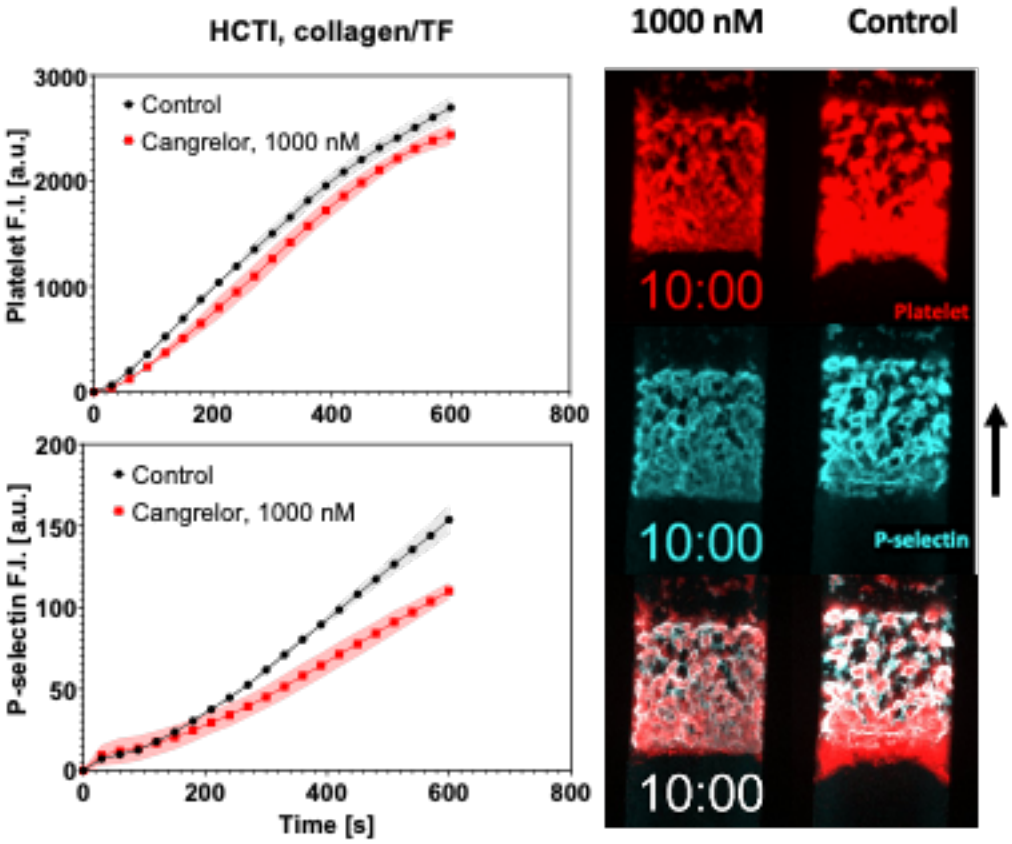

Figure 4-12. Cangrelor affects the morphology of the clot and reduces P-selectin+ core region at venous shear rate in the presence of thrombin.
Cangrelor (1000 nM) was added to HCTI-treated whole blood and perfused over collagen/TF at 100 s^{-1}. Cangrelor had little effects on platelet deposition but affected the morphology of the clots.

In conclusion, we have tested cangrelor effects on platelet deposition at different shear rate with or without thrombin. We found that in the presence of thrombin generation, cangrelor only reduced platelet deposition at arterial shear rate but not venous shear rate. For the intensity of P-selectin, we also saw the effects on the platelet plug structure.

Cangrelor is often used with other antiplatelet drugs or anticoagulants. In the future, it would be interesting to see the effects of cangrelor with the combination with other antithrombosis agents. The surface concentration of tissue factor or direct thrombin inhibitor concentration can also be varied to test the effects of cangrelor at different thrombin concentration. The effects of cangrelor on platelet stability and the core/shell structure can also be investigated by a new microfluidic assay [118].

CHAPTER 5: FUTURE WORK

5.1 Introduction

There are few ways to estimate thrombin in clots forming under flow. I have used microfluidic devices combined with immunoassay to estimate the thrombin concentration. Based on the experimental data, I developed a reduced model to estimate the species. I also used the thrombin and fibrin fluxes in a convection-diffusion model to confirm the thrombin concentration. Furthermore, with normal variation of 5 plasma zymogens and 2 fibrin binding sites, I used the reduced model with Monte Carlo simulations to estimate the thrombin concentration distribution. Here, I developed two other assays to estimate thrombin in clots under flow. The followings are the primary results. These two methods will not only confirm previous estimation under venous flow rate, but also allow us to calculate the thrombin concentration in clots forming under arterial shear rate.

5.2 Estimation by thrombin active sites calibrated by standard curve

Our previous studies have shown that the fluorescein-PPACK was able to label the thrombin active site and was highly resistant to high shear rate wash out. We followed a similar method. First, let the clot grow under flow for 500 second at 100 s^{-1}. After washing the clots with HBS for 1 minute, we introduced the fluorescein-PPACK and labeled the active sites of thrombin. In order to get rid of the unbinding PPACK, we washed the clots again with HBS. The clots were ready for imaging. For quantitatively estimation of the fluorescein-PPACK, we filled the channels of microfluidic device with a series concentration of fluorescein-PPACK and used linear regression to come up with a calibration line (**Figure 5-1**). We estimated the thrombin concentration in the clots by assuming all the thrombin were in the porous core region in the clot. The height of the channels was 120 μm, and the porosity and height of the core were previously estimated

to be 0.5 and 15 μm by direct imaging. The concentration of thrombin in the clots was estimated to be 1.6 μM, which was not far away from other estimations. However, it is still a primary result and requires replicates.

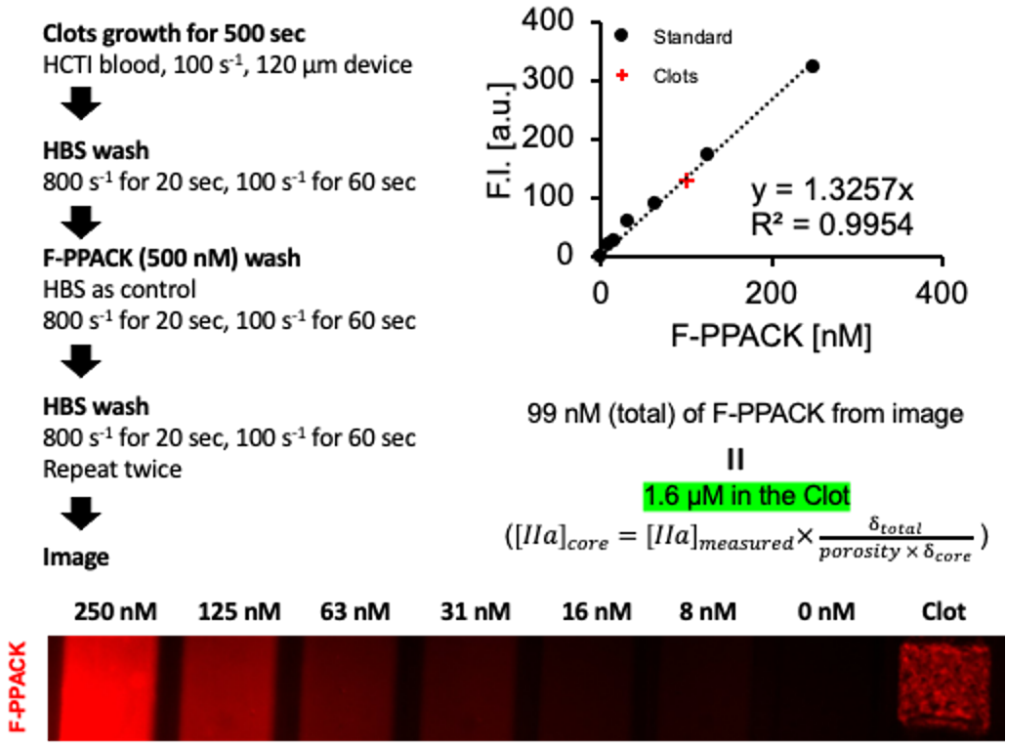

Figure 5-1. Estimation of thrombin concentration by active sites.
Clots were formed at 100 s^{-1} with HCTI-treated blood perfused over collagen/TF surface. Washed by HBS, the thrombin in clots was labeled by fluorescein-PPACK. Calculated by calibration line, the thrombin in clots was estimated to be 1.6 μM.

5.3 Estimation by fluorogenic thrombin substrate and known kinetics property

The recent work of Haynes [18] studied clot-bound thrombin with flow chambers and thrombin substrate. Followed by similar approach, I used small thrombin substrate (Z-GGR-MCA) to investigate the thrombin activities in the clots grown under flow with healthy human blood. First, I let the clots grow with HCTI-treated blood perfused over collagen/TF surface at 100 s^{-1} for 500 seconds. Washed by HBS, the clots were introduced with fluorogenic thrombin substrate. Under flow, fluorescence intensity reached to steady state quickly. When the flow stopped, the substrate was cleaved by thrombin and the fluorescence product accumulated (**Figure 5-2**). By using the first few points in the linear region, we can estimate the thrombin concentration by Michaelis–Menten kinetics. Here, I presented the primary results, and the thrombin was calculated to be 11.8 μM when the substrate concentration was 100 μM. However, it requires replicates and tests at different conditions. It would also be useful to simulate with COMSOL.

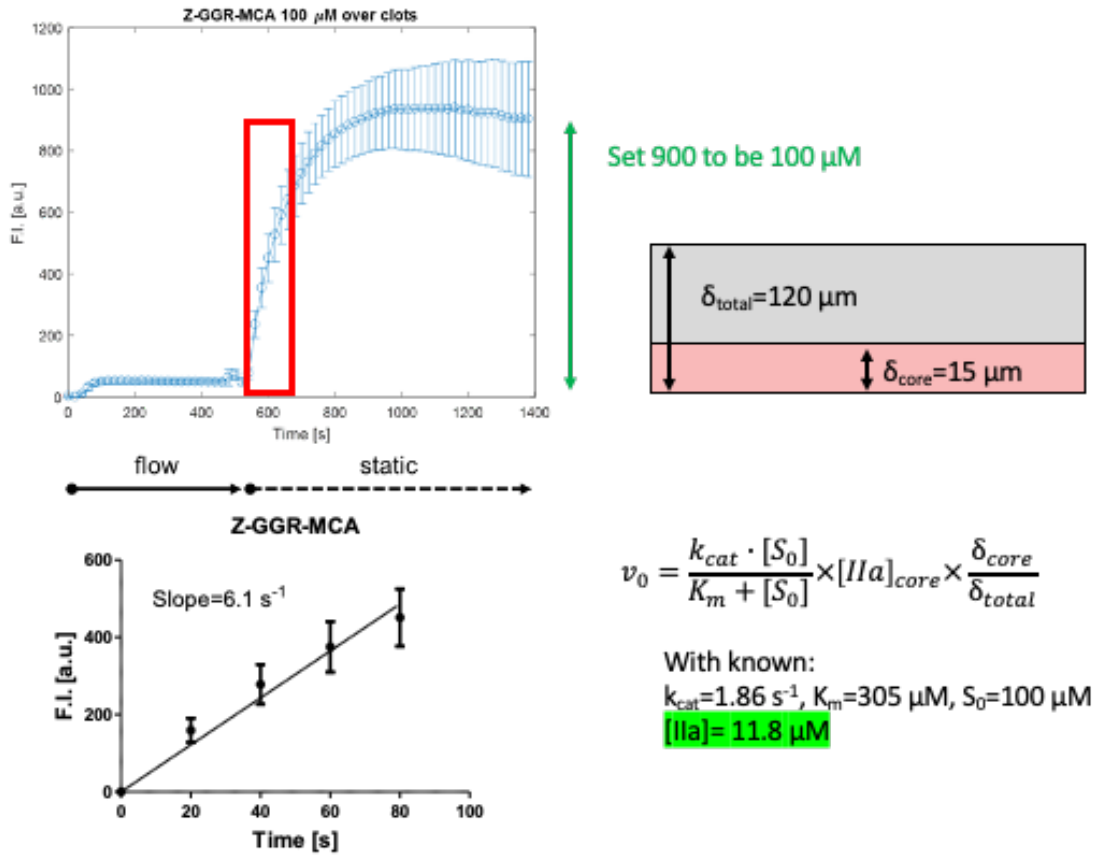

Figure 5-2. Estimation of thrombin concentration in clots by fluorogenic substrate.
Clots were formed at 100 s^{-1} with HCTI-treated blood perfused over collagen/TF surface. Washed by HBS, the clots were introduced to thrombin substrate. The concentration was estimated by Michaelis–Menten kinetics.

Here, I developed two methods to estimate thrombin concentration in the clots. The primary results were shown in **Figure 5-3** and **Table 5-1** compared with other published results. Although it requires replicates in both methods, it is going to be helpful for establishing mass balance at arterial shear rate.

Method	**$[IIa]_{core}$ at 500 sec**	**Experimental Set up**	**Methods**	**Publication**
Transient Mass Balance	15 µM	High CTI 1-inlet 1-outlet device (60 µm) 200 s^{-1}	TAT, F1.2 ELISA	ATVB (2018)
Reduced Model	9 µM		7 rates, 2 K_D, enzyme half-lives=1 min	PLOS comp. bio. 2019)
Convection-Diffusion Model	5.5 µM		COMSOL F1.2, D-dimer ELISA 2 K_D	PLOS comp. bio. (2019)
Active sides labeled by F-PPACK	1.6 µM	High CTI 8-channel device (120 µm) 100 s^{-1}	8-channel standard curve	
Thrombin Activity by Z-GGR-AMC	11.8 µM (100 µM) 3.9 µM (200 µM)	High CTI 8-channel device (120 µm) 100 s^{-1}	Dynamic parameters	

Table 5-1. Results of thrombin concentration in the clots by different methods.

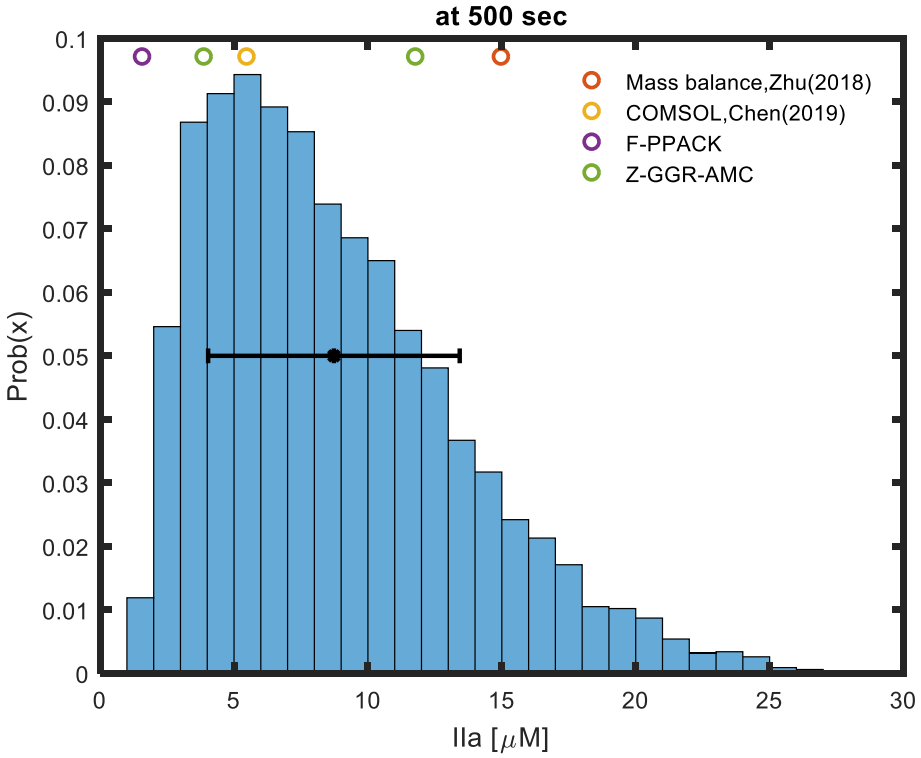

Figure 5-3. Results of thrombin concentration in the clots by different methods.
The mean and distribution are from sensitivity analysis described previously. Estimation of thrombin in the clots by active sites labeling and fluorogenic substrate is shown in the figure compared other published results.

CHAPTER 6: APPENDIX I (SUPPLEMENTAL MATERIALS)

Calculation of free thrombin concentration in clots

To calculate the concentration of free thrombin, two reactions were considered. Thrombin can bind reversibly to weak sites (Eq. 1) and γ' sites (Eq. 2) of fibrin. According to the mass conservation principle, at equilibrium, the total thrombin ($C_{IIa,total}$) is the sum of free thrombin (C_{IIa}), thrombin on low-affinity binding sites (^{weak}S) and thrombin on γ' sites ($^{\gamma'}S$). The total numbers of each sites ($^{weak}\theta_{total}$, $^{\gamma'}\theta_{total}$) are the sum of vacancy ($^{weak}\theta$, $^{\gamma'}\theta$) and filled sites (^{weak}S, $^{\gamma'}S$), respectively. With the equilibrium constant of both reactions, we were able to determine the concentration of every species.

$$\begin{cases} IIa + {}^{weak}\theta \Leftrightarrow {}^{weak}S & (1) \\ IIa + {}^{\gamma'}\theta \Leftrightarrow {}^{\gamma'}S & (2) \end{cases}$$

$$\begin{cases} \frac{1}{{}^{weak}K_d} = \frac{{}^{weak}S}{C_{IIa} \times {}^{weak}\theta} = \frac{{}^{weak}S}{(C_{IIa,total} - {}^{weak}S - {}^{\gamma'}S)\,({}^{weak}\theta_{total} - {}^{weak}S)} & (3) \\ \frac{1}{{}^{\gamma'}K_d} = \frac{{}^{\gamma'}S}{C_{IIa} \times {}^{\gamma'}\theta} = \frac{{}^{\gamma'}S}{(C_{IIa,total} - {}^{weak}S - {}^{\gamma'}S)\,({}^{\gamma'}\theta_{total} - {}^{\gamma'}S)} & (4) \end{cases}$$

$$^{weak}\theta_{total} = {}^{weak}\theta + {}^{weak}S \quad (5)$$

$$^{\gamma'}\theta_{total} = {}^{\gamma'}\theta + {}^{\gamma'}S \quad (6)$$

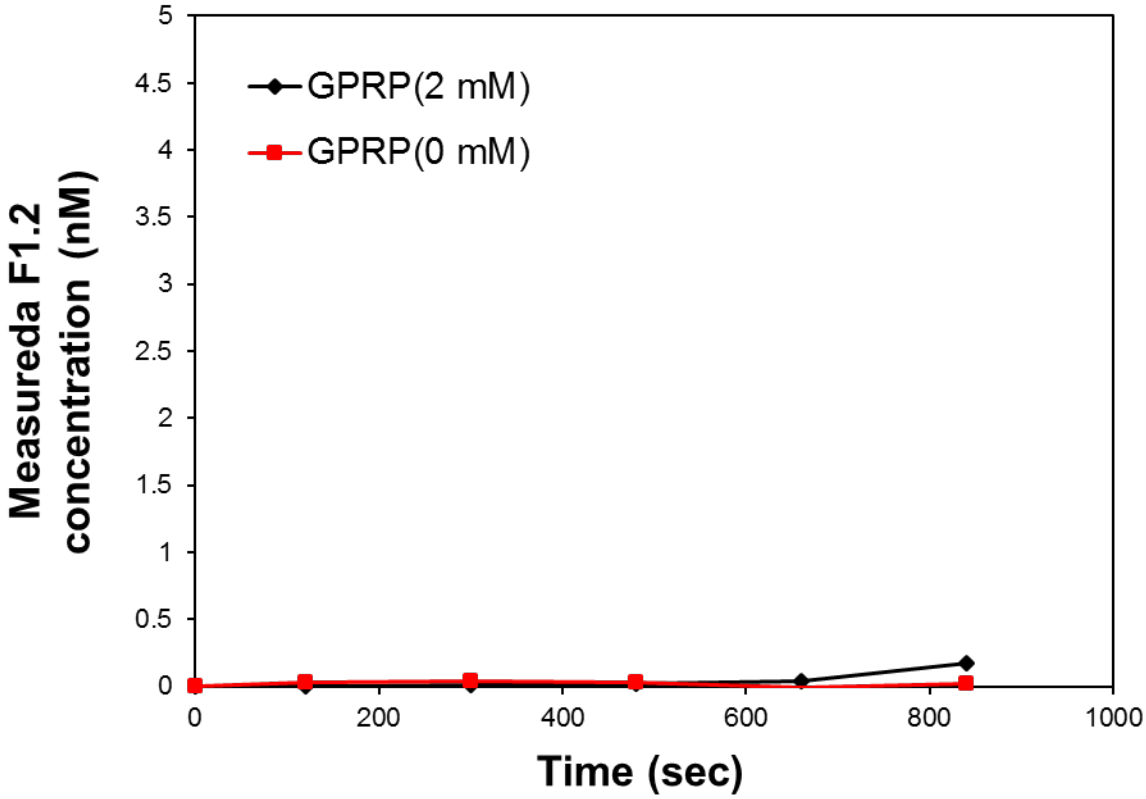

Supplemental Figure I High CTI treated whole blood perfused through blank channels (no collagen/no TF) produced essentially undetectable levels of F1.2 regardless of presence or absence of GPRP. This indicated that high dose CTI of 40 µg/ml quenches FXIIa in the inlet reservoir and flow channels of the microfluidic device.

Estimation of core thickness and core porosity

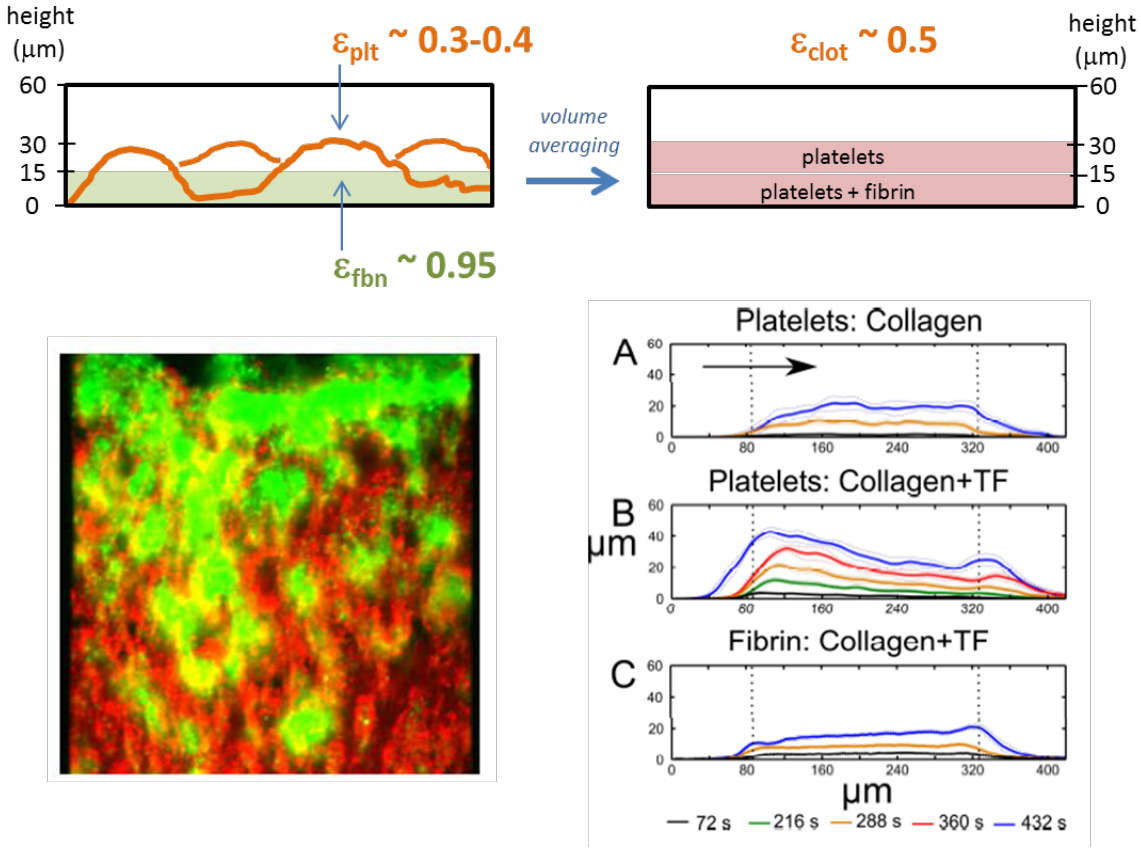

Supplemental Figure II Measurements of 15-micron thick fibrin-rich layer within thrombus formed under flow. With assumption that thrombin and fibrin cannot exist inside a platelet, thrombin and fibrin exist in the pore space around the platelets. Averaging through the clot with two compartments, the platelet compartment and the fibrin compartment, we have a core height δ=15 μm and porosity ε=0.5.

Calculation of intrathrombus thrombin levels using TAT Elisa and F1.2 Elisa

By collection of microfluidic device effluent, the exit concentration of discrete samples was measured at discrete time points t_i and then averaged ($\bar{c}_i$ for *n* donors). Over the first 500 sec of clotting under flow, the flux of thrombin from the surface increased linearly with time (Fig. 4A). By either summing up cumulative mass in each sample volume (V_i * $\bar{c}_i$ for i samples) or equivalently by integrating the fitted flux $J_{FIIa}(t)$, the total average amount of thrombin generated per total collagen/TF area was calculated.

Over the first 500 sec, the average thrombin generation as estimated by TAT (with GPRP present) was statistically identical to F1.2 generation (with no GPRP present). F1.2 was assumed to be a gold standard metric of thrombin generation since one molecule of F1.2 is generated per molecule of thrombin generated. From Fig. 4A, thrombin flux determined via F1.2 assay (without GPRP) increased linearly with time and reached a value of ~0.5 x 10^{-12} nmole/μm^2-sec by 500 sec, essentially identical to thrombin flux determined with TAT assay with GPRP present. Thus, the thrombin generated over the first 500 seconds was calculated by integration of the F1.2 flux from the surface:

$$FIIa\ generated\ over\ 500\,\text{sec} = F1.2\ generated\ over\ 500\ sec$$

$$= \int_0^{500} J_{F1.2}(t)\ dt \cong 92000\ \frac{molecules}{\mu m^2}$$

Of the 92,000 molecules of thrombin made per μm^2 over the first 500 sec of flow, the TAT assay indicated that only 15 % of the thrombin escaped the clot to form TAT when fibrin was present. A mass balance at 500 sec on thrombin requires:

FIIa generated (***by F1.2 assay***) = FIIa escaped and complexed at TAT (***15% by TAT Elisa***)

+ FIIa escaped and complexed to other inhibitors (***estimated[1]***)

+ FIIa captured by fibrin (***Calculated***)

For 92000 molecules of thrombin, 15 % escapes the clot as detected as TAT (15% of 92000 = 13800 molecules TAT). We estimate that 70% of the escaped thrombin will

complex with antithrombin to form TAT (13800 molecules) and 30% of escaped thrombin will go undetected (eg. thrombin-macroglobulin, thrombin-C1 inhibitor) (5,900 molecules) (*See footnote 1*). For 92000 molecules of thrombin made, of which 19,700 escape the clot as either TAT or other inhibited forms, a total of 72300 molecules of thrombin are captured within the clot. We calculate the thrombin concentration in the fibrin space (50% of the clot volume) of the clot core (the 15-micron layer) to be:

Intrathrombus [thrombin] = 72300 molecules/μm^2 ÷ (7.5 μm^3 -fibrin gel/μm^2-collagenTF area),which corresponds to a local concentration of ~ 15 μM of intrathrombus thrombin in the fibrin space.

[1]We observed that the amount of F1.2 made in the presence of GPRP was ~30-50% greater than the amount of TAT detected in the presence of GPRP (Fig. 4A). This difference is expected, in part, since some of the thrombin released from the clot might be inhibited by C1 inhibitor or α_2MG and not detected as TAT. From here, we can estimate that about 70% of escaped thrombin complexes with antithrombin and 30% captured by other inhibitors.

Calculating intrathrombus fibrin levels from D-dimer endpoint assay Elisa and FPA Elisa.

From D-dimer endpoint ELISA, each D-dimer detected was considered equivalent to a single fibrin monomer containing two D domains. The volume of pore space of clot core (V) was calculated using the following equation, where A is the thrombotic area per channel (A = 8 channels x 250μm x 250μm), δ is the core thickness (δ = 15 μm) and ε = 0.5 is overall porosity averaged over the entire collagen-TF surface (**Supplement Fig. II**), which is covered relatively equally by dense platelet-rich thrombus deposits ($\varepsilon_{thrombus}$~ 0.3) and dense fibrin deposits (ε_{fibrin}=0.95):

Average volume of the pore space of the clot core, $V = A \times \delta \times \varepsilon$

All the D-dimer molecules (or equivalently fibrin monomers) detected in the endpoint assay were then placed in the pore space of core layer. This allowed the determination of the final average fibrin concentration at 800 sec in the clot to be 28.3 ± 11.4 mg/mL. From the 800-sec endpoint measurement to calibrate the dynamic fluorescence signal obtained by microscopy (**Fig. 4C**), the intrathrombus fibrin concentration in the pore space of the clot at 500 sec is 15 mg/mL, and fibrin porosity was calculated to be ε_{fibrin} = 0.95, based on a fibrin fiber density of 280 mg-fibrin/mL-fiber. For fibrin at a density of 15 mg/mL, the copy number of fibrin monomer is 203000 in a volume of 7.5 μm^3. The concentration is 45 μM with 13.5 μM γ'-sites (0.3 sites/monomer) and 72 μM low affinity sites (1.6 sites/monomer).

Estimating intrathrombus prothrombinase level from Michaelis–Menten kinetic model.

From the activation of prothrombin (II) by the prothrombinase complex (XaVa)

$$II + XaVa \leftrightarrow II{:}XaVa \xrightarrow{k_{cat}} IIa + XaVa$$

Given that thrombin flux increased linearly and reached a value of ~0.5 x 10^{-12} nmole/μm^2-sec by 500 sec, we assume that prothrombinase concentration to be

$$[XaVa](t) = \beta \cdot t, \qquad \beta\ [=]\ \mu M/s$$

We can get the following equation from Michaelis–Menten model,

$$[IIa] = \int_0^{500\ s} \frac{k_{cat}\,[II]}{K_m + [II]} [XaVa](t)\ dt$$

We calculated β to be 6.48 x 10^{-6} μM/s, for 20 μM (92,000 molecules per 7.5 μm^3) of thrombin made by the first 500 sec, 1.4 μM of prothrombin, k_{cat} = 30 s^{-1} and K_m = 0.3 μM (Leiderman and Fogelson, 2010). We then calculate the prothrombinase concentration to be 3.2 nM in the pore space (ε = 0.5) of the clot core (δ = 15 μm), which corresponds to a total number of 15 molecules of intrathrombus prothrombinase in active form. We expect ~10^2 of Factor Xa were made over the first 500 sec, but 90% was inhibited by the antithrombin III system.

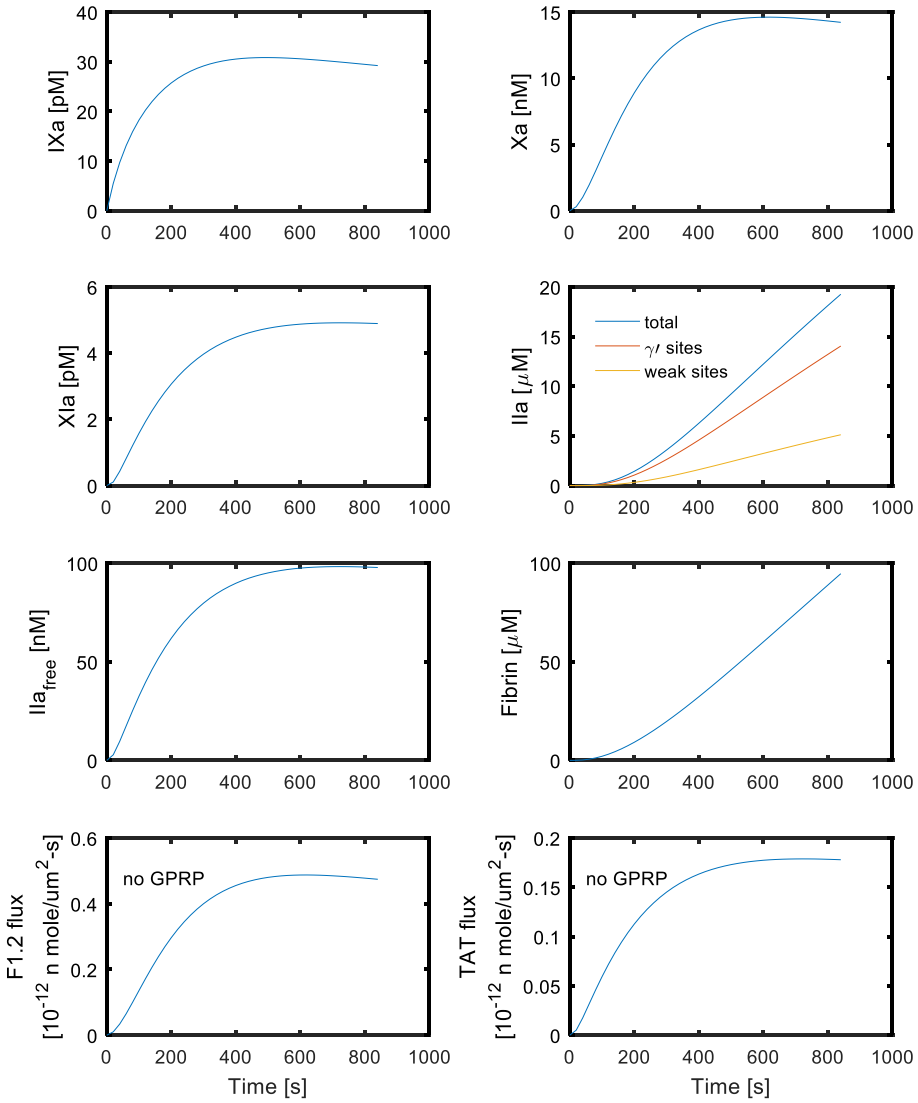

Supplement Figure III. The concentration of the procoagulants (A, B, C), thrombin distribution (D, E), fibrin, flux of F1.2 and TAT (G,H) with the normal plasma protein levels and thrombin binding sites.

CHAPTER 7: BIBLIOGRAPHY

1 Wolfenstein-Todel C, Mosesson MW. Human plasma fibrinogen heterogeneity: evidence for an extended carboxyl-terminal sequence in a normal gamma chain variant (gamma'). *Proc Natl Acad Sci* 1980; **77**: 5069–73.

2 Lovely RS, Yang Q, Massaro JM, Wang J, D'Agostino RB, O'Donnell CJ, Shannon J, Farrell DH. Assessment of genetic determinants of the association of γ′ fibrinogen in relation to cardiovascular disease. *Arterioscler Thromb Vasc Biol* 2011; **31**: 2345–52.

3 Cheung EYL, Vos HL, Kruip MJHA, den Hertog HM, Jukema JW, de Maat MPM. Elevated fibrinogen gamma' ratio is associated with cardiovascular diseases and acute phase reaction but not with clinical outcome. *Blood* 2009; **114**: 4603–4; author reply 4604-5.

4 Stalker TJ, Traxler EA, Wu J, Wannemacher KM, Cermignano SL, Voronov R, Diamond SL, Brass LF. Hierarchical organization in the hemostatic response and its relationship to the platelet-signaling network. *Blood* 2013; **121**: 1875–85.

5 Zhu S, Herbig BA, Yu X, Chen J, Diamond SL. Contact pathway function during human whole blood clotting on procoagulant surfaces. *Front Med* 2018; **5**: 1–8.

6 Zhu S, Herbig BA, Li R, Colace T V., Muthard RW, Neeves KB, Diamond SL. In microfluidico: Recreating in vivo hemodynamics using miniaturized devices. *Biorheology*. IOS Press; 2015. p. 303–18.

7 Zhu S, Travers RJ, Morrissey JH, Diamond SL. FXIa and platelet polyphosphate as therapeutic targets during human blood clotting on collagen/tissue factor surfaces under flow. *Blood* American Society of Hematology; 2015; **126**: 1494–502.

8 Welsh JD, Poventud-Fuentes I, Sampietro S, Diamond SL, Stalker TJ, Brass LF. Hierarchical organization of the hemostatic response to penetrating injuries in the mouse macrovasculature. *J Thromb Haemost* 2017; **15**: 526–37.

9 Welsh JD, Colace T V., Muthard RW, Stalker TJ, Brass LF, Diamond SL. Platelet-targeting sensor reveals thrombin gradients within blood clots forming in microfluidic assays and in mouse. *J Thromb Haemost* 2012; **10**: 2344–53.

10 Muthard RW, Diamond SL. Side view thrombosis microfluidic device with controllable wall shear rate and transthrombus pressure gradient. *Lab Chip* 2013; **13**: 1883.

11 Muthard RW, Welsh JD, Brass LF, Diamond SL. Fibrin, γ′-Fibrinogen, and Transclot Pressure Gradient Control Hemostatic Clot Growth during Human Blood Flow over a Collagen/Tissue Factor Wound. *Arterioscler Thromb Vasc Biol* 2015; **35**: 645–54.

12 Tomaiuolo M, Stalker TJ, Welsh JD, Diamond SL, Sinno T, Brass LF. A systems approach to hemostasis: 2. Computational analysis of molecular transport in the thrombus microenvironment. *Blood* 2014; **124**: 1816–23.

13 Zhu S, Lu Y, Sinno T, Diamond SL. Dynamics of Thrombin Generation and Flux from Clots during Whole Human Blood Flow over Collagen/Tissue Factor Surfaces. *J Biol Chem* 2016; **291**: 23027–35.

14 Mosesson MW, Finlayson JS, Umfleet RA, Galanakis D. Human fibrinogen heterogeneities. I. Structural and related studies of plasma fibrinogens which are high solubility catabolic intermediates. *J Biol Chem* 1972; **247**: 5210–9.

15 Mosesson MW. Update on antithrombin I (fibrin). *Thromb Haemost* 2007; **98**: 105–8.

16 Liu CY, Nossel HL, Kaplan KL. The binding of thrombin by fibrin. *J Biol Chem* 1979; **254**: 10421–5.

17 Lovely RS, Moaddel M, Farrell DH. Fibrinogen gamma' chain binds thrombin exosite II. *J Thromb Haemost* 2003; **1**: 124–31.

18 Haynes LM, Orfeo T, Mann KG, Everse SJ, Brummel-Ziedins KE. Probing the Dynamics of Clot-Bound Thrombin at Venous Shear Rates. *Biophys J* Biophysical Society; 2017; **112**: 1634–44.

19 Bänninger H, Lämmle B, Furlan M. Binding of alpha-thrombin to fibrin depends on the quality of the fibrin network. *Biochem J* 1994; **298 (Pt 1**: 157–63.

20 Brass LF, Diamond SL. Transport physics and biorheology in the setting of hemostasis and thrombosis. *J Thromb Haemost* 2016; **14**: 906–17.

21 Hockin MF, Jones KC, Everse SJ, Mann KG. A model for the stoichiometric regulation of blood coagulation. *J Biol Chem* 2002; **277**: 18322–33.

22 Chatterjee MS, Denney WS, Jing H, Diamond SL. Systems biology of coagulation initiation: Kinetics of thrombin generation in resting and activated human blood. Beard DA, editor. *PLoS Comput Biol* Public Library of Science; 2010; **6**: e1000950.

23 Kuharsky AL, Fogelson AL. Surface-mediated control of blood coagulation: The role of binding site densities and platelet deposition. *Biophys J* 2001; **80**: 1050–74.

24 Fogelson AL, Hussain YH, Leiderman K. Blood clot formation under flow: the importance of factor XI depends strongly on platelet count. *Biophys J* 2012; **102**: 10–8.

25 Lu Y, Lee MY, Zhu S, Sinno T, Diamond SL. Multiscale simulation of thrombus growth and vessel occlusion triggered by collagen/tissue factor using a data-driven model of combinatorial platelet signalling. *Math Med Biol* 2017; **34**: 523–546.

26 Maloney SF, Brass LF, Diamond SL. P2Y12 or P2Y1 inhibitors reduce platelet deposition in a microfluidic model of thrombosis while apyrase lacks efficacy under flow conditions. *Integr Biol* 2010; **2**: 183.

27 Zhu S, Travers RJ, Morrissey JH, Diamond SL. FXIa and platelet polyphosphate as therapeutic targets during human blood clotting on collagen/tissue factor surfaces under flow. *Blood* American Society of Hematology; 2015; **126**: 1494–

502.

28 Colace T V, Muthard RW, Diamond SL. Thrombus growth and embolism on tissue factor-bearing collagen surfaces under flow: role of thrombin with and without fibrin. *Arter Thromb Vasc Biol* 2012; **32**: 1466–76.

29 Carr ME, Hermans J. Size and Density of Fibrin Fibers from Turbidity. *Macromolecules* 1978; **11**: 46–50.

30 Vindigni A, Di Cera E. Release of Fibrinopeptides by the Slow and Fast Forms of Thrombin †. *Biochemistry* 1996; **35**: 4417–26.

31 Higgins DL, Lewis SD, Shafer JA. Steady state kinetic parameters for the thrombin-catalyzed conversion of human fibrinogen to fibrin. *J Biol Chem* 1983; **258**: 9276–82.

32 Voronov RS, Stalker TJ, Brass LF, Diamond SL. Simulation of intrathrombus fluid and solute transport using in vivo clot structures with single platelet resolution. *Ann Biomed Eng* 2013; **41**: 1297–307.

33 Welsh JD, Stalker TJ, Voronov R, Muthard RW, Tomaiuolo M, Diamond SL, Brass LF. A systems approach to hemostasis: 1. The interdependence of thrombus architecture and agonist movements in the gaps between platelets. *Blood* 2014; **124**: 1808–15.

34 Talens S, Leebeek FWG, Demmers JAA, Rijken DC. Identification of fibrin clot-bound plasma proteins. Reitsma PH, editor. *PLoS One* 2012; **7**: e41966.

35 Leiderman K, Fogelson AL. Grow with the flow: A spatial-temporal model of platelet deposition and blood coagulation under flow. *Math Med Biol* 2011; **28**: 47–84.

36 Elizondo P, Fogelson AL. A Mathematical Model of Venous Thrombosis Initiation. *Biophys J* Biophysical Society; 2016; **111**: 2722–34.

37 Fredenburgh JC, Stafford AR, Leslie BA, Weitz JI. Bivalent Binding to γ_A /γ′-Fibrin Engages Both Exosites of Thrombin and Protects It from Inhibition by the Antithrombin-Heparin Complex. *J Biol Chem* 2008; **283**: 2470–7.

38 Weitz JI, Hudoba M, Massel D, Maraganore J, Hirsh J. Clot-bound thrombin is protected from inhibition by heparin-antithrombin III but is susceptible to inactivation by antithrombin III-independent inhibitors. *J Clin Invest* 1990; **86**: 385–91.

39 Tsiang M, Jain AK, Gibbs CS. Functional requirements for inhibition of thrombin by antithrombin III in the presence and absence of heparin. *J Biol Chem* 1997; **272**: 12024–9.

40 Ellis V, Scully MF, Kakkar V V. The acceleration of the inhibition of platelet prothrombinase complex by heparin. *Biochem J* Portland Press Limited; 1986; **233**: 161–5.

41 Uitte de Willige S, de Visser MC, Houwing-Duistermaat JJ, Rosendaal FR, Vos HL, Bertina RM. Genetic variation in the fibrinogen gamma gene increases the risk for deep venous thrombosis by reducing plasma fibrinogen gamma' levels.

Blood 2005; **106**: 4176–83.

42 Macrae FL, Domingues MM, Casini A, Ariëns RASS. The (Patho)physiology of Fibrinogen γ′. *Semin Thromb Hemost* 2016; **42**: 344–55.

43 Müller F, Mutch NJ, Schenk WA, Smith SA, Esterl L, Spronk HM, Schmidbauer S, Gahl WA, Morrissey JH, Renné T. Platelet Polyphosphates Are Proinflammatory and Procoagulant Mediators In Vivo. *Cell* 2009; **139**: 1143–56.

44 Kamikubo Y, Mendolicchio GL, Zampolli A, Marchese P, Rothmeier AS, Orje JN, Gale AJ, Krishnaswamy S, Andr´ A, Gruber A, Østergaard H, Petersen LC, Ruf W, Ruggeri ZM. Selective factor VIII activation by the tissue factor-factor VIIa-factor Xa complex. *Blood* 2017; **130**: 1661–70.

45 Bungay SD, Gentry PA, Gentry RD, Bungay SD. A mathematical model of lipid-mediated thrombin generation. *Mathematical Medicine and Biology*. 2003.

46 Coenraad Hemker H, Giesen P, Al Dieri R, Regnault V, De Smedt E, Wagenvoord R, Lecompte T, Béguin S, Hemker HC. Calibrated Automated Thrombin Generation Measurement in Clotting Plasma. *Pathophysiol Haemost Thromb* 2003; **33**: 4–15.

47 Fogelson AL, Neeves KB. Fluid Mechanics of Blood Clot Formation. *Annu Rev Fluid Mech* 2015; **47**: 377–403.

48 Diamond SL. Systems Analysis of Thrombus Formation. *Circ Res* 2016; **118**: 1348–62.

49 Leiderman K, Fogelson A. An overview of mathematical modeling of thrombus formation under flow. *Thromb Res* 2014; **133**.

50 Zhu S, Chen J, Diamond SL. Establishing the Transient Mass Balance of Thrombosis: From Tissue Factor to Thrombin to Fibrin Under Venous Flow. *Arterioscler Thromb Vasc Biol* American Heart Association, Inc.; 2018; : ATVBAHA.118.310906.

51 Berny MA, Munnix ICA, Auger JM, Schols SEM, Cosemans JMEM, Panizzi P, Bock PE, Watson SP, McCarty OJT, Heemskerk JWM. Spatial distribution of factor xa, thrombin, and fibrin(ogen) on thrombi at venous shear. *PLoS One* 2010; **5**.

52 Zhu S, Lu Y, Sinno T, Diamond SL. Dynamics of thrombin generation and flux from clots during whole human blood flow over collagen/tissue factor surfaces. *J Biol Chem* American Society for Biochemistry and Molecular Biology; 2016; **291**: 23027–35.

53 Nesheim ME, Tracy RP, Tracy PB, Boskovic DS, Mann KG. Mathematical Simulation of Prothrombinase. *Methods Enzymol* Academic Press; 1992; **215**: 316–28.

54 Higgins DL, Lewis SD, Shafer JA, Higginss DL, Lewis SD, Shaferg JA, Higgins DL, Lewis SD, Shafer JA. Steady State Kinetic Parameters for the Thrombin-catalysed Conversion of Human Fibrinogen to Fibrin. *J Biol Chem* 1983; **258**: 9276–82.

55 Welsh JD, Stalker TJ, Voronov R, Muthard RW, Tomaiuolo M, Diamond SL, Brass LF. A systems approach to hemostasis: 1. The interdependence of thrombus architecture and agonist movements in the gaps between platelets. *Blood* 2014; **124**: 1808–15.

56 Zhu S, Tomaiuolo M, Diamond SL. Minimum wound size for clotting: Flowing blood coagulates on a single collagen fiber presenting tissue factor and von Willebrand factor. *Integr Biol (United Kingdom)* 2016; **8**: 813–20.

57 Lovely RS, Kazmierczak SC, Massaro JM, D'Agostino RB, O'Donnell CJ, Farrell DH. γ′ fibrinogen: Evaluation of a new assay for study of associations with cardiovascular disease. *Clin Chem* 2010; **56**: 781–8.

58 Renné T, Pozgajová M, Grüner S, Schuh K, Pauer H-U, Burfeind P, Gailani D, Nieswandt B. Defective thrombus formation in mice lacking coagulation factor XII. *J Exp Med* 2005; **202**: 271–81.

59 Colace T V., Fogarty PF, Panckeri KA, Li R, Diamond SL. Microfluidic assay of hemophilic blood clotting: Distinct deficits in platelet and fibrin deposition at low factor levels. *J Thromb Haemost* 2014; **12**: 147–58.

60 Muthard RW, Diamond SL. Blood Clots Are Rapidly Assembled Hemodynamic Sensors. *Arterioscler Thromb Vasc Biol* 2012; **32**: 2938–45.

61 Lobanova ES, Ataullakhanov FI. Unstable trigger waves induce various intricate dynamic regimes in a reaction-diffusion system of blood clotting. *Phys Rev Lett* 2003; **91**: 1–4.

62 Panteleev MA, Balandina AN, Lipets EN, Ovanesov M V., Ataullakhanov FI. Task-Oriented modular decomposition of biological networks: Trigger mechanism in blood coagulation. *Biophys J* Biophysical Society; 2010; **98**: 1751–61.

63 Galochkina T, Bouchnita A, Kurbatova P, Volpert V. Reaction-diffusion waves of blood coagulation. *Math Biosci* 2017; **288**: 130–9.

64 Xu Z, Chen N, Kamocka MM, Rosen ED, Alber M. A multiscale model of thrombus development. *J R Soc Interface* 2008; **5**: 705–22.

65 Flamm MH, Colace T V, Chatterjee MS, Jing H, Zhou S, Jaeger D, Brass LF, Sinno T, Diamond SL. Multiscale prediction of patient-specific platelet function under flow. *Blood* 2012; **120**: 190–8.

66 Wu WT, Jamiolkowski MA, Wagner WR, Aubry N, Massoudi M, Antaki JF. Multi-Constituent Simulation of Thrombus Deposition. *Sci Rep* Nature Publishing Group; 2017; **7**: 1–16.

67 Lu Y, Lee MY, Zhu S, Sinno T, Diamond SL. Multiscale simulation of thrombus growth and vessel occlusion triggered by collagen/tissue factor using a data-driven model of combinatorial platelet signalling. *Math Med Biol* 2017; **34**: 523–46.

68 Tsiklidis E, Sims C, Sinno T, Diamond SL. Multiscale systems biology of trauma-induced coagulopathy. 2018; : 1–10.

69 Danforth CM, Orfeo T, Mann KG, Brummel-Ziedins KE, Everse SJ. The impact of uncertainty in a blood coagulation model. *Math Med Biol* 2009; **26**: 323–36.

70 Danforth CM, Orfeo T, Everse SJ, Mann KG, Brummel-Ziedins KE. Defining the Boundaries of Normal Thrombin Generation: Investigations into Hemostasis. *PLoS One* 2012; **7**: 30385.

71 Link KG, Stobb MT, Di Paola JA, Neeves KB, Fogelson AL, Sindi SS, Leiderman K. A local and global sensitivity analysis of a mathematical model of coagulation and platelet deposition under flow. 2018; .

72 Kelley M, Leiderman K. A Mathematical Model of Bivalent Binding Suggests Physical Trapping of Thrombin within Fibrin Fibers. *Biophys J* Biophysical Society; 2019; **117**: 1442–55.

73 Chen J, Diamond SL. Reduced model to predict thrombin and fibrin during thrombosis on collagen/tissue factor under venous flow: Roles of γ'-fibrin and factor XIa. *PLoS Comput Biol* 2019; **15**.

74 Chen J, Diamond SL. Reduced model to predict thrombin and fibrin during thrombosis on collagen/tissue factor under venous flow: Roles of γ'-fibrin and factor XIa. *PLOS Comput Biol* 2019; **15**: e1007266.

75 Chen J, Verni CCCC, Jouppila A, Lassila R, Diamond SLSL. Dual antiplatelet and anticoagulant (APAC) heparin proteoglycan mimetic with shear-dependent effects on platelet-collagen binding and thrombin generation. *Thromb Res* Elsevier; 2018; **169**: 143–51.

76 Colace T V., Muthard RW, Diamond SL. Thrombus growth and embolism on tissue factor-bearing collagen surfaces under flow: Role of thrombin with and without fibrin. *Arterioscler Thromb Vasc Biol* 2012; **32**: 1466–76.

77 Zhu S, Diamond SL. Contact activation of blood coagulation on a defined kaolin/collagen surface in a microfluidic assay. *Thromb Res* Pergamon; 2014; **134**: 1335–43.

78 Weitz JI, Chan NC. Novel antithrombotic strategies for treatment of venous thromboembolism. *Blood* 2020; **135**: 351–9.

79 Nossent AY, Eikenboom JCJ, Bertina RM. Plasma Coagulation Factor Levels in Venous Thrombosis. *Semin Hematol* 2007; **44**: 77–84.

80 Van Hylckama Vlieg A, Van Der Linden IK, Bertina RM, Rosendaal FR. High levels of factor IX increase the risk of venous thrombosis. *Blood* American Society of Hematology; 2000; **95**: 3678–82.

81 Meijers JCM, Tekelenburg WLH, Bouma BN, Bertina RM, Rosendaal FR. High Levels of Coagulation Factor XI as a Risk Factor for Venous Thrombosis. *New England Journal of Medicine*. 2000.

82 Susree M, Anand · M, Anand M, In AA. Importance of Initial Concentration of Factor VIII in a Mechanistic Model of In Vitro Coagulation. *Acta Biotheor* 2018; **66**: 201–12.

83 Pieters M, Kotze RC, Jerling JC, Kruger A, Ariëns RAS. Evidence that fibrinogen γ' regulates plasma clot structure and lysis and relationship to cardiovascular risk factors in black Africans. *Blood* American Society of Hematology; 2013; **121**: 3254–60.

84 Siebenlist KR, Mosesson MW, Hernandez I, Bush LA, Di Cera E, Shainoff JR, Di Orio JP, Stojanovic L. Studies on the basis for the properties of fibrin produced from fibrinogen-containing chains. 2005; .

85 Rein-Smith CM, Anderson NW, Farrell DH. Differential regulation of fibrinogen γ chain splice isoforms by interleukin-6. *Thromb Res* Pergamon; 2013; **131**: 89–93.

86 Link KG, Stobb MT, Monroe DM, Fogelson AL, Neeves KB, Sindi SS, Leiderman K. Computationally Driven Discovery in Coagulation. *Arterioscler Thromb Vasc Biol* 2020; : 79–86.

87 Gailani D, Gruber A. Factor XI as a Therapeutic Target. *Arterioscler Thromb Vasc Biol* 2016; **36**: 1316–22.

88 Sikka P, Bindra VK. Newer antithrombotic drugs. *Indian J Crit Care Med* 2010; **14**: 188–95.

89 Watson RDS, Chin BSP, Lip GYH. Antithrombotic therapy in acute coronary syndromes. *BMJ (Clinical Res ed)* 2002; **325**: 1348–51.

90 Warner TD, Nylander S, Whatling C. Anti-platelet therapy: Cyclo-oxygenase inhibition and the use of aspirin with particular regard to dual anti-platelet therapy. *Br J Clin Pharmacol* 2011; **72**: 619–33.

91 Stangl PA, Lewis S. Review of currently available GP IIb/IIIa inhibitors and their role in peripheral vascular interventions. *Semin Intervent Radiol* 2010; **27**: 412–21.

92 Lijnen HR, Collen D. Fibrinolytic agents: Mechanisms of activity and pharmacology. *Thromb Haemost* 1995; **74**: 387–90.

93 Holmes DR, Kereiakes DJ, Kleiman NS, Moliterno DJ, Patti G, Grines CL. Combining Antiplatelet and Anticoagulant Therapies. *J Am Coll Cardiol* American College of Cardiology Foundation; 2009; **54**: 95–109.

94 Lamberts M, Olesen JB, Ruwald MH, Hansen CM, Karasoy D, Kristensen SL, Køber L, Torp-Pedersen C, Gislason GH, Hansen ML. Bleeding after initiation of multiple antithrombotic drugs, including triple therapy, in atrial fibrillation patients following myocardial infarction and coronary intervention: A nationwide cohort study. *Circulation* 2012; **126**: 1185–93.

95 Hirsh J, Anand SS, Halperin JL, Fuster V. Mechanism of Action and Pharmacology of Unfractionated Heparin. *Arterioscler Thromb Vasc Biol* 2001; **21**: 1094–6.

96 Machovich R. Mechanism of action of heparin through thrombin on blood coagulation. *BBA - Protein Struct* 1975; **412**: 13–7.

97 Lassila R, Lindstedt K, Kovanen PT. Native macromolecular heparin proteoglycans exocytosed from stimulated rat serosal mast cells strongly inhibit platelet-collagen interactions. *ArteriosclerThrombVascBiol* 1997; **17**: 3578–87.

98 Lassila R, Jouppila A. Mast cell-Derived heparin proteoglycans As a model for a local antithrombotic. *Semin Thromb Hemost* 2014; **40**: 837–44.

99 Tchougounova E, Pejler G. Regulation of extravascular coagulation and fibrinolysis by heparin-dependent mast cell chymase. *FASEB J* 2001; **15**: 2763–5.

100 San Antonio JD, Lander AD, Karnovsky MJ, Slayter HS. Mapping the heparin-binding sites on type I collagen monomers and fibrils. *J Cell Biol* 1994; **125**: 1179–88.

101 Kauhanen P, Kovanen PT, Lassila R. Coimmobilized native macromolecular heparin proteoglycans strongly inhibit platelet-collagen interactions in flowing blood. *Arterioscler Thromb Vasc Biol* 2000; **20**: E113–9.

102 Tuuminen R, Jouppila A, Salvail D, Laurent CE, Benoit MC, Syrjälä S, Helin H, Lemström K, Lassila R. Dual antiplatelet and anticoagulant APAC prevents experimental ischemia–reperfusion-induced acute kidney injury. *Clin Exp Nephrol* 2017; **21**: 436–45.

103 Zhu S, Travers RJ, Morrissey JH, Diamond SL. FXIa and platelet polyphosphate as therapeutic targets during human blood clotting on collagen / tissue factor surfaces under flow. *Blood* 2015; **126**: 1494–503.

104 Li R, Diamond SL. Detection of platelet sensitivity to inhibitors of COX-1, $P2Y_1$, and $P2Y_{12}$ using a whole blood microfluidic flow assay. *Thromb Res* 2014; **133**: 203–10.

105 Li R, Fries S, Li X, Grosser T, Diamond SL. Microfluidic assay of platelet deposition on collagen by perfusion of whole blood from healthy individuals taking aspirin. *Clin Chem* 2013; **59**: 1195–204.

106 Hwang D, Leblanc P. Heparin inhibits the formation of endoperoxide metabolites in rat platelets : aspirin-like activity . *Prostaglandins Med* 1981; **6**: 341–4.

107 Sweeney SM, Guy CA, Fields GB, San Antonio JD. Defining the domains of type I collagen involved in heparin- binding and endothelial tube formation. *Proc Natl Acad Sci U S A* 1998; **95**: 7275–80.

108 Ricard-Blum S, Beraud M, Raynal N, Farndale RW, Ruggiero F. Structural requirements for heparin/heparan sulfate binding to type V collagen. *J Biol Chem* 2006; **281**: 25195–204.

109 Wilson SJ, Ismat FA, Wang Z, Cerra M, Narayan H, Raftis J, Gray TJ, Connell S, Garonzik S, Ma X, Yang J, Newby DE. PAR4 (Protease-Activated Receptor 4) Antagonism with BMS-986120 Inhibits Human Ex Vivo Thrombus Formation. *Arterioscler Thromb Vasc Biol* 2018; **38**: 448–56.

110 Pinto DJP, Orwat MJ, Smith LM, Quan ML, Lam PYS, Rossi KA, Apedo A, Bozarth JM, Wu Y, Zheng JJ, Xin B, Toussaint N, Stetsko P, Gudmundsson O, Maxwell B, Crain EJ, Wong PC, Lou Z, Harper TW, Chacko SA, et al. Discovery of a Parenteral Small Molecule Coagulation Factor XIa Inhibitor Clinical Candidate (BMS-962212). *J Med Chem* 2017; **60**: 9703–23.

111 Meah MN, Raftis J, Wilson SJ, Perera V, Garonzik SM, Murthy B, Gerry Everlof J, Aronson R, Luettgen J, Newby DE. Antithrombotic effects of combined PAR (protease-activated receptor)-4 antagonism and factor Xa inhibition. *Arterioscler Thromb Vasc Biol* 2020; : 2678–85.

112 Bostwick JS, Bird JE, Hua J, Bouvier M, Miller MM, Callejo M, Lawrence RM, Marinier A, Seiffert D, Banville J, Gordon DA, Wong PC, Wexler RR, Priestley ES, Maxwell BD, Guay J, Yang J, Harden D, Giancarli M, Schumacher WA, et al. Blockade of protease-activated receptor-4 (PAR4) provides robust antithrombotic activity with low bleeding. *Sci Transl Med* 2017; **9**: eaaf5294.

113 Verni CC. Role of Soluble Fibrin and Fibrin Degradation Products on Platelet Signaling During Trauma. *Diss available from ProQuest* 2020; .

114 Li R, Diamond SL. Detection of platelet sensitivity to inhibitors of COX-1, P2Y1, and P2Y12 using a whole blood microfluidic flow assay. *Thromb Res* 2014; **133**: 203–10.

115 André P, LaRocca T, Delaney SM, Lin PH, Vincent D, Sinha U, Conley PB, Phillips DR. Anticoagulants (Thrombin Inhibitors) and Aspirin Synergize with P2Y 12 Receptor Antagonism in Thrombosis. *Circulation* 2003; **108**: 2697–703.

116 Van Giezen JJJ, Humphries RG. Preclinical and clinical studies with selective reversible direct P2Y 12 antagonists. *Seminars in Thrombosis and Hemostasis*. Copyright © 2005 by Thieme Medical Publishers, Inc., 333 Seventh Avenue, New York, NY 10001, USA. Tel: +1(212) 584-4662.; 2005. p. 195–204.

117 Akers WS, Oh JJ, Oestreich JH, Ferraris S, Wethington M, Steinhubl SR. Pharmacokinetics and Pharmacodynamics of a Bolus and Infusion of Cangrelor: A Direct, Parenteral P2Y12 Receptor Antagonist. *J Clin Pharmacol* John Wiley & Sons, Ltd; 2010; **50**: 27–35.

118 DeCortin ME, Brass LF, Diamond SL. Core and shell platelets of a thrombus: A new microfluidic assay to study mechanics and biochemistry. *Res Pract Thromb Haemost* 2020; **4**: 1158–66.